

UNCLASSIFIED

NASA TECHNICAL MEMORANDUM

NASA TM X-72711

NASA TM X-72711



AERODYNAMIC CHARACTERISTICS OF
THE 10-PERCENT-THICK NASA
SUPERCRITICAL AIRFOIL 33 DESIGNED FOR A
NORMAL-FORCE COEFFICIENT OF 0.7

(NASA-TM-X-72711) AERODYNAMIC
CHARACTERISTICS OF THE 10-PERCENT-THICK NASA
SUPERCRITICAL AIRFOIL 33 DESIGNED FOR A
NORMAL-FORCE COEFFICIENT OF 0.7 (NASA)
105 P HC A06/MF A01

83-11075


CSCL 01A G3/02 Unclas 32179

NATIONAL SECURITY INFORMATION
Unauthorized Disclosure Subject
to Criminal Sanctions

This informal documentation medium is used to provide accelerated or special release of technical information to selected users. The contents may not meet NASA formal editing and publication standards, may be revised, or may be incorporated in another publication.

NATIONAL AERONAUTICS AND SPACE ADMINISTRATION
LANGLEY RESEARCH CENTER, HAMPTON, VIRGINIA 23665

NASA/Langley LTR dtd. 2/10/81


AERODYNAMIC CHARACTERISTICS OF
THE 10-PERCENT-THICK NASA
SUPERCRITICAL AIRFOIL 33 DESIGNED FOR A
NORMAL-FORCE COEFFICIENT OF 0.7

By Charles D. Harris
Langley Research Center

SUMMARY

A 10-percent-thick supercritical airfoil based on an off-design sonic-pressure plateau criterion has been developed and experimental aerodynamic characteristics measured. The airfoil had a design normal-force coefficient of 0.7 and was identified as supercritical airfoil 33. Results show the airfoil to have good drag rise characteristics over a wide range of normal-force coefficients with no measurable shock losses up to the Mach numbers at which drag divergence occurred for normal-force coefficients up to 0.7. Comparisons of experimental and theoretical characteristics were made and composite drag rise characteristics were derived for normal-force coefficients of 0.5 and 0.7 and a Reynolds number of 40 million.

INTRODUCTION

Continued development of supercritical airfoil technology has resulted in recognition of design criteria which permit the design of family related supercritical airfoils. Based on these criteria, two supercritical airfoils have been designed - the 10-percent thick airfoil 33 reported herein and the 14-percent-thick airfoil of reference 1. The design normal-force coefficient was 0.7 for both airfoils.

5
[REDACTED]

OFFICE OF
OF [REDACTED]

SYMBOLS

Values are given in both SI and U.S. Customary Units. Measurements and calculations are made in U.S. Customary Units.

C_p	pressure coefficient, $\frac{P_1 - P_\infty}{q_\infty}$
$C_{p, \text{sonic}}$	pressure coefficient corresponding to local Mach number of 1.0
c	chord of airfoil, 63.5 centimeters (25.0 inches)
c_d	section drag coefficient
$\Delta c_{d,s}$	drag increment due to shock wave losses
c_l	section lift coefficient
c_m	section pitching-moment coefficient about the quarter-chord point
c_n	section normal-force coefficient
K	surface curvature, reciprocal of local radius of curvature
M	Mach number
m	surface slope, dy/dx
P	static pressure, newtons per meter ² (pounds per foot ²)
Δp_t	total-pressure loss, newtons per meter ² (pounds per foot ²)
q	dynamic pressure, newtons per meter ² (pounds per foot ²)
R	Reynolds number based on airfoil chord
x	ordinate along airfoil reference line measured from airfoil leading edge, centimeters (inches)
y	ordinate normal to airfoil reference line, centimeters (inches)
z	vertical distance in wake profile measured from bottom of rake, centimeters (inches)
α	geometric angle of attack of airfoil reference line, degrees

[REDACTED]

Subscripts:

- 1 local point on airfoil
- ∞ undisturbed stream

APPARATUS AND TECHNIQUES

Model Configuration

The supercritical airfoil basic concept and detailed design philosophy are discussed in reference 2.

Background.- During initial phases of the two-dimensional supercritical airfoil development program, emphasis was placed upon developing a 10-percent-thick airfoil with the highest drag divergence Mach number attainable at a normal-force coefficient of 0.7. The normal-force coefficient of 0.7 was chosen as the design goal since, when account was taken of the sweep effect, it was representative of lift coefficients at which the advanced technology near-sonic transports utilizing the supercritical airfoil concept were then expected to cruise. These initial phases resulted in supercritical airfoil 11 which has been reported in reference 3. This airfoil exhibited an undesirable creep or gradual increase in the variation of drag coefficient with Mach number of about 14 counts (c_d increment of 0.0014) between $M = 0.50$ and the drag divergent Mach number at the design normal-force coefficient.

Subsequent design studies of advanced technology transport configurations suggested that the near-sonic cruise lift coefficient requirements would be somewhat lower than originally anticipated. Consequently, the improved supercritical airfoil 26a (ref. 4) was developed with a design normal-force coefficient of about 0.55. The wind-tunnel tests required for this airfoil also provided the opportunity to explore the drag creep problem noted with airfoil 11. Airfoil 26a had no drag creep at normal-force coefficients up to about 0.6 and

[REDACTED]

~~SECRET~~

the drag divergence Mach number varied from approximately 0.82 at a normal-force coefficient of 0.30 to 0.78 at a normal-force coefficient of 0.80. As discussed in reference 4 these improved drag creep characteristics were largely attributed to a more favorable flow recompression over the forward upper surface and the elimination of a region of overexpansion near the three-quarter-chord station.

Recent emphasis on fuel economy has generated considerable interest in a fuel-conserving aircraft envisioned to cruise at Mach numbers near those of current transports. Such an aircraft could utilize supercritical airfoil technology to achieve weight and drag reductions by permitting the use of thicker wings with higher aspect ratios and less sweep. Because the wings with higher aspect ratio would require airfoils with design normal-force coefficients higher than 0.55, airfoil 31 (ref. 5) was developed with the same design normal-force coefficient as the earlier airfoil 11 ($c_n = 0.7$) but with significant improvements in the drag characteristics. Drag creep was practically eliminated at normal-force coefficients between about 0.4 and 0.7 and greatly reduced at other normal-force coefficients. Substantial reductions in the drag levels preceding drag divergence were also achieved at all normal-force coefficients.

Airfoils through 31 were developed experimentally through intuitive contour modifications in the wind tunnel. It was an iterative process consisting of evaluating experimental pressure distributions at design and off-design conditions and physically altering the airfoil profile to yield the best drag characteristics over a range of test conditions.

The experimental results for these earlier airfoils suggested design criteria which would yield the best compromise in drag characteristics over a

[REDACTED]

range of test conditions. These design criteria consist essentially of three principal guidelines which may be used in designing supercritical airfoils. There are several additional, more detailed, design guidelines (treatment of leading and trailing edges, and local minimum thickness constraints, for example) which are beyond the intended scope of this report and will be discussed in a later report.

The first principal guideline, referred to as the sonic plateau criterion, is that at some incremental normal-force coefficient below the design normal-force coefficient the pressure distribution on the upper and lower surfaces be flat with the upper surface pressures just below the sonic value. The increment is a function of the design normal-force coefficient and appears to be about -0.25 to -0.30 for a design normal-force coefficient of 0.7.

On the upper surface the plateau extends from near the leading edge to the start of the aft pressure recovery and on the lower surface from near the leading edge to the recompression region entering into the cusp. The rearward extent of the upper surface plateau is determined by the second principal design guideline which requires that the gradient of the aft pressure recovery be gradual enough to avoid separation problems for lift coefficients and Mach numbers up to the design value. Consequently, the rearward extent of the upper surface plateau would depend on thickness ratio since the thicker the airfoil, the higher the induced velocities from which the flow must recover and, therefore, the further forward the aft pressure recovery must begin. The upper surface plateau extends from approximately 3- to 80-percent chord on the 10-percent-thick airfoil 33 and approximately 5- to 66-percent chord on the 14-percent-thick airfoil of reference 1.

~~SECRET~~

The third principal guideline requires that the airfoil have sufficient aft camber so that at design conditions the angle of attack be about zero. This prevents a too-forward location of the upper surface crest with the negative pressure coefficients over the mid-chord region acting over a rearward facing surface. Both experiments and theoretical analyses (ref. 6) have indicated that an increase in angle of attack to positive values results in an abrupt increase in wave drag.

Based on these criteria two supercritical airfoils were designed - the 14-percent-thick airfoil reported in reference 1 and the 10-percent-thick airfoil 33 reported herein. The design normal-force coefficient was 0.7 for both airfoils. An iterative design process was used which consisted of altering the airfoil coordinates until the viscous, airfoil analysis program of reference 6 indicated that the aforementioned design criteria had been satisfied. Geometric characteristics of the experimental 10-percent-thick airfoil 33 are presented in figures 1 and 2 and compared with those of the earlier 10-percent-thick airfoil 31 (ref. 5). Measured section coordinates of both airfoils are presented in table I.

The incremental ordinates between airfoils 31 and 33 delineated in table I show that the ordinates were modified over the forward upper and lower surfaces, decreased over the rear upper surface, and increased in the vicinity of the 80-percent chord on the lower surface. Referring to the pressure distribution for airfoil 31 which approaches the off-design sonic-plateau criterion (fig. 15(c) of ref. 5; $M = 0.76$ and $c_n = 0.46$), the alterations over the upper surface and forward lower surface were necessary to obtain the desired plateau pressure distributions and to reduce the upper surface aft pressure recovery gradient. The ordinates on the rear lower surface were increased, with the maximum increase

[REDACTED]

at 80-percent, to provide increased depth for control surface and flap structural requirements. Subtracting from the upper surface and adding to the lower surface over the aft portion of the airfoil in this manner reduced the aft camber and, therefore, increased the angle of attack required to achieve a given normal-force coefficient. The ordinates on the lower surface were progressively increased until the third design criterion was met; that is, that the angle of attack required for the design normal-force coefficient of 0.7 was approximately 0° .

Since the best drag characteristics are often obtained on airfoils with a small amount of upper surface trailing-edge separation and since theoretical treatments of the flow at trailing-edge regions are generally unreliable, theoretically-predicted flow separation at the 98-percent chord location was accepted during the design process. Attempts to achieve a more rearward location of theoretical separation by reducing the aft pressure recovery gradient would have forced the rear terminus of the sonic plateau forward, resulting in higher induced velocities in the plateau region and a probable reduction in drag rise Mach number.

Wind-tunnel model.- The coordinates of the experimental airfoil 33 deviated slightly from the design profile (not presented). On the upper surface, the deviation was nowhere greater than $\Delta x/c = 0.0003$ and generally less than 0.0001. On the lower surface, deviation was somewhat greater; as much as 0.0005 on the forward region. These small deviations should not significantly affect the results.

Irregularities in the curvature distributions (fig. 2) are due to small surface irregularities that become greatly exaggerated when examined from the standpoint of local curvature. Such irregularities are not as apparent in the slope distributions (fig. 2). Both airfoils included a trailing-edge cavity

[REDACTED]

[REDACTED]

(see the insert in fig. 1 and the photographs of fig. 3) which had a favorable effect on the wake as discussed in reference 3.

The wind-tunnel models, mounted in an inverted position, spanned the width of the tunnel with a span-chord ratio of 3.43. They were constructed with metal leading and trailing edges and a metal core around which plastic fill was used to form the contours of the airfoils. Angle of attack was changed manually by rotating the model about pivots in the tunnel sidewalls. A photograph and a drawing of a typical airfoil model installed in the tunnel are shown in figures 3 and 4, respectively.

Wind Tunnel

The investigation was conducted in the Langley 8-foot transonic pressure tunnel (ref. 7). This tunnel is a continuous-flow, variable-pressure wind tunnel with controls that permit the independent variation of Mach number, stagnation pressure and temperature, and dewpoint. It has a 2.16-meter-square (85.2-inch-square) test section with filleted corners so that the total cross-sectional area is equivalent to that of a 2.44-meter-diameter (8-foot-diameter) circle. The upper and lower test-section walls are axially slotted to permit testing through the transonic speed range. The total slot width at the position of the model averaged about 5 percent of the width of the upper and lower walls.

The solid sidewalls and slotted upper and lower walls make this tunnel well suited to the investigation of two-dimensional models since the sidewalls act as endplates and the slots permit development of the flow field in the vertical direction.

Boundary-Layer Transition

Based on the technique discussed in reference 8, boundary-layer transition was fixed along the 28-percent chord line on the upper and lower surfaces of

~~SECRET~~

the models in an attempt to simulate full-scale Reynolds numbers by providing the same relative trailing-edge boundary-layer displacement thickness at model scale as would exist at full-scale flight conditions. The simulation technique, which requires that laminar flow be maintained ahead of the transition trip, is limited to those test conditions in which shock waves or steep adverse pressure gradients occur behind the point of fixed transition so that the flow is not tripped prematurely. The transition trips consisted of 0.25-cm-wide (0.10-in.) bands of No. 90 Carborundum grains. Analysis of drag and boundary-layer displacement thickness at the trailing edge theoretically computed using reference 6 indicated that the simulated full-scale Reynolds number was around 40 million rather than the 20 to 30 million quoted for earlier supercritical airfoil investigations (ref. 3, for example).

Measurements

Surface-pressure measurements.- Normal force and pitching moments on the airfoils were determined from surface static-pressure measurements. The surface-pressure measurements were obtained from a chordwise row of orifices located approximately $0.32c$ from the tunnel center line. Orifices were more concentrated near the leading and trailing edges of the airfoil to define the pressure gradients in these regions. In addition, a rearward facing orifice was included in the cavity at the trailing edge (identified at an upper surface x/c location of 1.00). The transducers used in the differential pressure scanning valves to measure the static pressure at the airfoil surface had a range of $\pm 68.9 \text{ kN/m}^2$ (10 lb/in^2).

Wake measurements.- Drag forces were determined from vertical variations of the total and static pressures measured across the wake with the profile drag rake shown in figure 4(b). The profiles, schematically illustrated in figure 5, represent the momentum losses as indicated by stagnation-pressure deficits

~~SECRET~~

across the wake. The middle section of these profiles reflects viscous and separation losses in the boundary layer, whereas the "wings" of the profile reflect direct losses in stagnation pressure across the shock waves.

The rake was positioned in the vertical center-line plane of the tunnel, approximately 1 chord length rearward of the trailing edge of the airfoil. The total-pressure tubes were flattened horizontally and closely spaced vertically (0.36 percent of the airfoil chord) in the region of the wake associated with skin-friction boundary-layer losses. Outside this region, the tube vertical spacing progressively widened until in the region above the wing where only shock losses were anticipated, the total-pressure tubes were spaced apart about 7.2 percent of the chord. Static-pressure tubes were distributed as shown in figure 4(b). Each static pressure measured was used over a section of the rake to determine local flow conditions in the vicinity of the static-pressure tube rather than using an average of all the static pressures measured. The rake was attached to the conventional center line sting mount of the tunnel; this arrangement permitted it to be moved vertically to center the close concentration of tubes in the boundary-layer wake. The transducer in the differential-pressure scanning valve connected to total-pressure tubes intended to measure boundary-layer losses had a range of $\pm 17.2 \text{ kN/m}^2$ (2.5 lb/in^2), and the transducers in the valves for measuring shock losses and static pressure had a range of $\pm 6.9 \text{ kN/m}^2$ (1 lb/in^2).

Reduction of Data

Calculation of c_n and c_m .- Section normal-force and pitching-moment coefficients were obtained by numerical integration (based on the trapezoidal method) of the local surface-pressure coefficient measured at each orifice multiplied by an appropriate weighting factor (incremental area).

~~XX~~

Calculation of c_d . - To obtain section drag coefficients, point drag coefficients were computed for each total-pressure measurement in the wake by using the procedure of reference 9. These point drag coefficients were then summed by numerical integration across the wake, again based on the trapezoidal method. Drag increments due to shock wave losses ($\Delta c_{d,s}$) were determined from integration of the drag measured across the wings (fig. 5) of the wake profile.

Wind-Tunnel-Wall Effects

Because of the uncertainty in lift-induced interference effects and solid and wake blockage effects (particularly in the presence of local supercritical flow) no corrections for wall effects have been applied to the basic experimental data. Adjustments for blockage were applied to the composite drag rise data and are explained in the Discussion section.

TEST CONDITIONS

Tests were conducted at Mach numbers from 0.50 to 0.82 for a stagnation pressure of 0.1013 MN/m^2 (1 atm). The stagnation temperature of the tunnel air was automatically controlled at approximately 322 K (120°F) and the air was dried until the dewpoint in the test section was reduced sufficiently to avoid condensation effects. Resultant test Reynolds numbers based on the airfoil chord length were as shown in figure 6.

PRESENTATION OF RESULTS

The experimental data reported herein are presented in the following figures:

	Figure
Force and moment characteristics	7
Variation of measured section drag coefficient with Mach number.	8
Drag increment due to shock-wave losses.	9

D
██████████

	Figure
Composite drag curves.	10
Chordwise pressure distributions at -	
M = 0.50.	11
M = 0.60.	12
M = 0.70.	13
M = 0.74.	14
M = 0.76.	15
M = 0.77.	16
M = 0.78.	17
M = 0.79.	18
M = 0.80.	19
M = 0.81.	20
M = 0.82.	21
Comparisons of theoretical and experimental characteristics for -	
M = 0.76, $c_n = 0.414$	22
M = 0.79, $c_n = 0.535$	23
M = 0.77, $c_n = 0.707$	24

Complete surface pressure distributions for the earlier 10-percent-thick supercritical airfoil 31 are presented in reference 5 and for the family related 14-percent-thick airfoil in reference 1.

DISCUSSION

Measured Aerodynamic Characteristics

Sonic plateau.- Figure 15(c) indicates how close the analytically designed, experimental 10-percent-thick airfoil 33 came to satisfying the off-design sonic plateau criterion for $M = 0.76$ and $c_n = 0.41$. Irregularities in the plateau

██████████

pressures are due to small surface imperfections which become greatly exaggerated when the flow is right on the verge of sonic velocity. The upper surface plateau extends from approximately 3- to 80-percent chord and comes much nearer to satisfying the sonic-plateau criterion than that for airfoil 31 (ref. 5). The aft pressure recovery gradient is considerably reduced and the trailing-edge pressure recovery more positive, compared with airfoil 31.

The characteristic supercritical pressure distribution at near design conditions (slightly decelerating upper surface velocities terminated by a very weak recompression near the midchord and followed by a near-sonic plateau before entering the final trailing-edge pressure recovery) for an angle of attack near the design value of 0° (fig. 24) occurs at the experimental conditions of $M = 0.77$ and $c_n = 0.71$ (fig. 16(f)). The increment between normal-force coefficients at design and off-design sonic plateau conditions is, therefore, about -0.25 to -0.30 as suggested.

Measured drag characteristics.- Figure 8 indicates that although airfoil 33 had slightly lower drag divergence Mach numbers than airfoil 31 because of earlier onset of shock losses (fig. 9), the drag characteristics of airfoil 33 preceding drag divergence were much improved compared to those of airfoil 31. The improved drag characteristics preceding drag divergence are associated primarily with reduced aft adverse pressure gradients which result in less profile drag. The increased wave losses are associated with the more positive angle of attack required to achieve the same normal-force coefficients as airfoil 31 because of the reduced aft camber and with the influence of the increased curvature over the upper surface mid-chord region (fig. 2(a)). These increased wave losses occur at conditions beyond the design conditions however, and were tolerated in exchange for enhanced performance preceding drag divergence.

~~CONFIDENTIAL~~

The apparent dips in the drag rise curves (fig. 8) should not be interpreted as being due to reductions in shock losses as the design Mach number is approached. At $c_n = 0.7$, for example, there is a dip near $M = 0.77$ but there are no shock losses evident (fig. 9) below $M = 0.77$. In an attempt to simulate full scale Reynolds numbers for the design Mach number, boundary-layer transition trips were fixed at 28-percent chord. At $M = 0.70$, the pressure distribution for $c_n = 0.7$ (fig. 13) was such that laminar flow could not be maintained back to the trip. The higher drag level preceding $M = 0.77$ was, therefore, due to premature boundary-layer transition with greater skin friction drag than there would have been if laminar flow could have been maintained back to the trip at 28-percent chord. Higher drag levels preceding the dip are not associated with increased form drag due to separation effects since no losses in trailing-edge pressure recovery were evident.

Measured pitching-moment characteristics.— The negative or leading edge down pitching moments of airfoil 31 (fig. 7) were reduced by about $\Delta c_m = 0.01$ because of the reduced aft camber incorporated into airfoil 33. At design conditions ($M \approx 0.78$ and $c_n = 0.7$ for airfoil 33 (fig. 7), and $M \approx 0.74$ and $c_n = 0.7$ for the 14-percent-thick airfoil of reference 1) pitching-moment coefficients were practically the same for the family related 10- and 14-percent airfoils.

Comparison With Theory

Correlation was established between experimental and theoretically predicted data using the viscous, analysis program of reference 6. Representative results are presented in figures 22 to 24. Since the viscous analysis program was known to overpredict trailing-edge pressure recovery, Mach number was varied, to achieve the best matches of the theoretical and experimental pressure

[REDACTED]

the transition point. Because of the lengthy run of laminar flow (28-percent) and its effect on the turbulent boundary-layer development on the model, the neglected laminar boundary had to be taken into account. This was accomplished by specifying a transition point forward of 28-percent chord in the theoretical calculations to get better agreement between the theoretical and experimental drag for flow conditions with no supercritical flow (zero wave losses) and where the experimental transition occurred at 28-percent chord. The theoretical calculations shown in figures 22 to 24 were, therefore, calculated for tunnel Reynolds numbers with transition fixed at 24-percent chord.

Composite Drag and Angle-of-Attack Characteristics

Drag.- A combination of experimental and theoretical drag characteristics for airfoil 33 is shown in figure 10 in order to synthesize a realistic drag rise curve for a full-scale Reynolds number. Theoretical drag values (solid line) based on 40 million Reynolds number and boundary-layer transition at 3-percent chord are used for Mach numbers up to the Mach number at which shock losses become evident in the experimental data. Because of the inaccuracy of the theoretical wave losses, experimental drag values (dashed line) are used beyond that point. The experimental and theoretical drag agree at the junction of the solid and dashed lines. The nominal Mach numbers for the experimental data were reduced by the increments indicated by figures 23 and 24 to be required to account for blockage effects.

The gradual increase in drag with Mach number up to drag divergence was associated with increased profile drag due to the effect of Mach number on the induced velocities. As noted in an earlier section there were no measurable shock losses up to the Mach numbers at which drag diverged.

[REDACTED]

Angle of attack.- Theoretical angles of attack required to obtain the desired section lift coefficients are also shown in figure 10 and are near zero at the design or cruise Mach numbers. The difference in angles of attack for $c_n = 0.5$ and 0.7 provide an indication of the lift curve slope in this lift range.

CONCLUDING REMARKS

A 10-percent-thick supercritical airfoil based on an off-design sonic pressure plateau criterion has been developed and experimental aerodynamic characteristics measured. The airfoil had good drag rise characteristics over a wide range of normal-force coefficients with no measurable shock losses up to the Mach numbers at which drag divergence occurred for normal-force coefficients up to 0.7. Comparisons of experimental and theoretical characteristics were made and composite drag rise characteristics were derived for normal-force coefficients of 0.5 and 0.7 and a Reynolds number of 40 million.

[REDACTED]

REFERENCES

1. Harris, Charles D.: Aerodynamic Characteristics of a 14-Percent-Thick NASA Supercritical Airfoil Designed for a Normal-Force Coefficient of 0.7. NASA TM X-72712, 1975.
2. Whitcomb, Richard T.: Review of NASA Supercritical Airfoils. ICAS Paper No. 74-10, Aug. 1974.
3. Harris, Charles D.: Wind-Tunnel Investigation of Effects of Trailing-Edge Geometry on a NASA Supercritical Airfoil Section. NASA TM X-2336, 1971.
4. Harris, Charles D.: Aerodynamic Characteristics of an Improved 10-Percent-Thick NASA Supercritical Airfoil. NASA TM X-2978, 1974.
5. Harris, Charles D.: Transonic Aerodynamic Characteristics of the 10-Percent-Thick NASA Supercritical Airfoil 31. NASA TM X-3203, 1975.
6. Bauer, F.; Garabedian, P.; Korn, D.; and Jameson, A.: Supercritical Wing Sections II. Lecture Notes in Economics and Mathematical Systems, M. Beckmann and H. P. Kunzi, eds., Springer-Verlag, c. 1975.
7. Schaefer, William T., Jr.: Characteristics of Major Active Wind Tunnels at the Langley Research Center. NASA TM X-1130, 1965.
8. Blackwell, James A., Jr.: Preliminary Study of Effects of Reynolds Number And Boundary-Layer Transition Location on Shock-Induced Separation. NASA TN D-5003, 1969.
9. Baals, Donald D.; and Mourhess, Mary J.: Numerical Evaluation of the Wake-Survey Equations for Subsonic Flow Including the Effect of Energy Addition. NACA WR L-5, 1945. (Formerly NACA ARR L5H27.)

- [REDACTED]
10. Davis, Don D., Jr.; and Moore, Dewey: Analytical Study of Blockage- and Lift-Interference Corrections for Slotted Tunnels Obtained by the Substitution of an Equivalent Homogeneous Boundary for the Discrete Slots. NACA RM L53E07b, 1953.

TABLE I.- SECTION COORDINATES

[c = 63.5 cm (25 in.); airfoil 31 has an upper-surface leading-edge radius of 0.0169c and a lower surface leading-edge radius of 0.0176c; airfoil 33 has a leading-edge radius of 0.015c; $\Delta(y/c) = (y/c)_{\text{airfoil 33}} - (y/c)_{\text{airfoil 31}}$]

x/c	(y/c) _u	(y/c) _l	(y/c) _u	(y/c) _l	$\Delta(y/c)_u$	$\Delta(y/c)_l$
	Airfoil 31		Airfoil 33			
0.0	0.0	0.0	0.0	0.0	0.0	0.0
.002	.0080	-.0081	.0075	-.0075	-.0005	.0006
.005	.0120	-.0123	.0116	-.0116	-.0004	.0007
.010	.0159	-.0164	.0156	-.0156	-.0003	.0008
.020	.0209	-.0215	.0206	-.0203	-.0003	.0012
.030	.0244	-.0250	.0240	-.0235	-.0004	.0015
.040	.0271	-.0274	.0267	-.0262	-.0004	.0012
.050	.0294	-.0295	.0289	-.0284	-.0005	.0011
.060	.0313	-.0314	.0308	-.0303	-.0005	.0011
.070	.0329	-.0330	.0325	-.0320	-.0004	.0010
.080	.0344	-.0344	.0340	-.0335	-.0004	.0009
.090	.0357	-.0358	.0354	-.0349	-.0003	.0009
.100	.0369	-.0370	.0367	-.0362	-.0002	.0008
.110	.0380	-.0381	.0379	-.0374	-.0001	.0007
.120	.0391	-.0392	.0389	-.0385	-.0002	.0007
.130	.0401	-.0402	.0399	-.0395	-.0002	.0007
.140	.0410	-.0411	.0408	-.0405	-.0002	.0006
.150	.0418	-.0420	.0417	-.0414	-.0001	.0006
.160	.0426	-.0427	.0425	-.0422	-.0001	.0005
.170	.0433	-.0434	.0432	-.0430	-.0001	.0004
.180	.0440	-.0440	.0439	-.0437	-.0001	.0003
.190	.0446	-.0446	.0446	-.0444	0.0	.0002

TABLE I.- SECTION COORDINATES - Continued

x/c	(y/c) _u	(y/c) _l	(y/c) _u	(y/c) _l	$\Delta(y/c)_u$	$\Delta(y/c)_l$
	Airfoil 31		Airfoil 33			
0.200	0.0452	-0.0452	0.0452	-0.0450	0.0	0.0002
.210	.0457	-.0457	.0457	-.0456	0.0	.0001
.220	.0462	-.0462	.0462	-.0462	0.0	0.0
.230	.0467	-.0467	.0467	-.0467	0.0	0.0
.240	.0471	-.0471	.0472	-.0472	.0001	-.0001
.250	.0475	-.0475	.0476	-.0476	.0001	-.0001
.260	.0478	-.0479	.0480	-.0480	.0002	-.0001
.270	.0481	-.0482	.0483	-.0484	.0002	-.0002
.280	.0484	-.0485	.0486	-.0487	.0002	-.0002
.290	.0487	-.0488	.0489	-.0490	.0002	-.0002
.300	.0489	-.0491	.0491	-.0493	.0002	-.0002
.310	.0491	-.0493	.0493	-.0495	.0002	-.0002
.320	.0493	-.0495	.0495	-.0497	.0002	-.0002
.330	.0495	-.0497	.0496	-.0499	.0001	-.0002
.340	.0497	-.0498	.0497	-.0500	0.0	-.0002
.350	.0498	-.0499	.0498	-.0501	0.0	-.0002
.360	.0499	-.0499	.0499	-.0502	0.0	-.0003
.370	.0500	-.0499	.0500	-.0502	0.0	-.0003
.380	.0500	-.0499	.0500	-.0502	0.0	-.0003
.390	.0500	-.0498	.0500	-.0502	0.0	-.0004
.400	.0500	-.0497	.0500	-.0501	0.0	-.0004
.410	.0500	-.0495	.0499	-.0500	-.0001	-.0005
.420	.0500	-.0493	.0498	-.0499	-.0002	-.0006
.430	.0499	-.0491	.0497	-.0497	-.0002	-.0006
.440	.0498	-.0488	.0496	-.0495	-.0002	-.0007
.450	.0497	-.0485	.0495	-.0492	-.0002	-.0007
.460	.0495	-.0482	.0493	-.0488	-.0002	-.0006
.470	.0493	-.0478	.0491	-.0484	-.0002	-.0006

TABLE I.- SECTION COORDINATES - Continued

x/c	(y/c) _u	(y/c) _l	(y/c) _u	(y/c) _l	$\Delta(y/c)_u$	$\Delta(y/c)_l$
	Airfoil 31		Airfoil 33			
0.480	0.0491	-0.0474	0.0489	-0.0480	-0.0002	-0.0006
.490	.0489	-.0470	.0487	-.0475	-.0002	-.0005
.500	.0487	-.0465	.0484	-.0470	-.0003	-.0005
.510	.0485	-.0459	.0481	-.0464	-.0004	-.0005
.520	.0482	-.0453	.0478	-.0457	-.0004	-.0004
.530	.0479	-.0446	.0475	-.0450	-.0004	-.0004
.540	.0476	-.0439	.0472	-.0442	-.0004	-.0003
.550	.0473	-.0431	.0468	-.0434	-.0005	-.0003
.560	.0469	-.0422	.0464	-.0425	-.0005	-.0003
.570	.0465	-.0413	.0460	-.0415	-.0005	-.0002
.580	.0461	-.0403	.0456	-.0405	-.0005	-.0002
.590	.0457	-.0392	.0451	-.0394	-.0006	-.0002
.600	.0453	-.0381	.0446	-.0382	-.0007	-.0001
.610	.0448	-.0369	.0441	-.0370	-.0007	-.0001
.620	.0443	-.0356	.0436	-.0357	-.0007	-.0001
.630	.0438	-.0342	.0430	-.0343	-.0008	-.0001
.640	.0433	-.0327	.0424	-.0329	-.0009	-.0002
.650	.0428	-.0311	.0418	-.0315	-.0010	-.0004
.660	.0422	-.0294	.0412	-.0300	-.0010	-.0006
.670	.0416	-.0277	.0405	-.0285	-.0011	-.0003
.680	.0409	-.0260	.0398	-.0270	-.0011	-.0010
.690	.0402	-.0242	.0391	-.0255	-.0011	-.0013
.700	.0395	-.0224	.0383	-.0239	-.0012	-.0015
.710	.0387	-.0206	.0375	-.0223	-.0012	-.0017
.720	.0379	-.0188	.0367	-.0207	-.0012	-.0019
.730	.0371	-.0171	.0358	-.0191	-.0013	-.0020
.740	.0363	-.0154	.0349	-.0175	-.0014	-.0021
.750	.0354	-.0137	.0340	-.0159	-.0014	-.0022

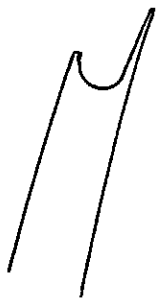
TABLE I.- SECTION COORDINATES - Concluded

x/c	(y/c) _u	(y/c) _l	(y/c) _u	(y/c) _l	$\Delta(y/c)_u$	$\Delta(y/c)_l$
	Airfoil 31		Airfoil 33			
0.760	0.0345	-0.0121	0.0330	-0.0143	-0.0015	-0.0022
.770	.0336	-.0105	.0320	-.0128	-.0016	-.0023
.780	.0326	-.0089	.0309	-.0113	-.0017	-.0024
.790	.0315	-.0074	.0298	-.0099	-.0017	-.0025
.800	.0304	-.0060	.0287	-.0085	-.0017	-.0025
.810	.0292	-.0047	.0275	-.0072	-.0017	-.0025
.820	.0280	-.0035	.0262	-.0060	-.0018	-.0025
.830	.0267	-.0024	.0248	-.0049	-.0019	-.0025
.840	.0254	-.0014	.0234	-.0038	-.0020	-.0024
.850	.0240	-.0006	.0219	-.0029	-.0021	-.0023
.860	.0225	0.0	.0204	-.0022	-.0021	-.0022
.870	.0210	.0005	.0188	-.0017	-.0022	-.0022
.880	.0194	.0007	.0171	-.0014	-.0023	-.0021
.890	.0176	.0007	.0153	-.0013	-.0023	-.0020
.900	.0157	.0005	.0135	-.0013	-.0022	-.0018
.910	.0137	.0001	.0116	-.0016	-.0021	-.0017
.920	.0116	-.0005	.0096	-.0021	-.0020	-.0016
.930	.0093	-.0014	.0075	-.0028	-.0018	-.0014
.940	.0069	-.0026	.0054	-.0039	-.0015	-.0013
.950	.0044	-.0041	.0032	-.0053	-.0012	-.0012
.960	.0019	-.0059	.0008	-.0069	-.0011	-.0010
.970	-.0008	-.0080	-.0017	-.0088	-.0009	-.0008
.980	-.0037	-.0105	-.0044	-.0110	-.0007	-.0005
.990	-.0068	-.0133	-.0074	-.0135	-.0006	-.0002
1.000	---	-.0164	---	-.0163	---	.0001

ORIGINAL QUALITY
OF PHOTO COPY

[REDACTED]

— Airfoil 31
- - - Airfoil 33



Sketch of T.E. at expanded scale

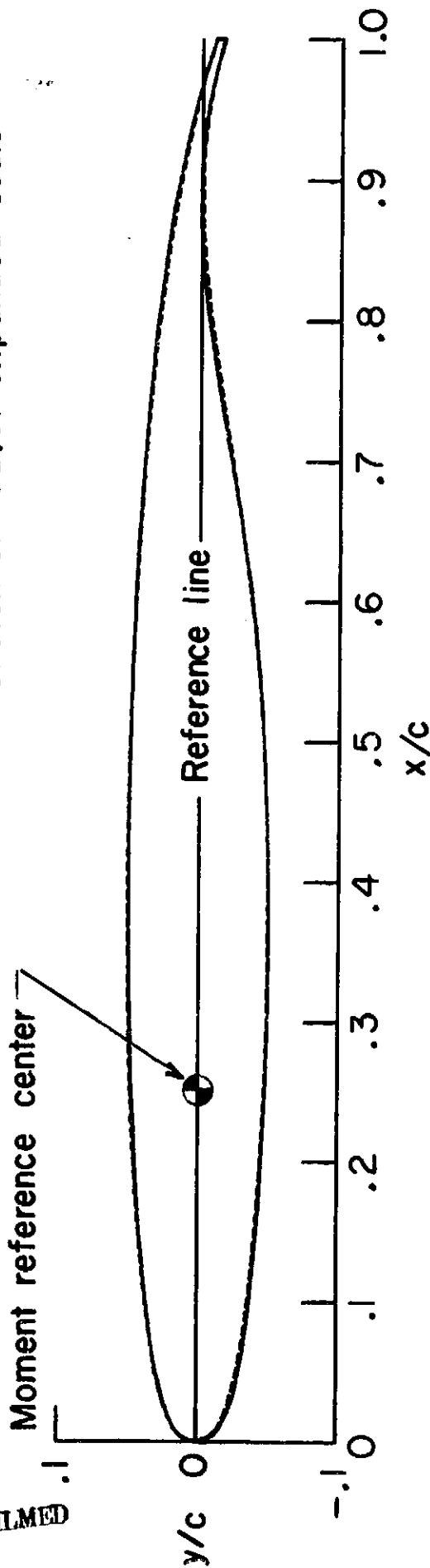
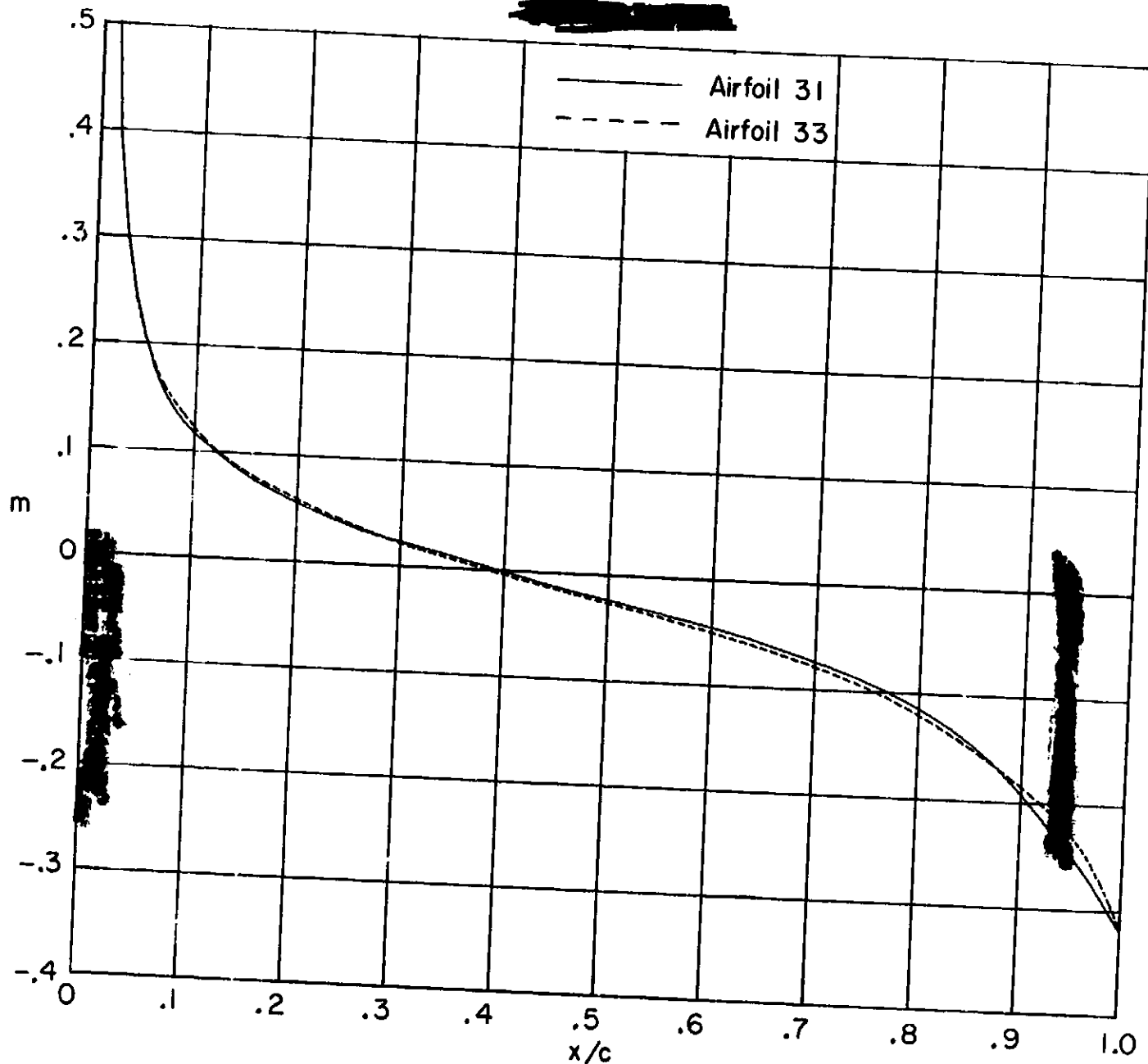


Figure 1. - Sketches of 10-percent-thick supercritical airfoils 31 and 33.

[REDACTED]

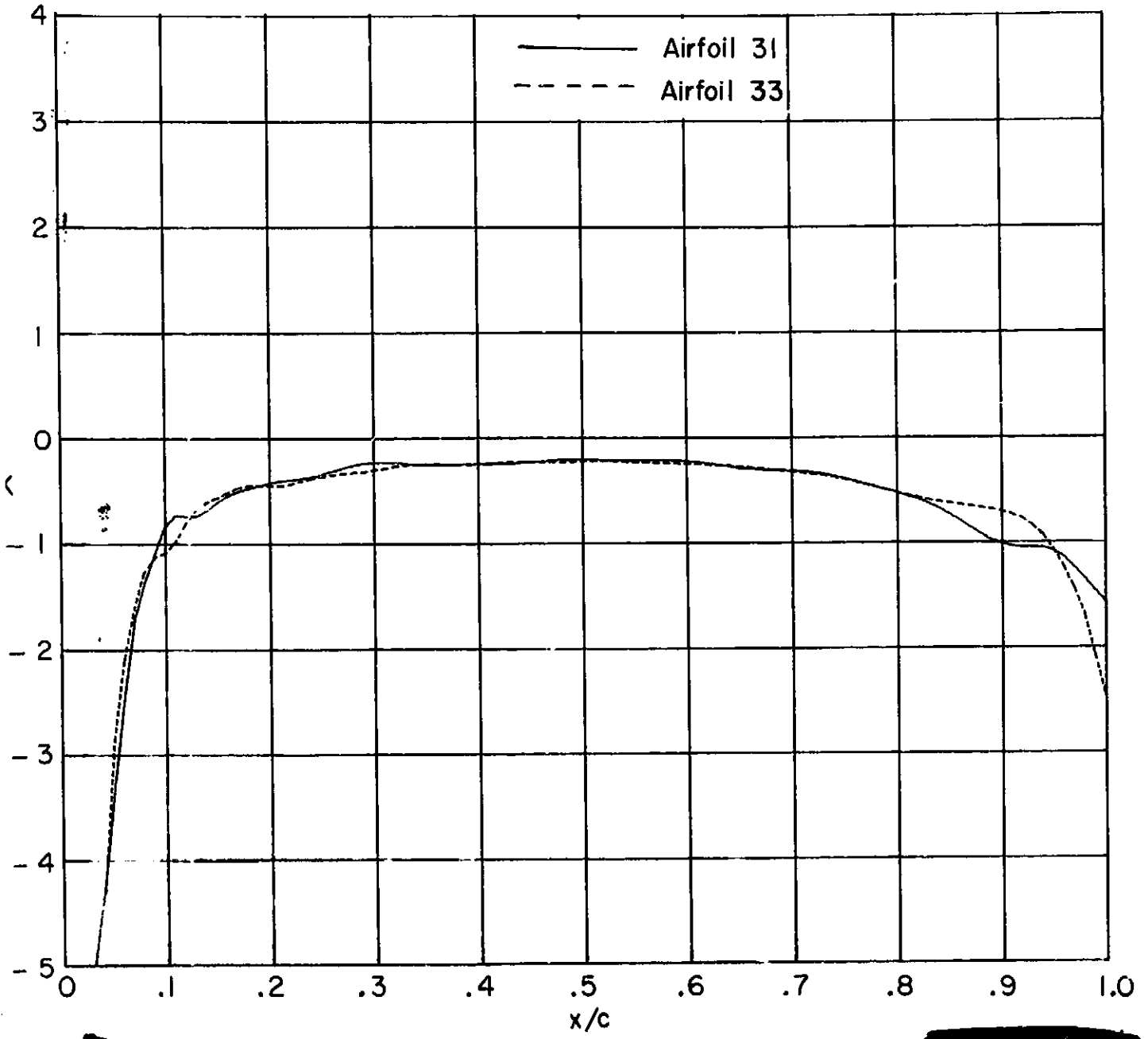
PRECEDING PAGE BLANK NOT FILMED



(a) Upper surface.

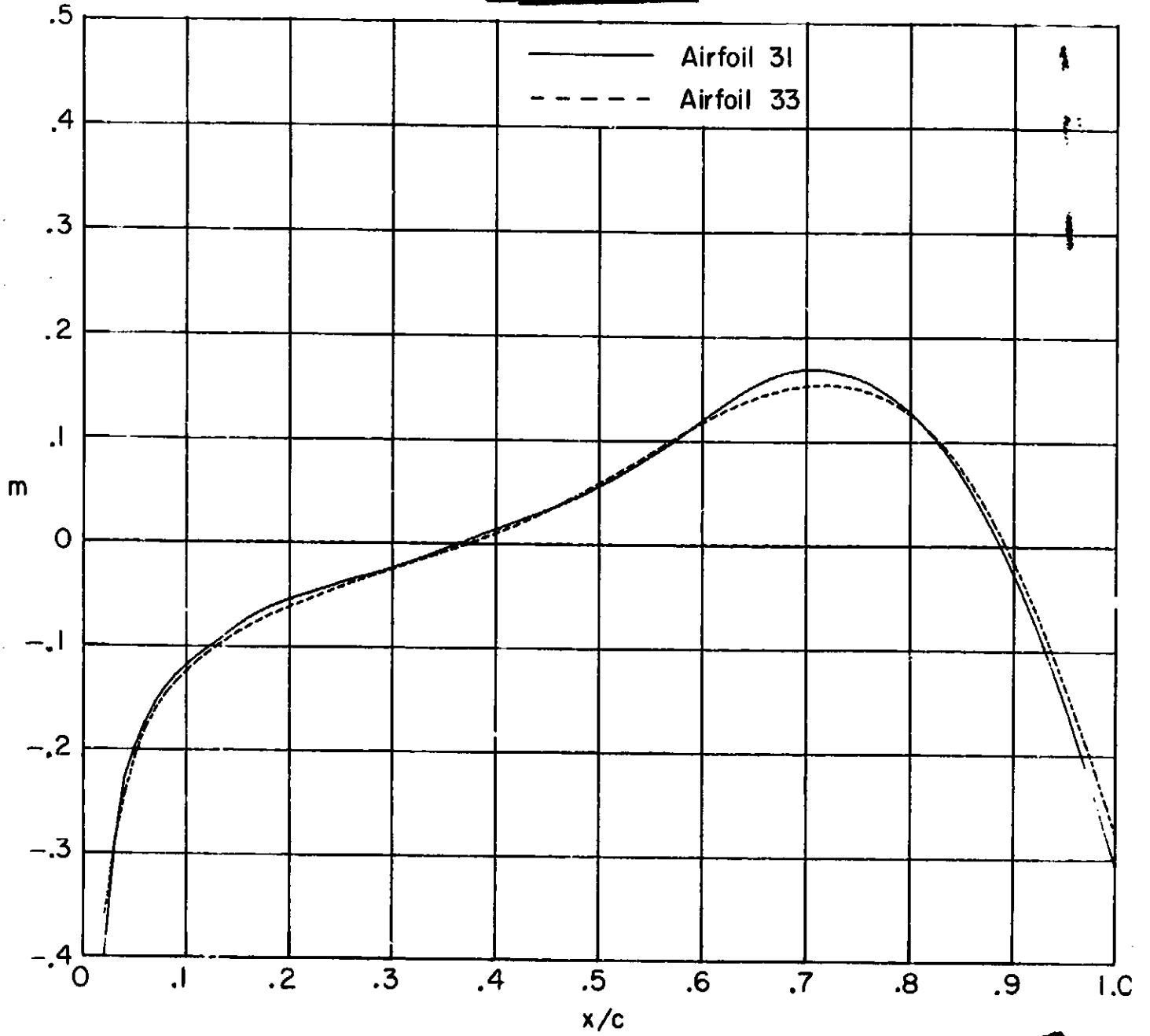
Figure 2. - Chordwise distribution of airfoil surface slopes and curvature.

ORIGINAL PAGE IS
OF POOR QUALITY



(a) Upper surface. Concluded.

Figure 2. - Continued.

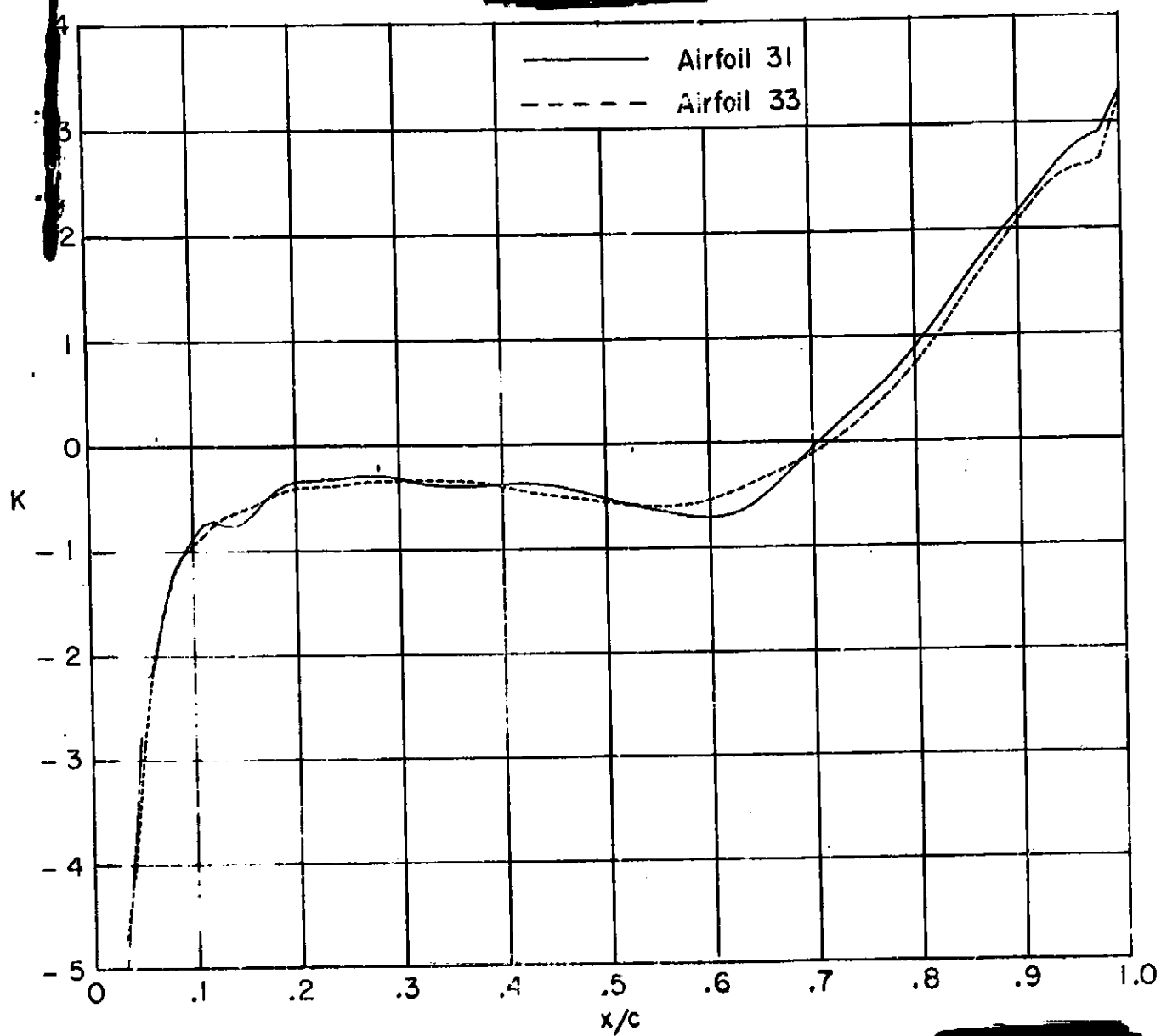


(b) Lower surface.

Figure 2. - Continued.

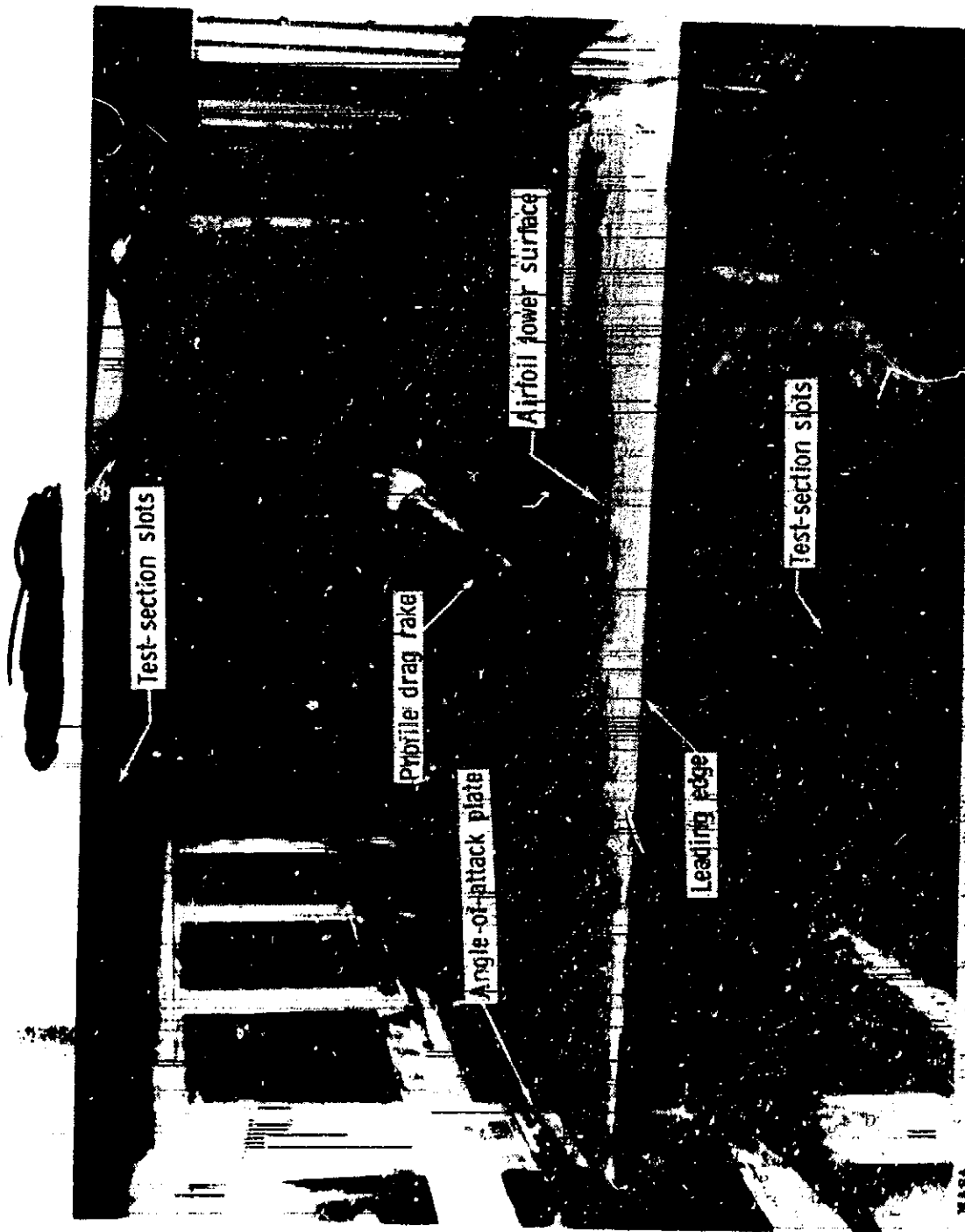
AL

ORIGINAL PAGE IS
OF POOR QUALITY



(b) Lower surface. Concluded.

Figure 2. - Concluded.



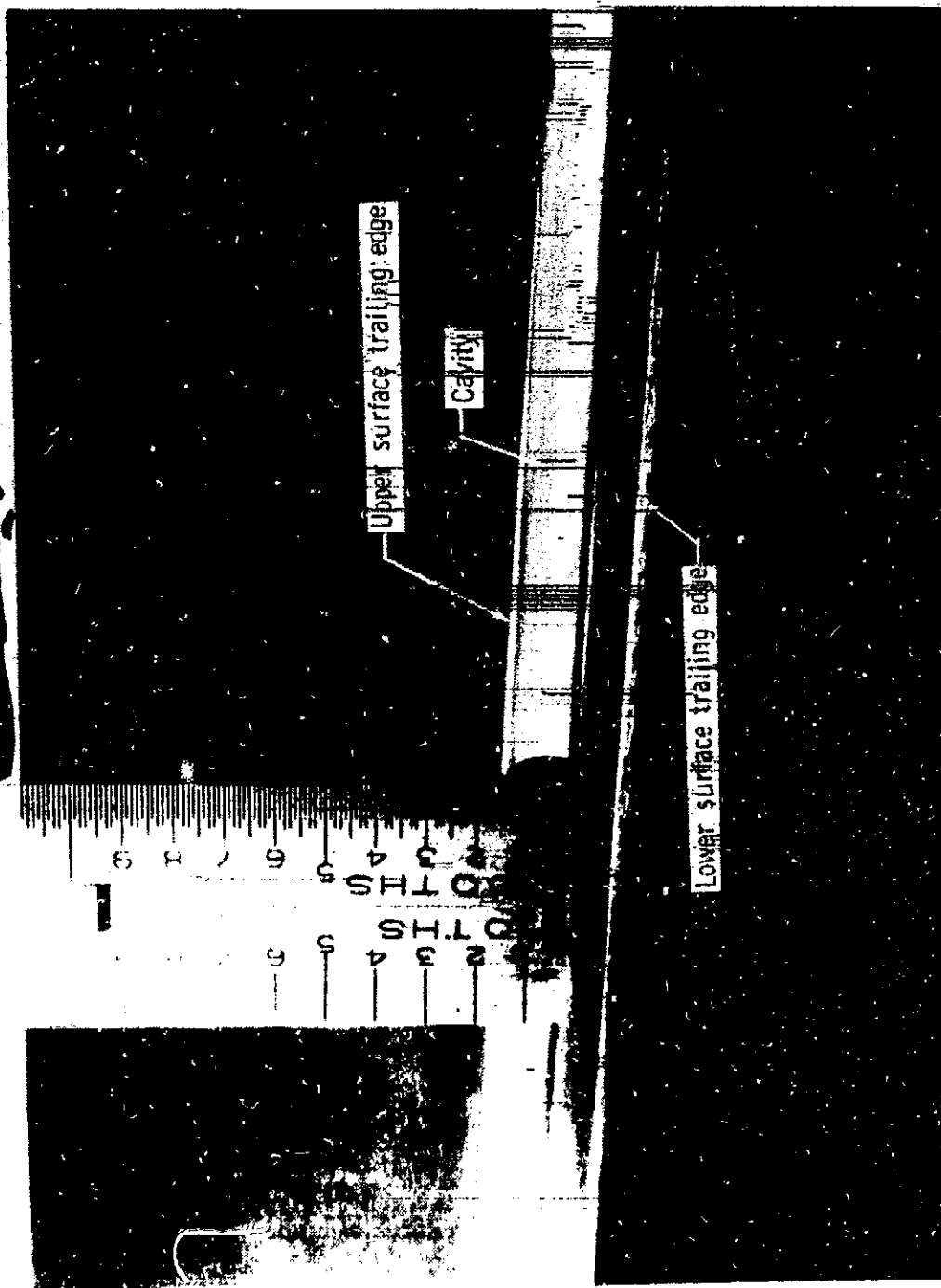
NASA
L-73-1225-2

(a) Supercritical airfoil and profile drag rake mounted in tunnel.

Figure 3.- Photographs of typical airfoil model in tunnel.

~~CONFIDENTIAL~~

ORIGINAL PAGE IS
OF POOR QUALITY



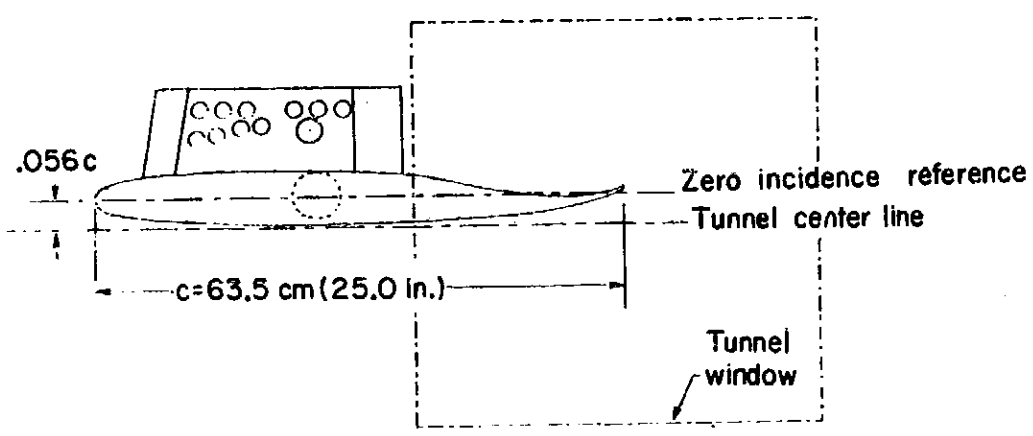
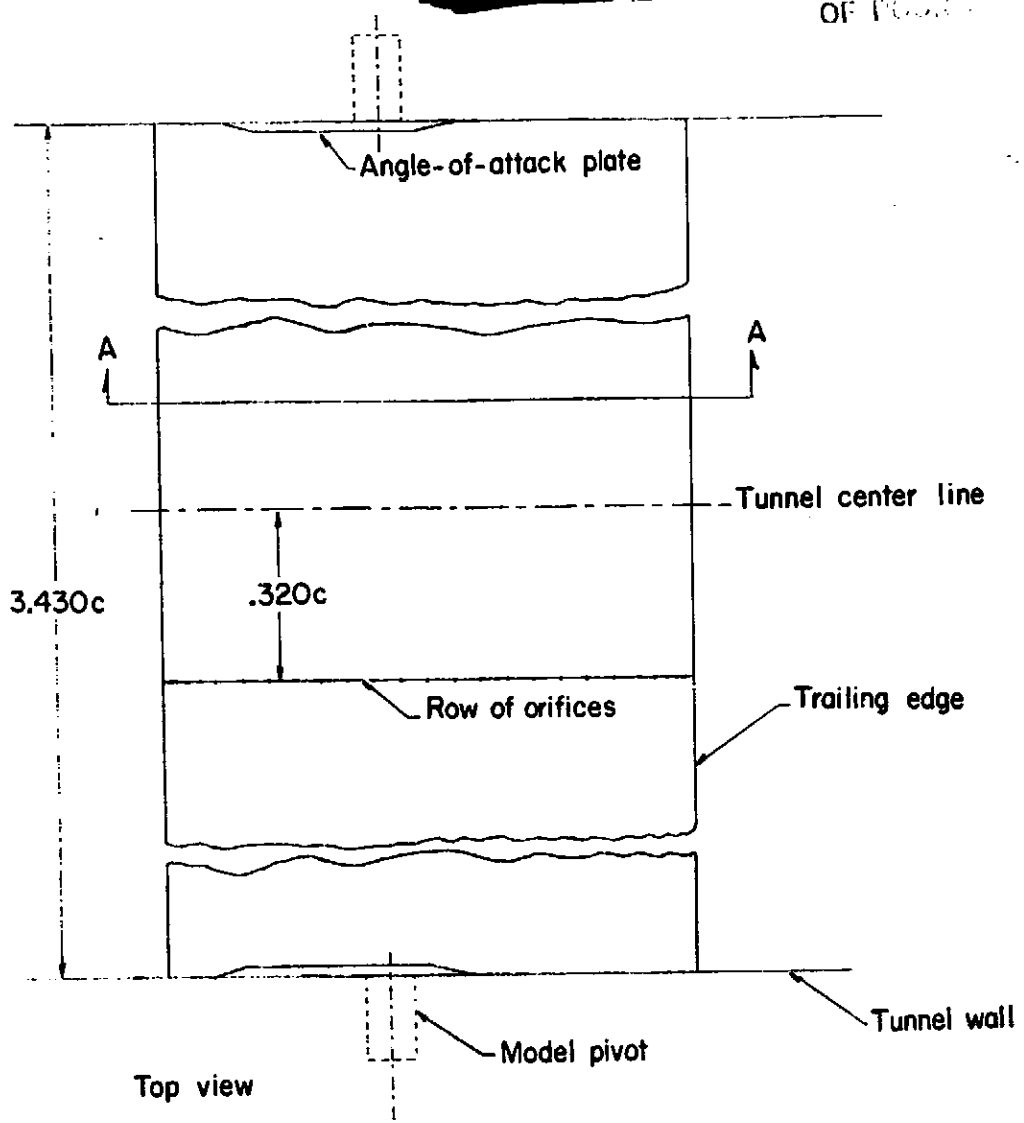
(b) Trailing-edge cavity.

Figure 3. - Concluded.

ORIGINAL PAGE IS
OF POOR QUALITY

10070

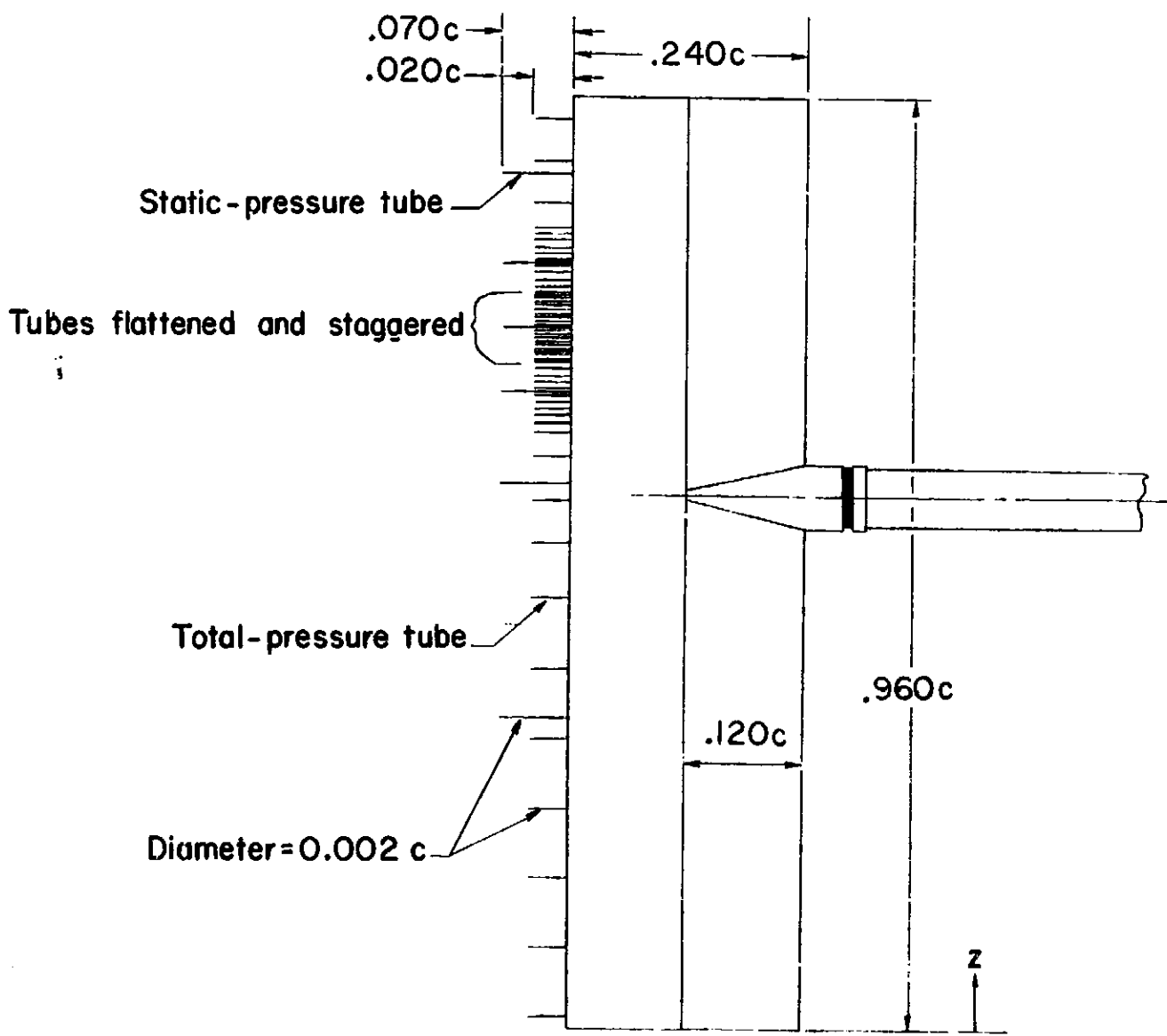
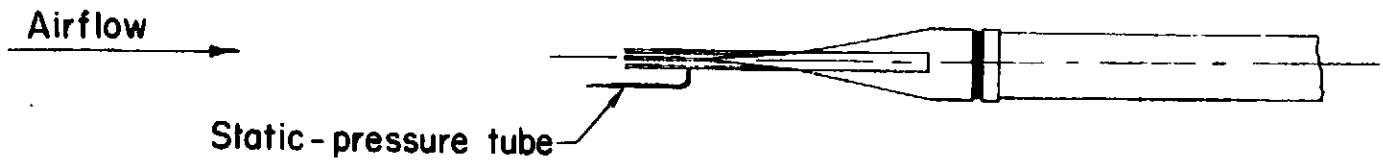
ORIGINAL FILED
OF POST OFFICE



End view, section A-A

(a) Airfoil mounted in tunnel.

Figure 4. - Apparatus dimensions in terms of chord. $c = 63.5 \text{ cm (25.0 in.)}$.



(b) Profile drag rake.

Figure 4. - Concluded.

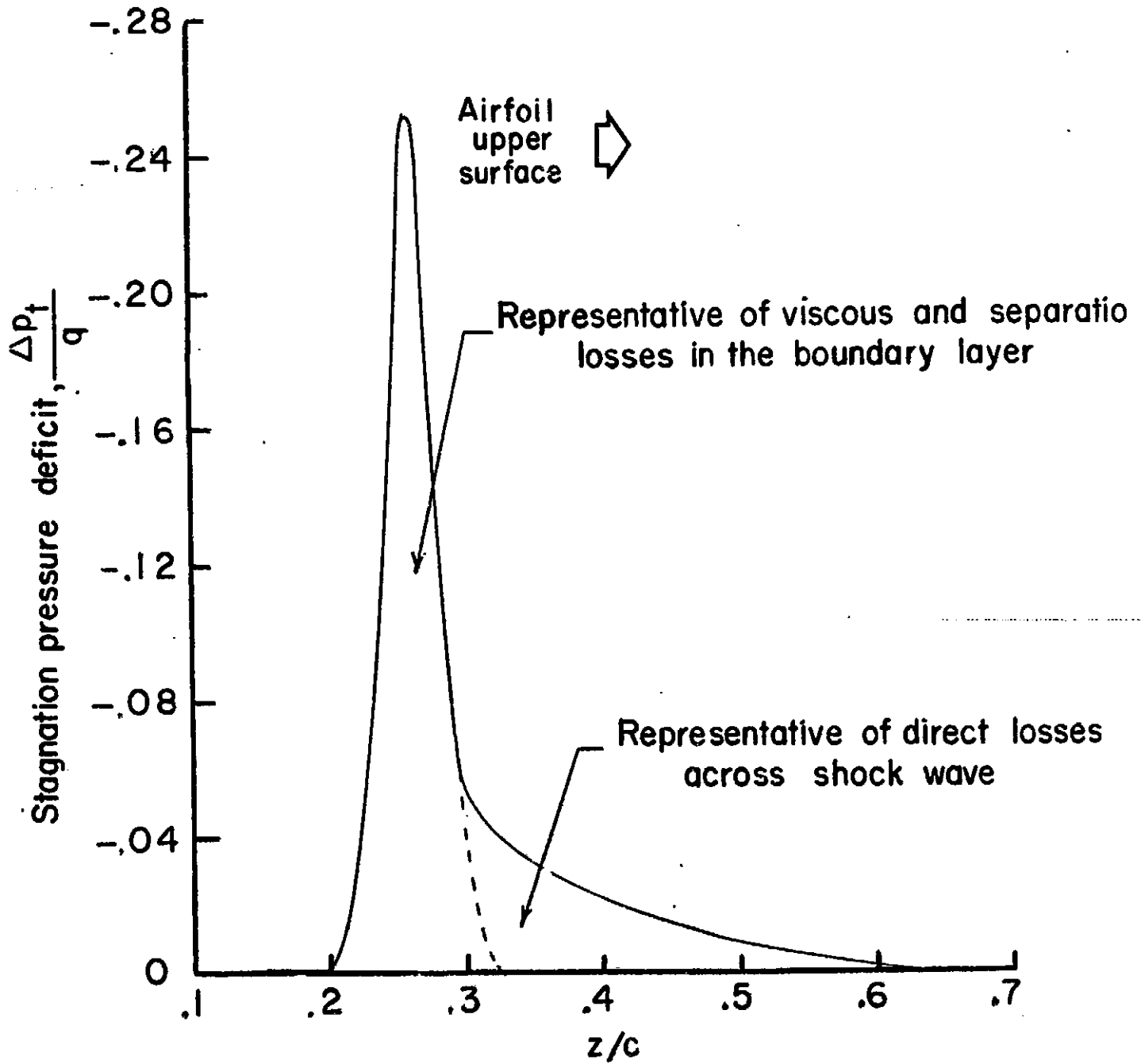


Figure 5. - Schematic of wake profiles.

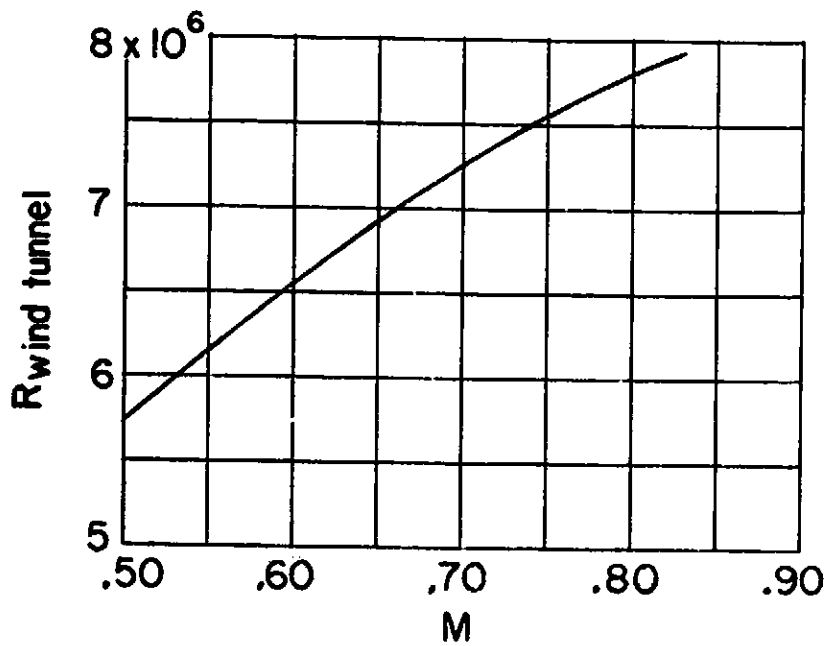
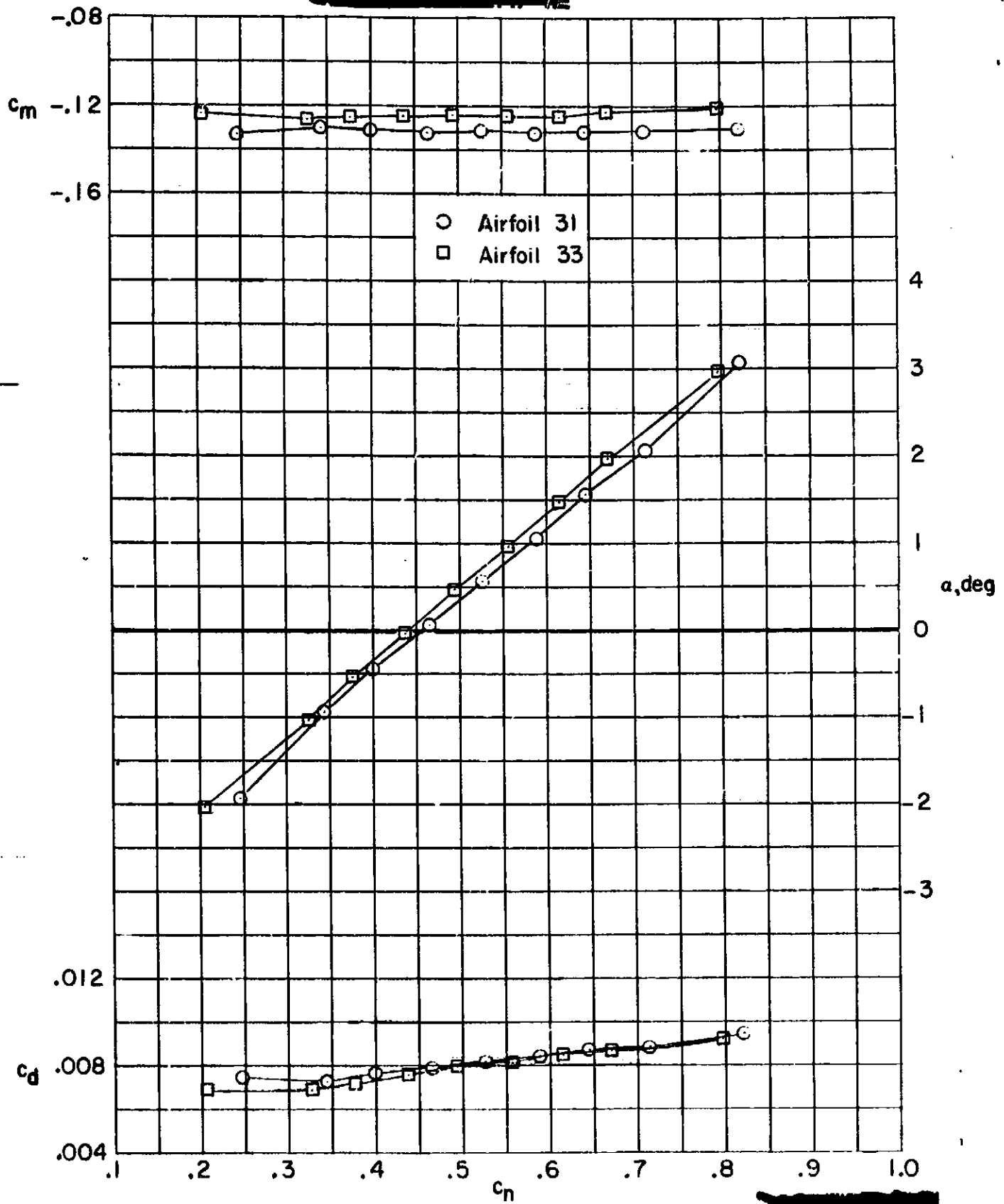


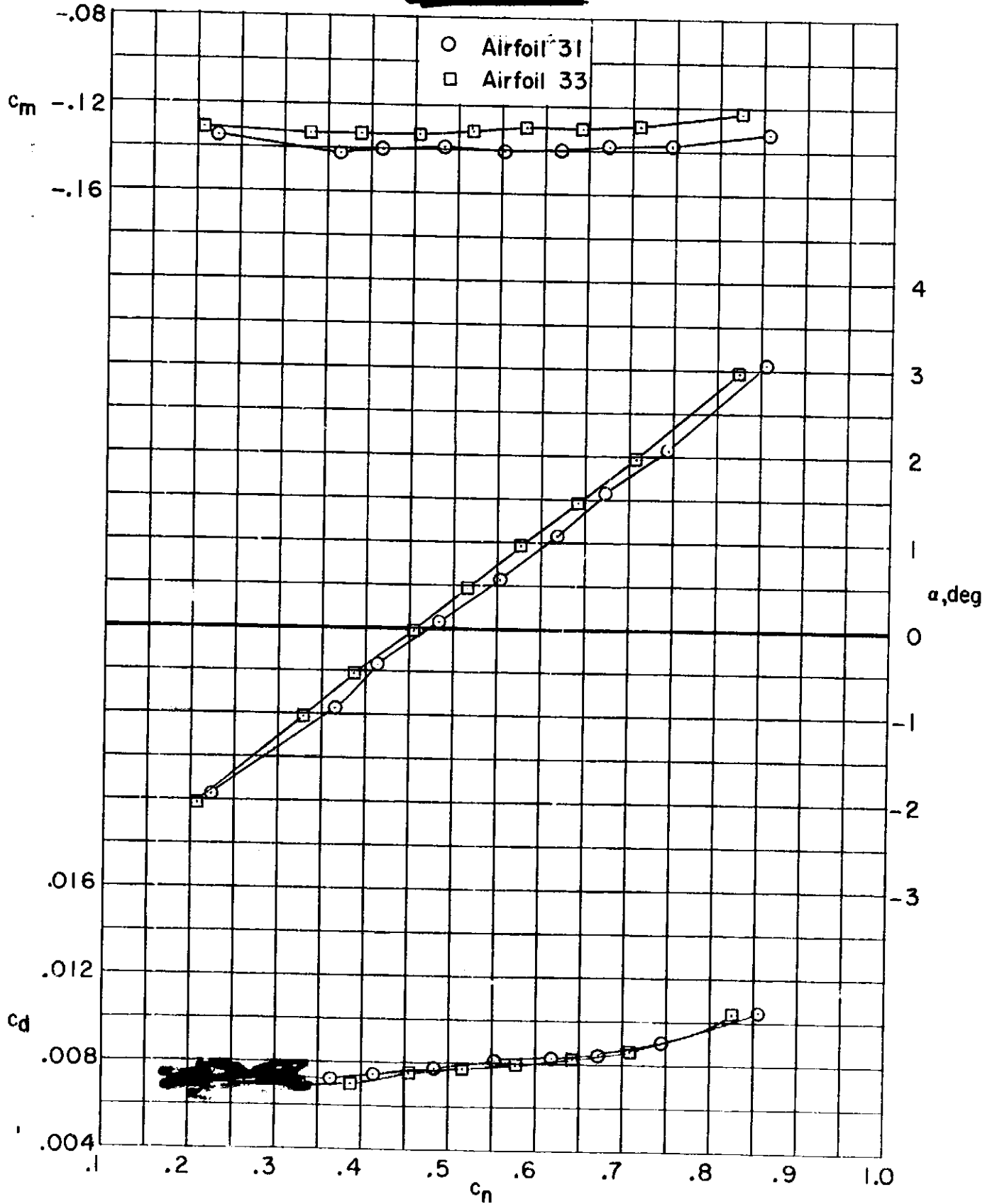
Figure 6. - Variation with Mach number of test wind-tunnel Reynolds number.

CONFIDENTIAL



(a) $M = 0.50$.

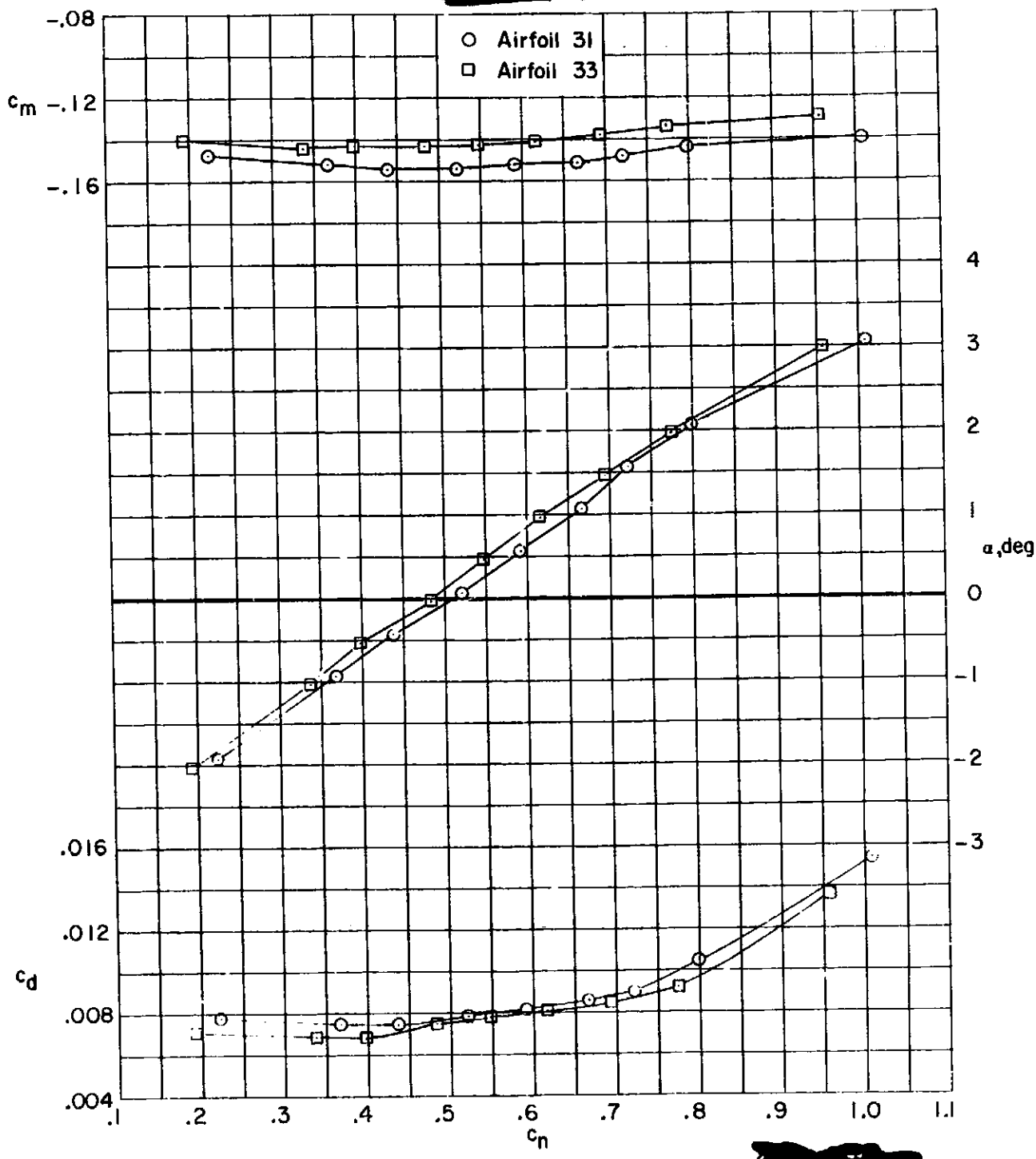
Figure 7. - Comparison of force and moment characteristics of 10-percent-thick supercritical airfoils 31 and 33.



(b) $M = 0.60$.

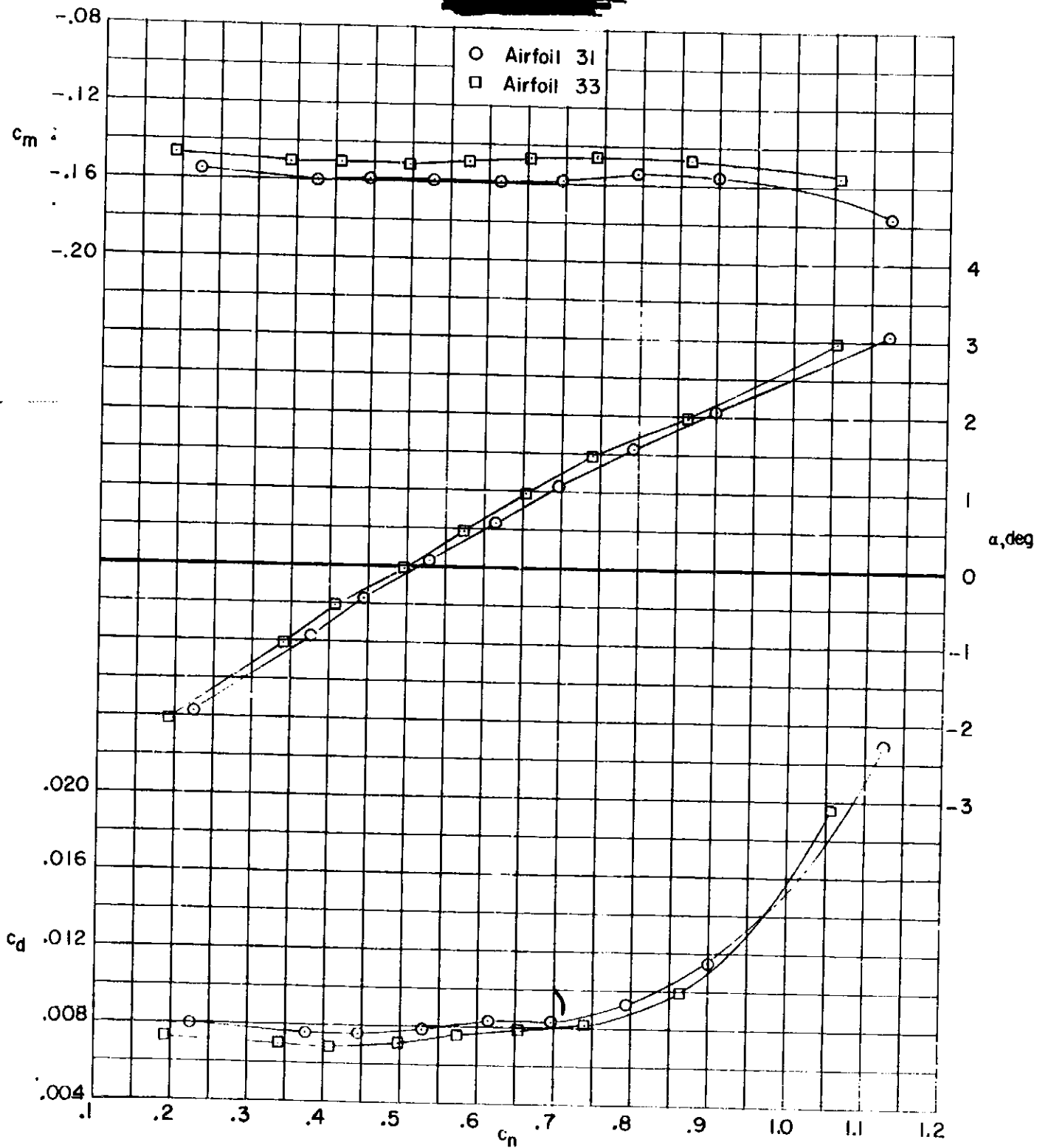
Figure 7. - Continued.

ORIGINAL OF 19



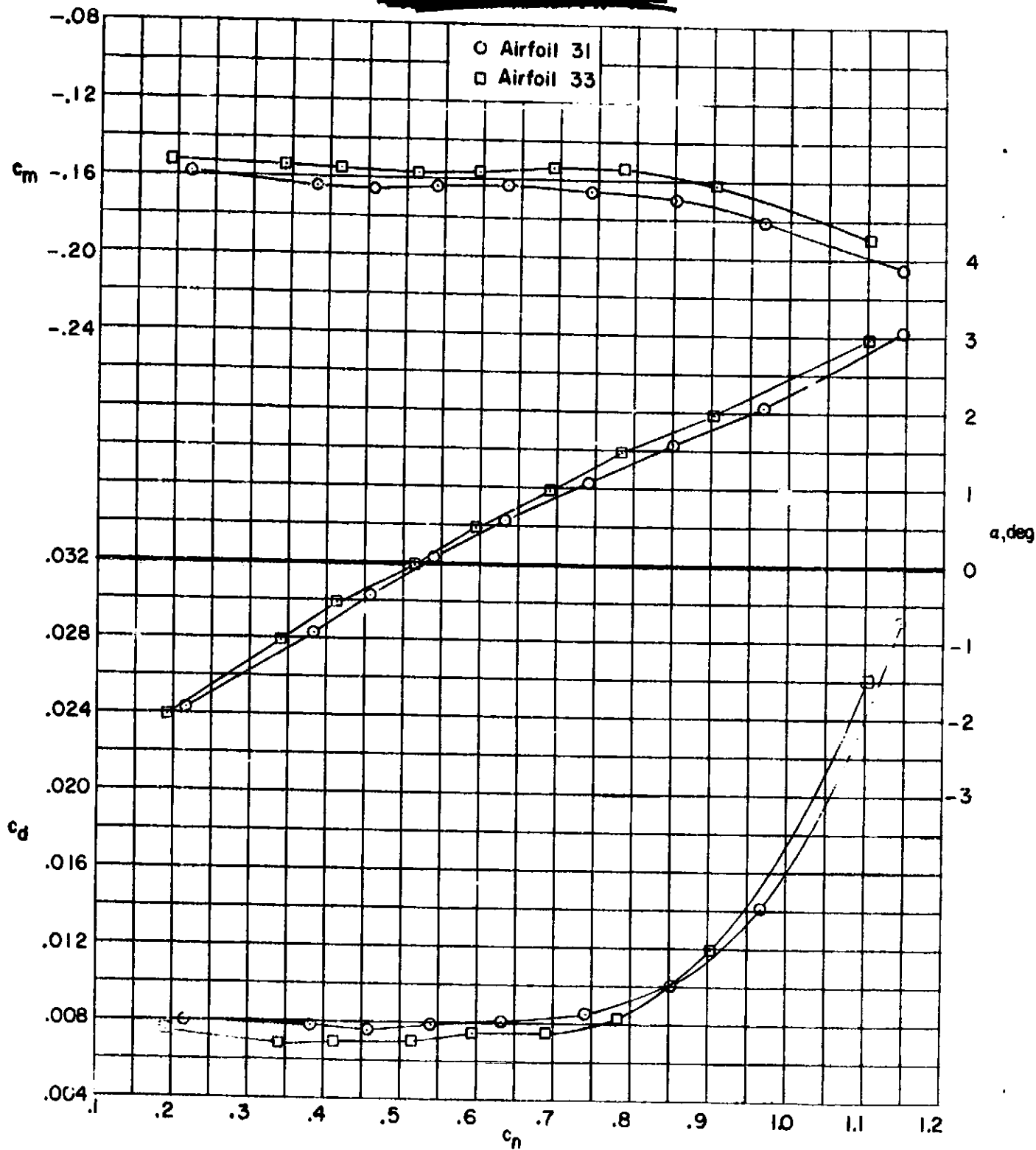
(c) $M = 0.70$.

Figure 7. - Continued.



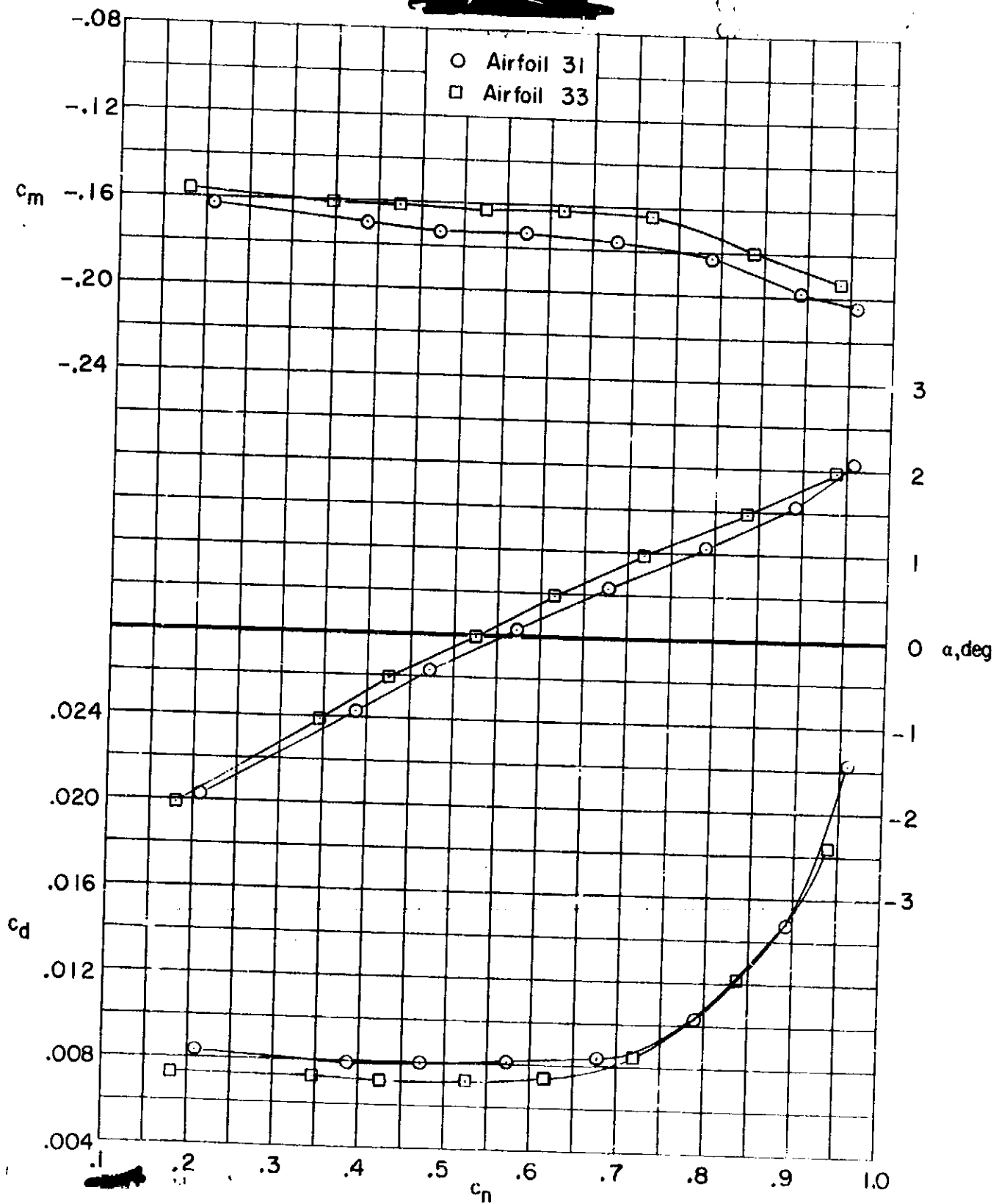
(d) $M = 0.74$.

Figure 7. - Continued.



(e) $M = 0.76$.

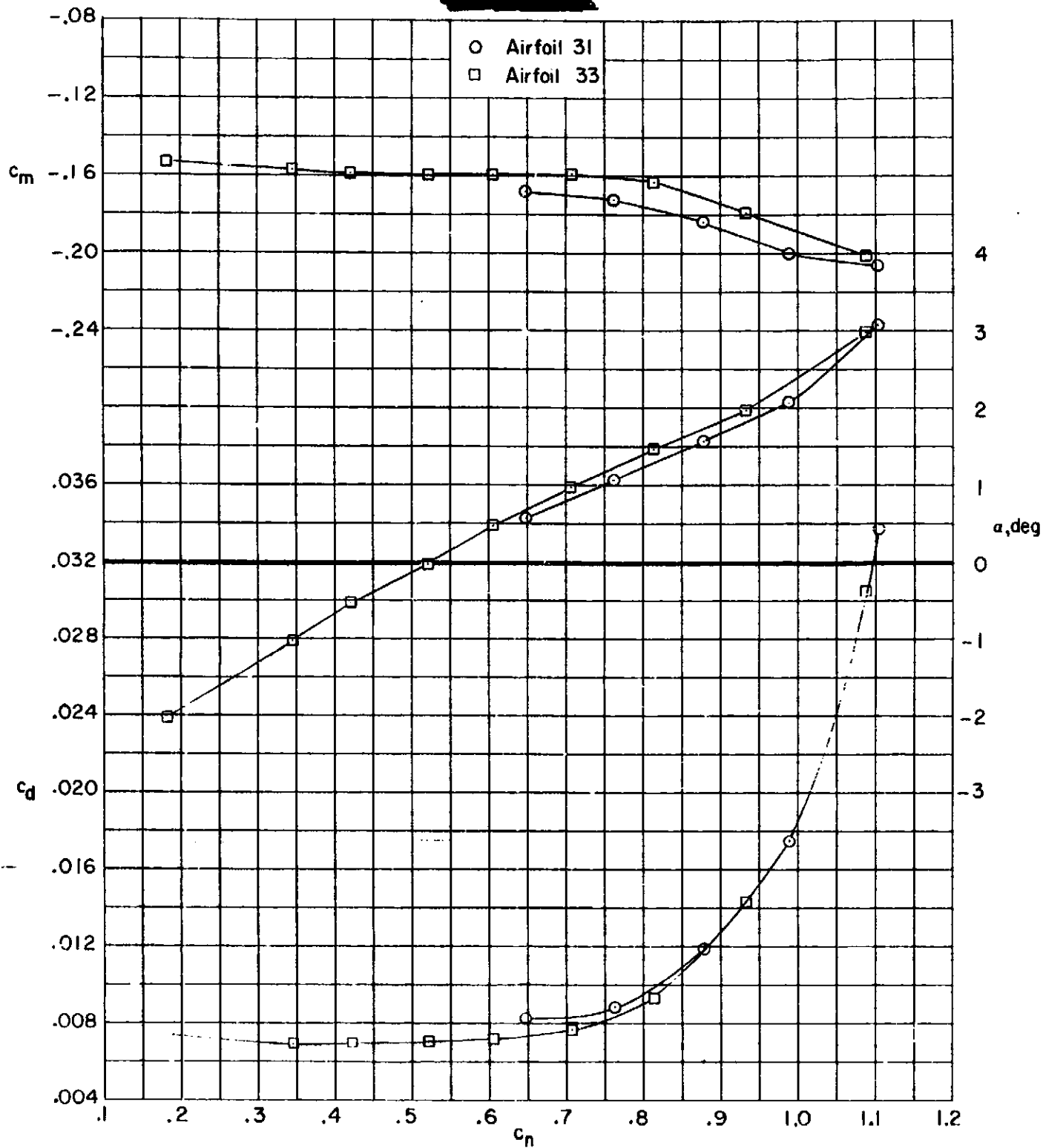
Figure 7. - Continued.



(g) $M = 0.78$.

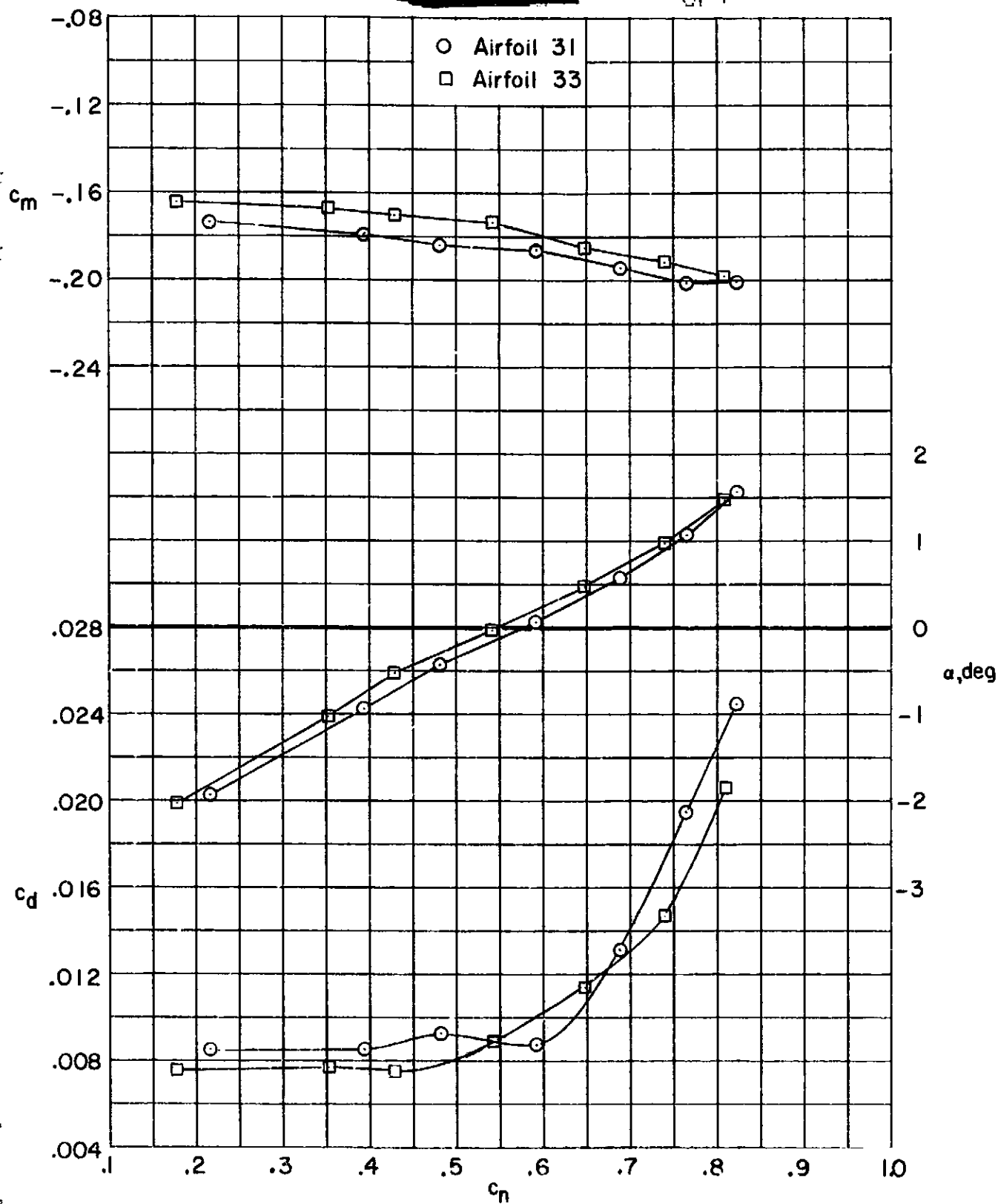
Figure 7. - Continued.

ORNL
CONF



(I) $M = 0.77$.

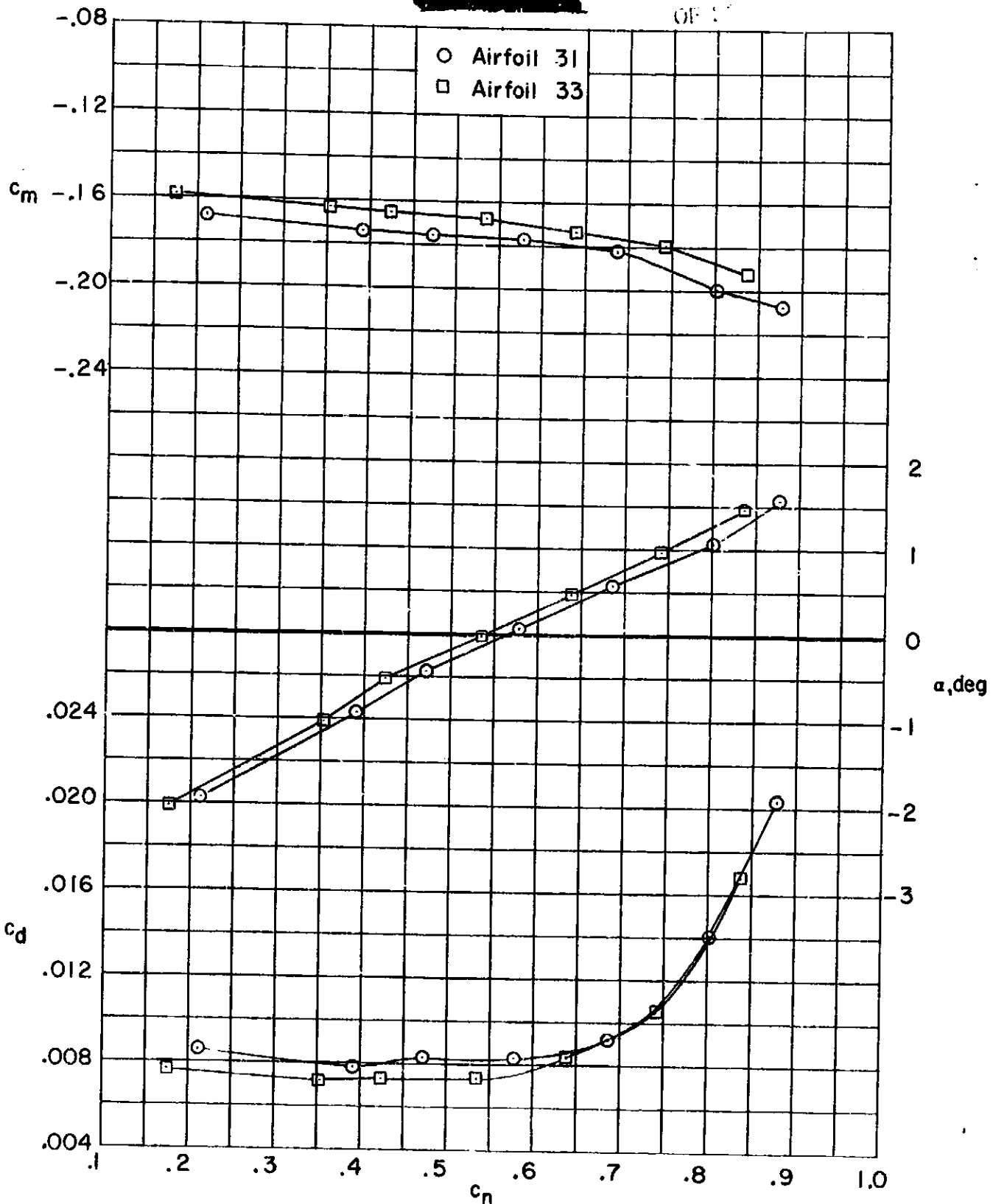
Figure 7. - Continued.



(I) $M = 0.80$.

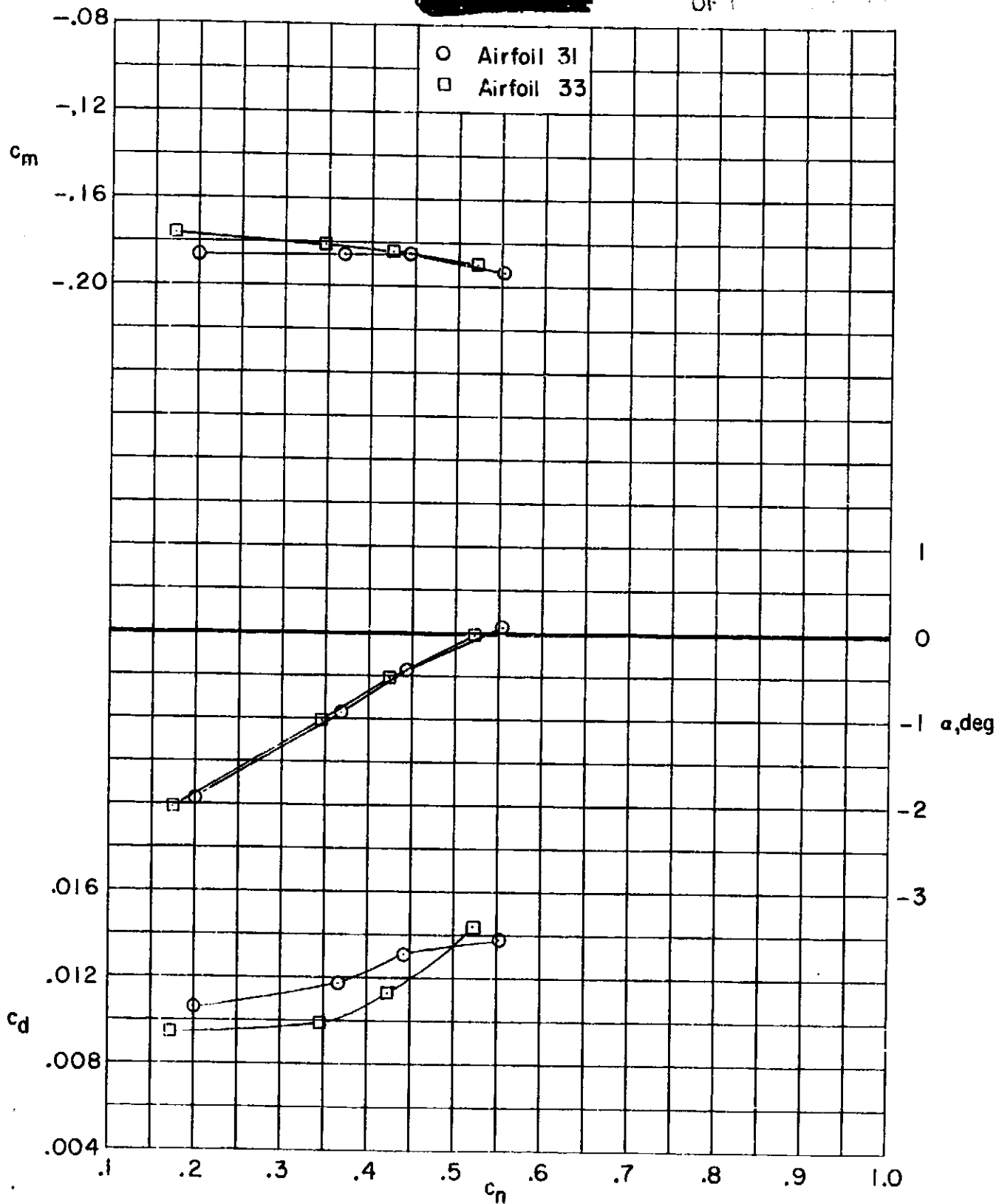
Figure 7. - Continued.

ORIGINAL
OF 17



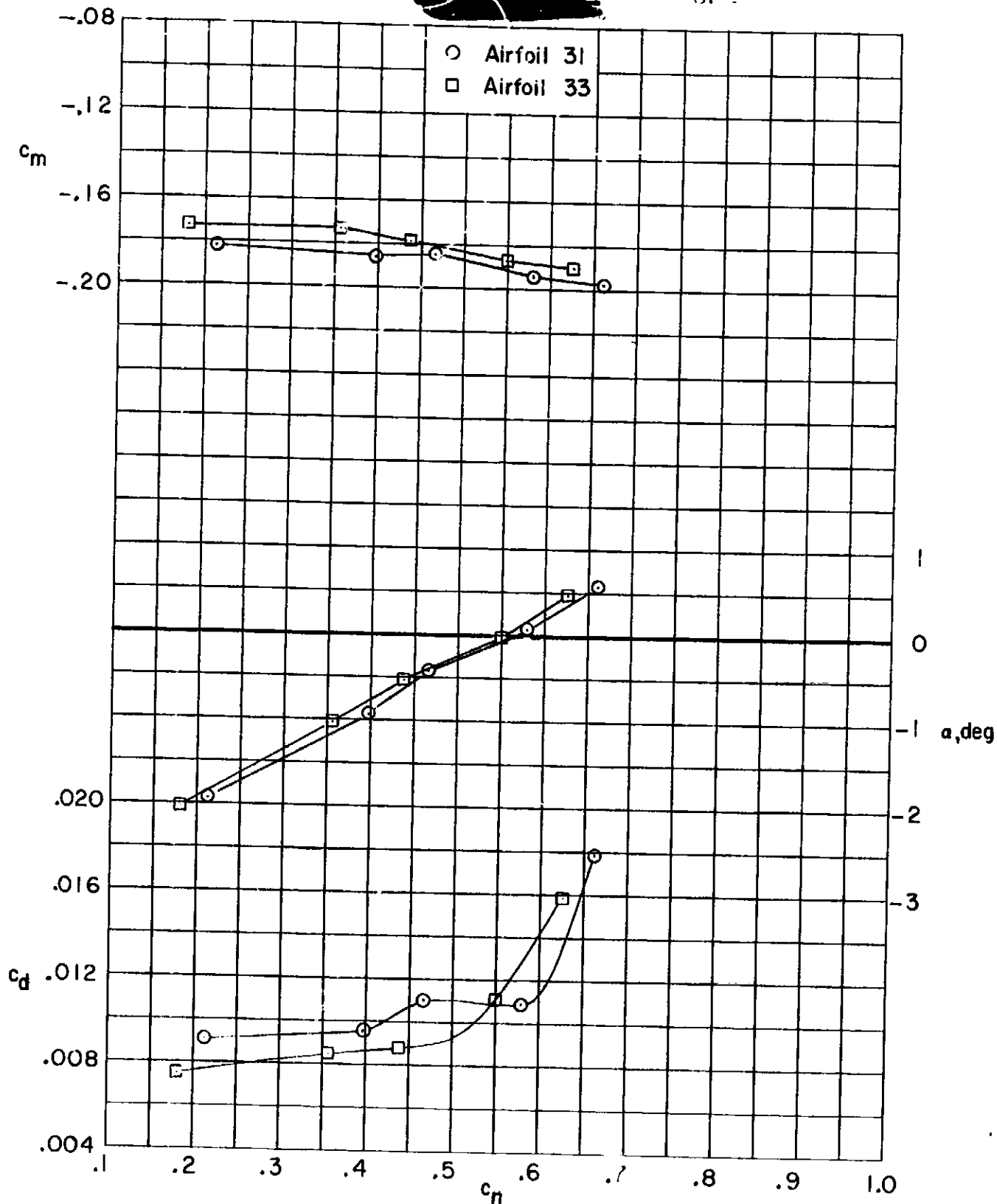
(h) $M = 0.79$.

Figure 7. - Continued.



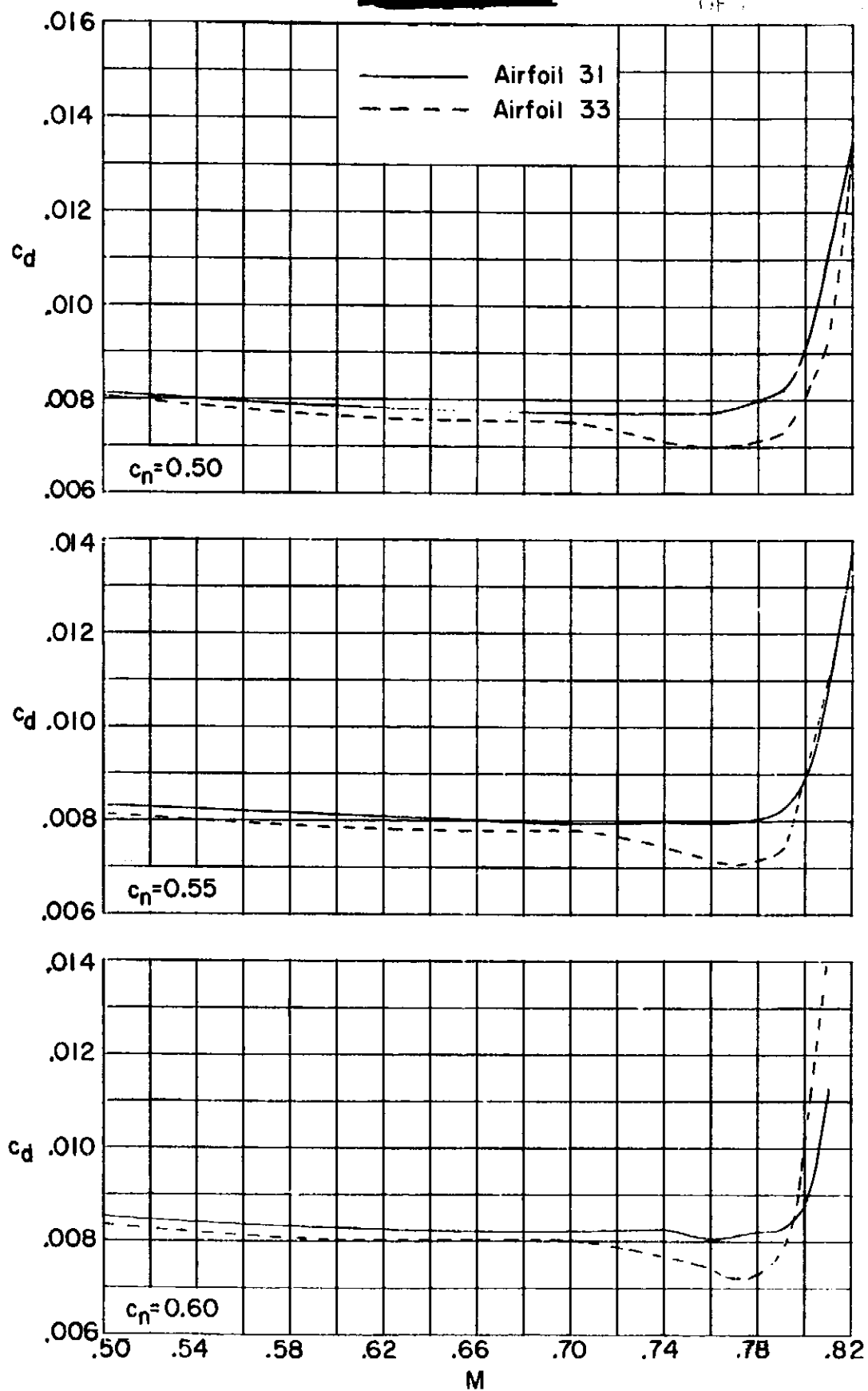
(k) $M = 0.82$.

Figure 7. - Concluded.



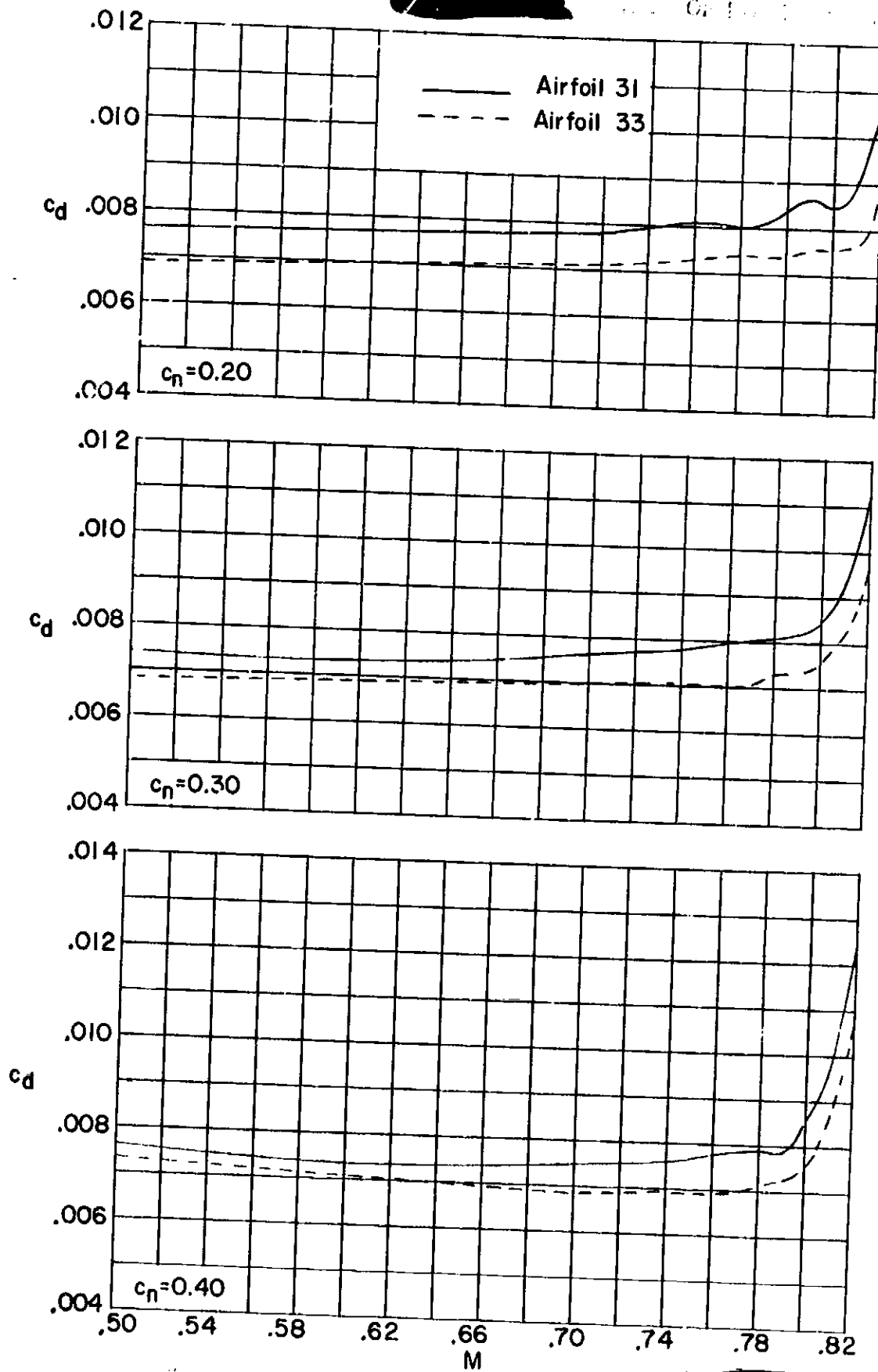
(j) $M = 0.81$.

Figure 7. - Continued.



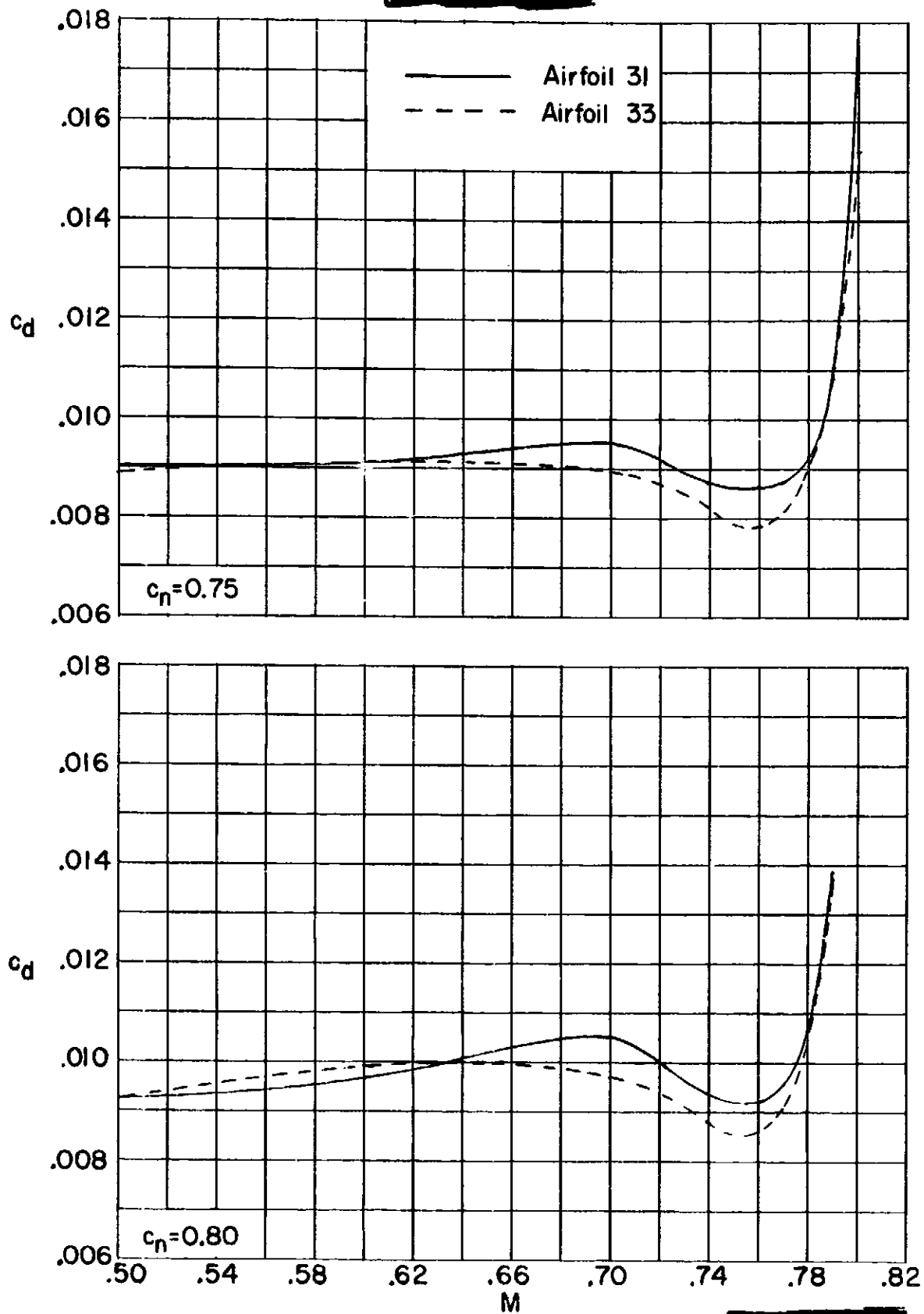
(b) $c_n = 0.50, 0.55$ and 0.60 .

Figure 8. - Continued.



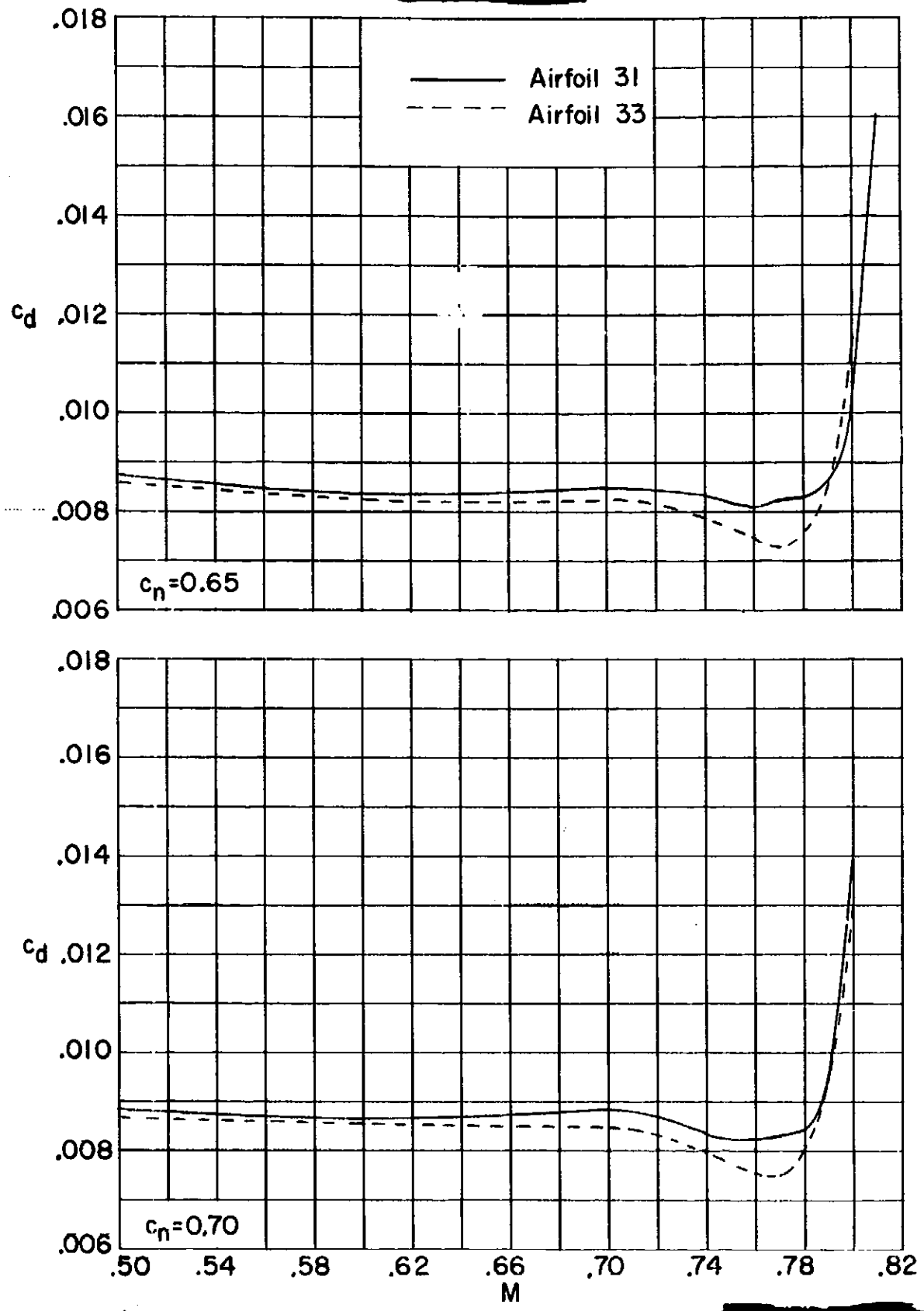
(a) $c_n = 0.20, 0.30$ and 0.40 .

Figure 8. - Variation of measured section drag coefficient with Mach number of 10-percent-thick supercritical airfoils 31 and 33.



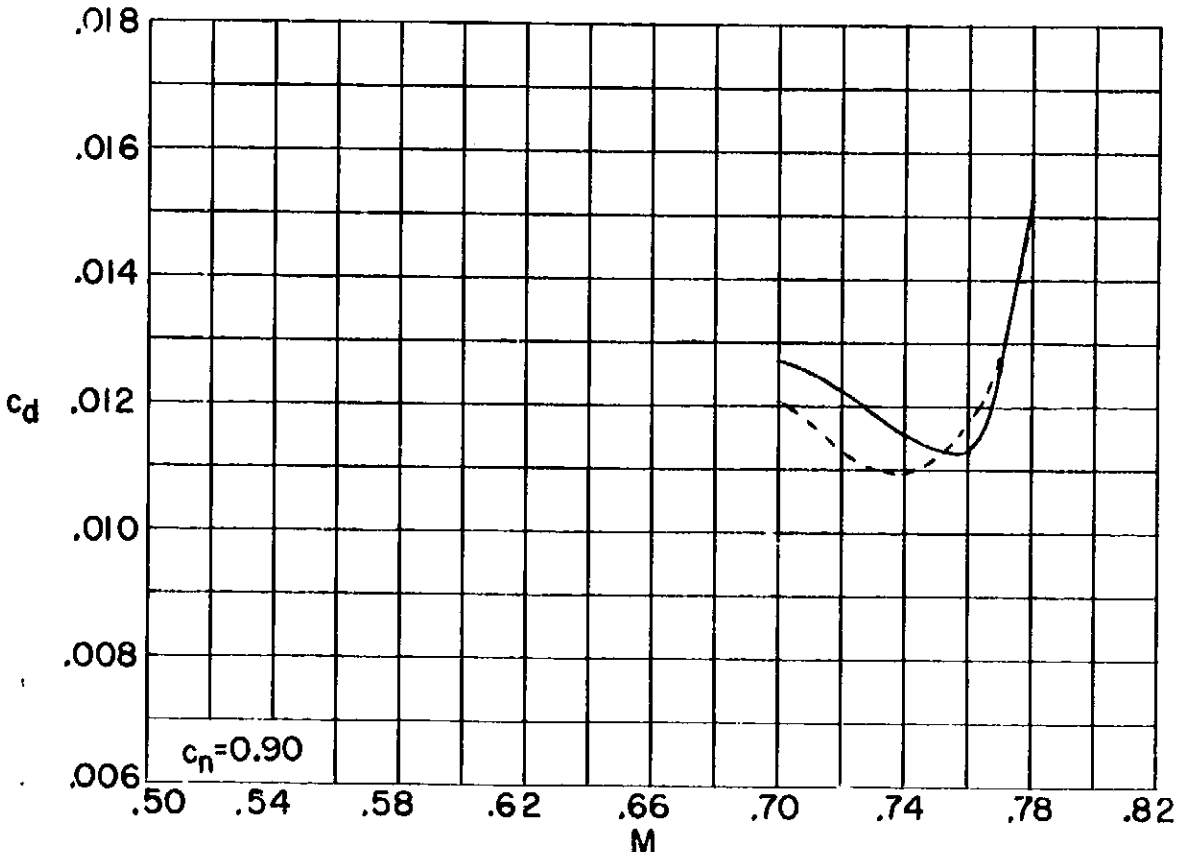
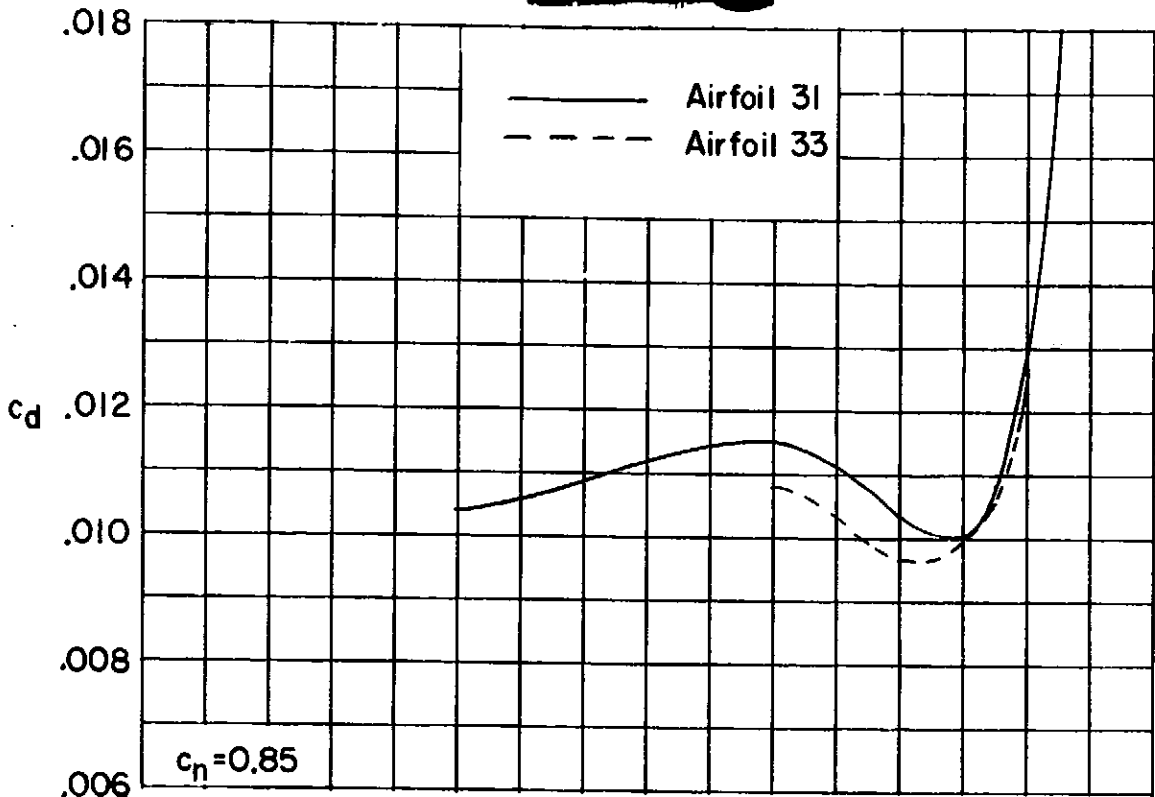
(d) $c_n = 0.75$ and 0.80 .

Figure 8. - Continued.



(c) $c_n = 0.65$ and 0.70 .

Figure 8. - Continued.



(e) $c_n = 0.85$ and 0.90 .

Figure 8. - Concluded.

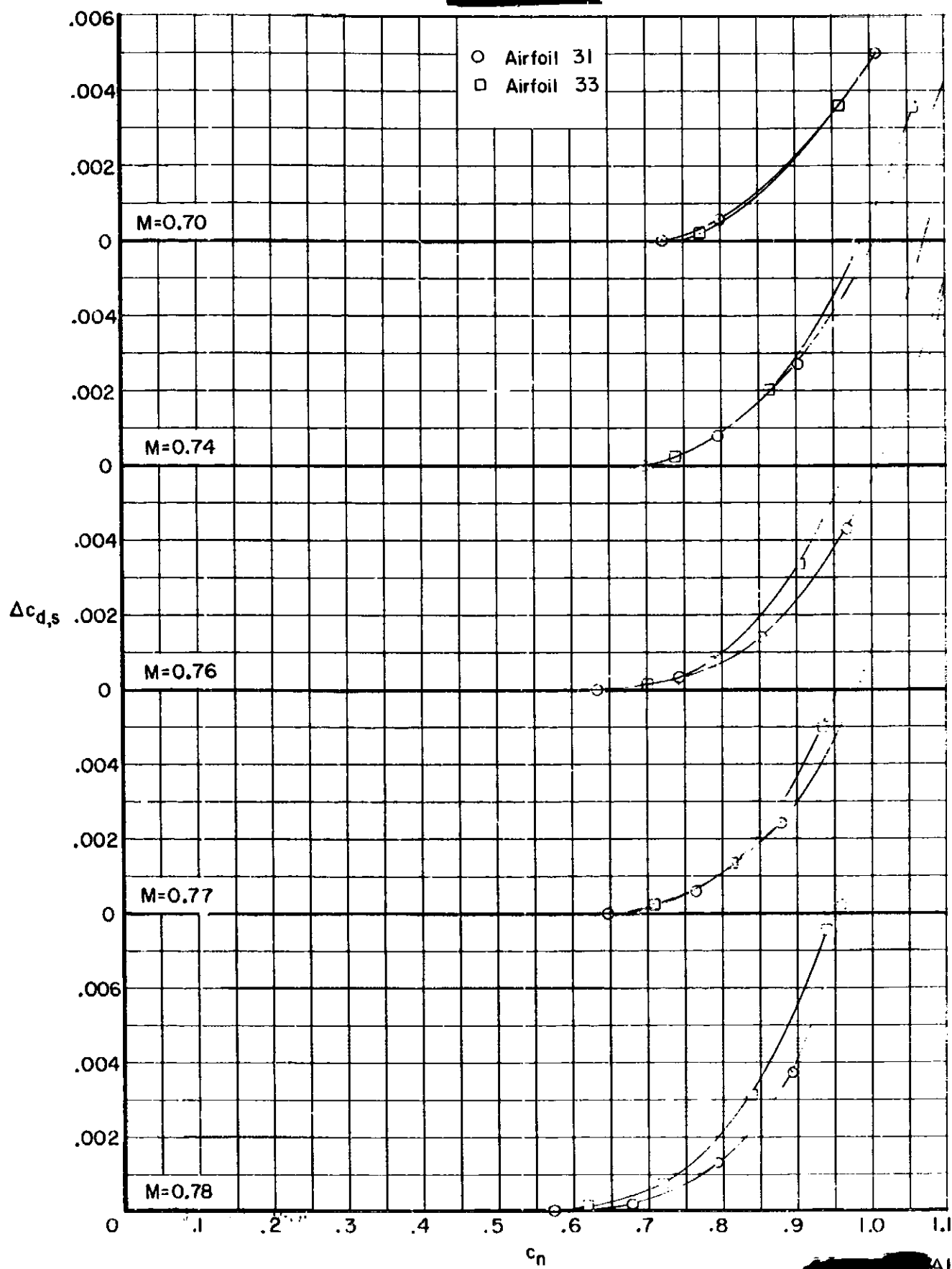


Figure 9. - Drag Increment due to shock wave losses.

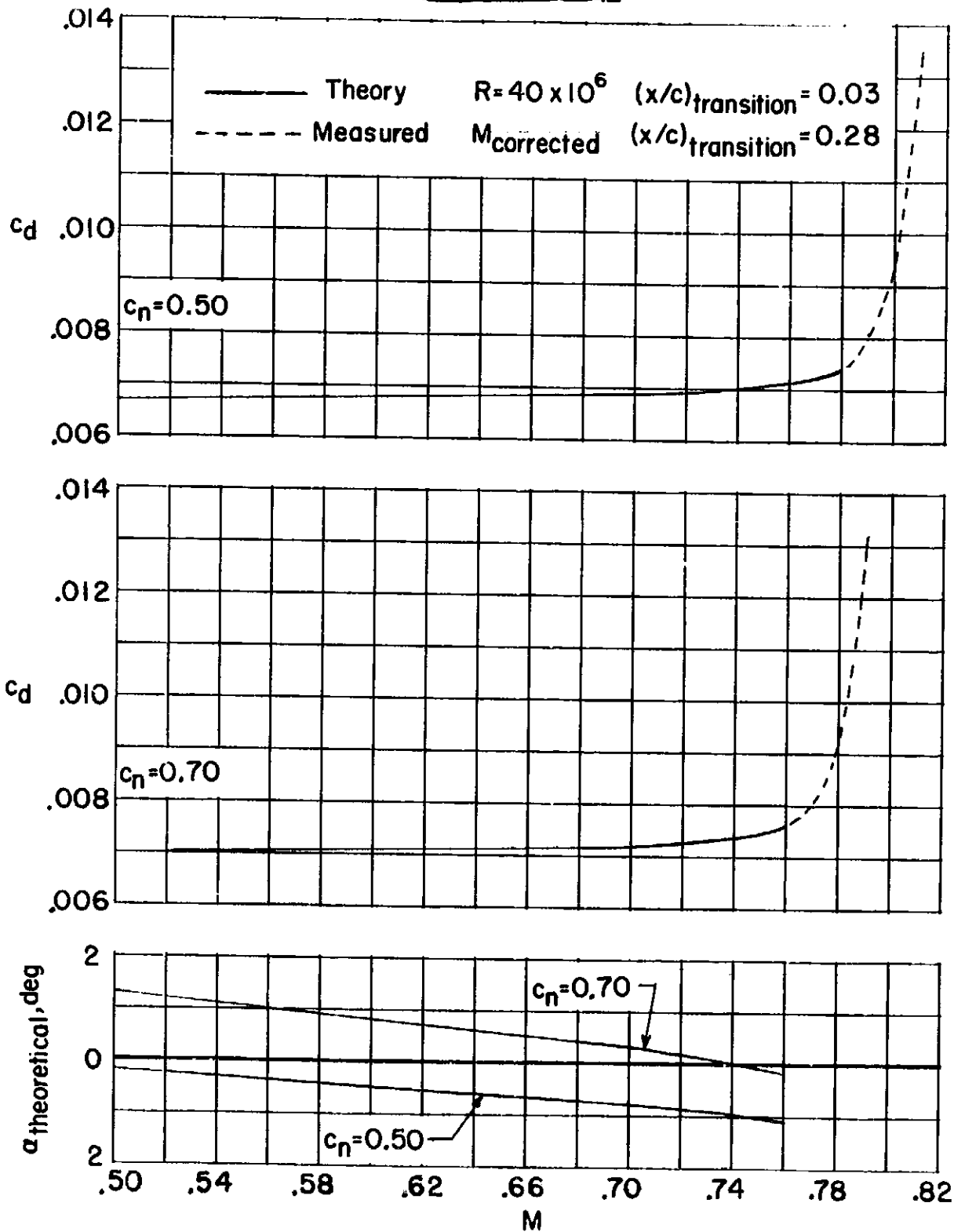


Figure 10. - Composite drag-rise curves and theoretical angles of attack for 10-percent-thick supercritical airfoil 33.

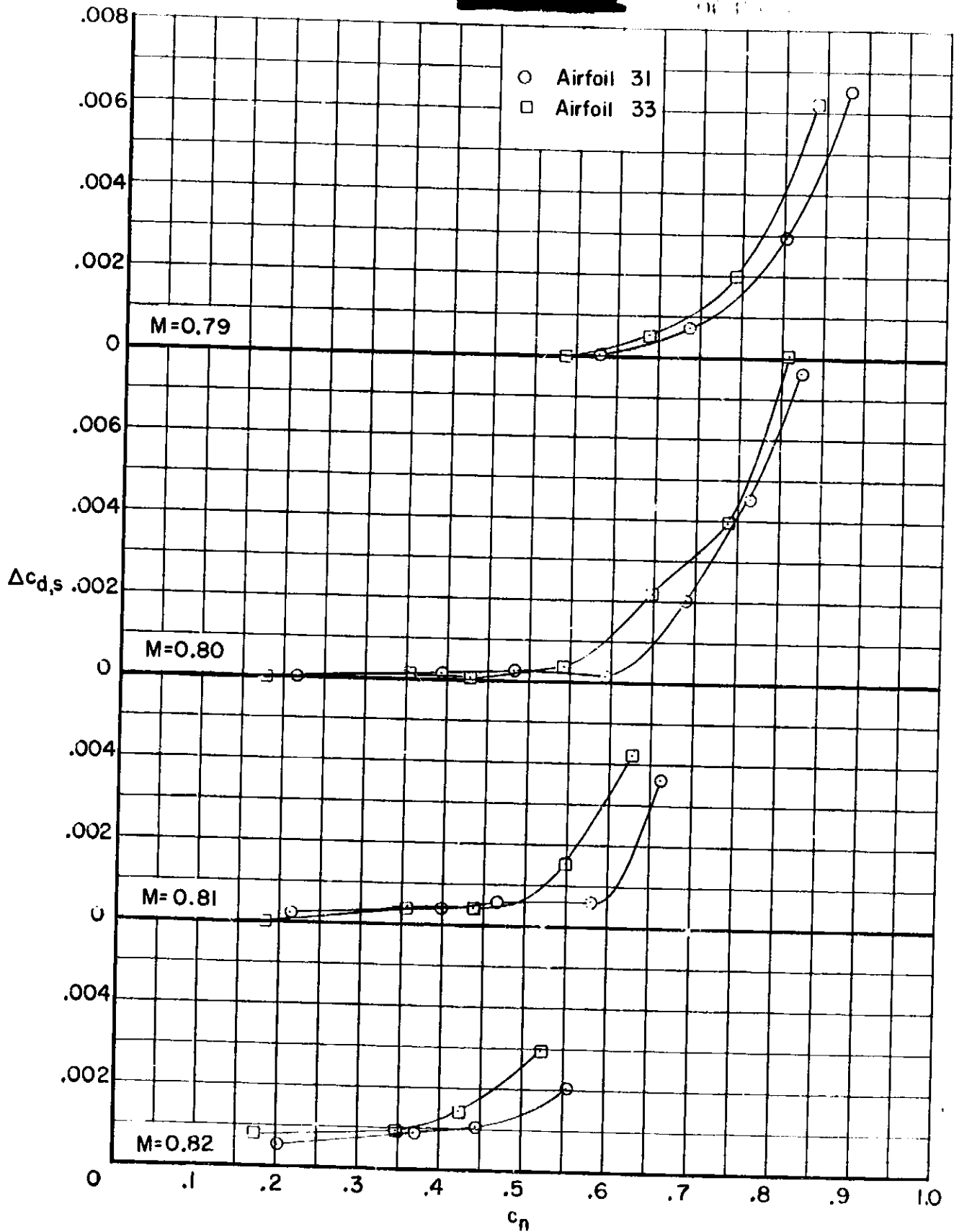
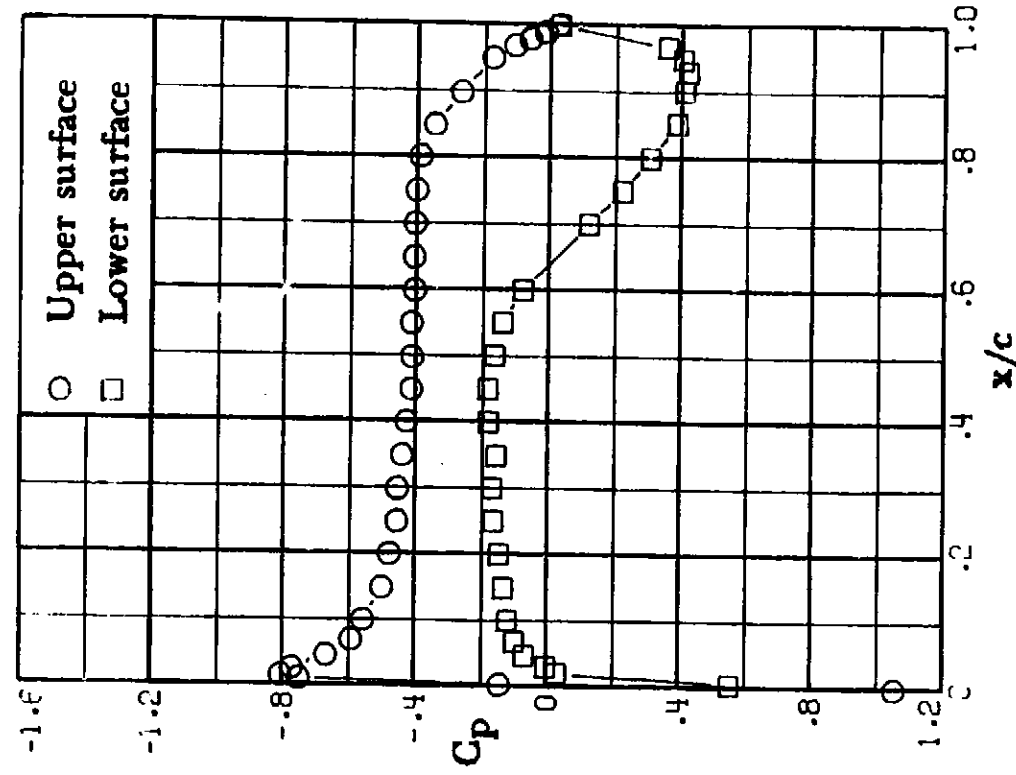
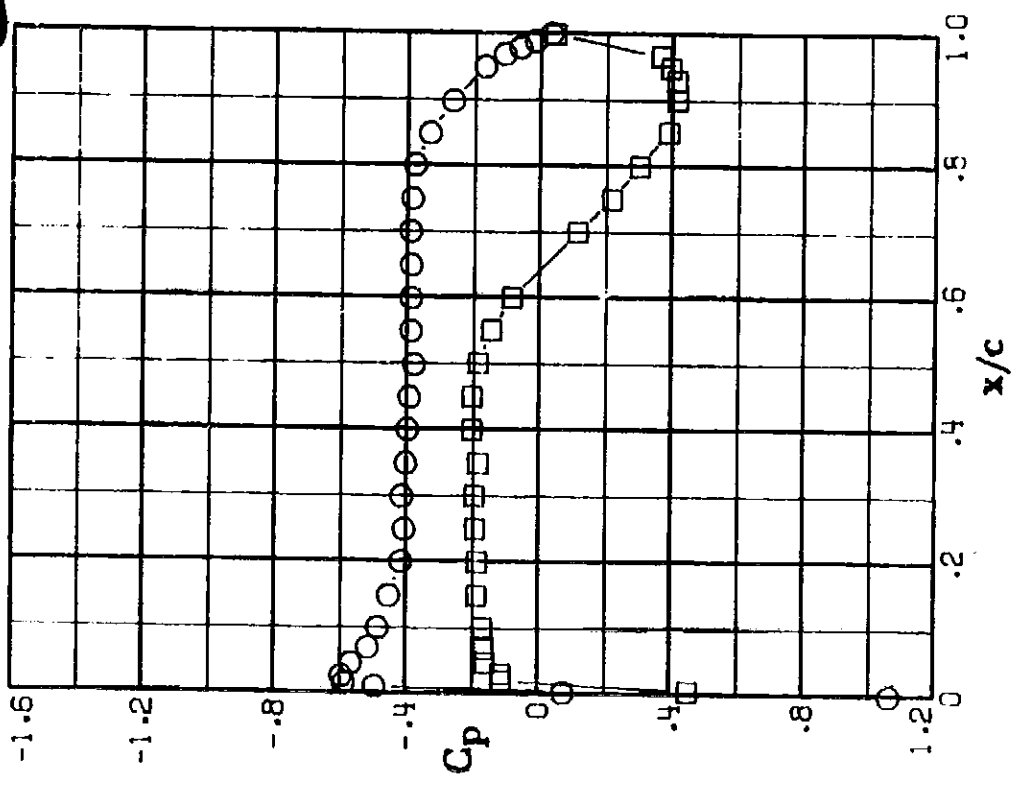


Figure 9. - Concluded.



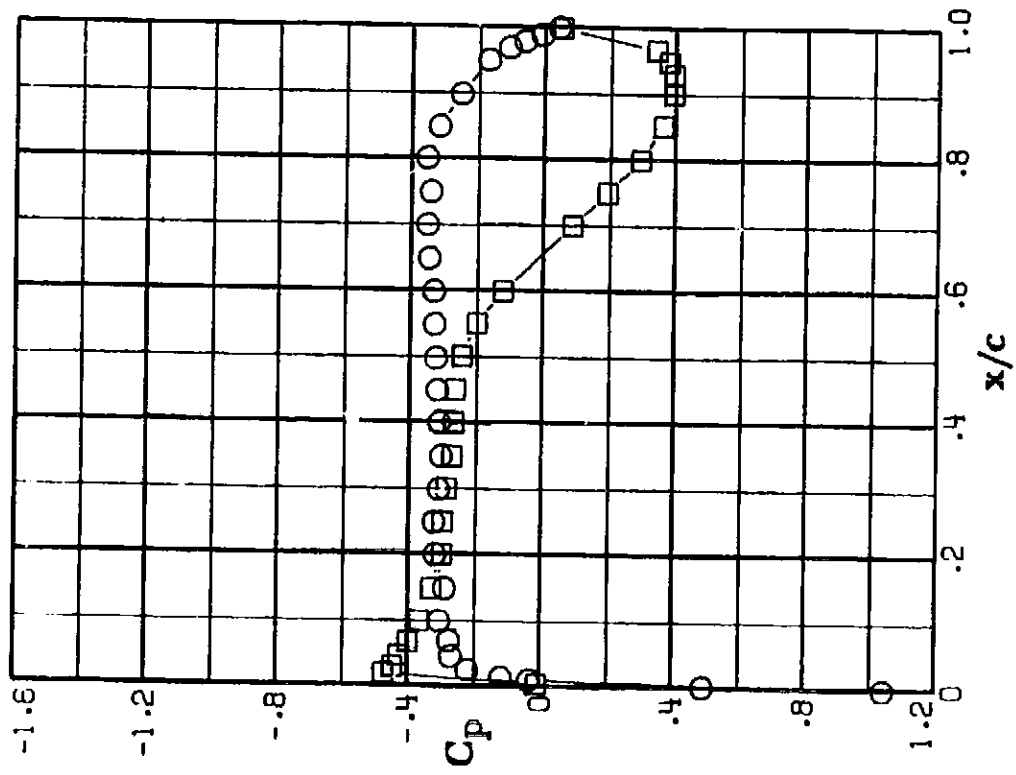


(d) $M = 0.50$; $c_n = 0.44$.

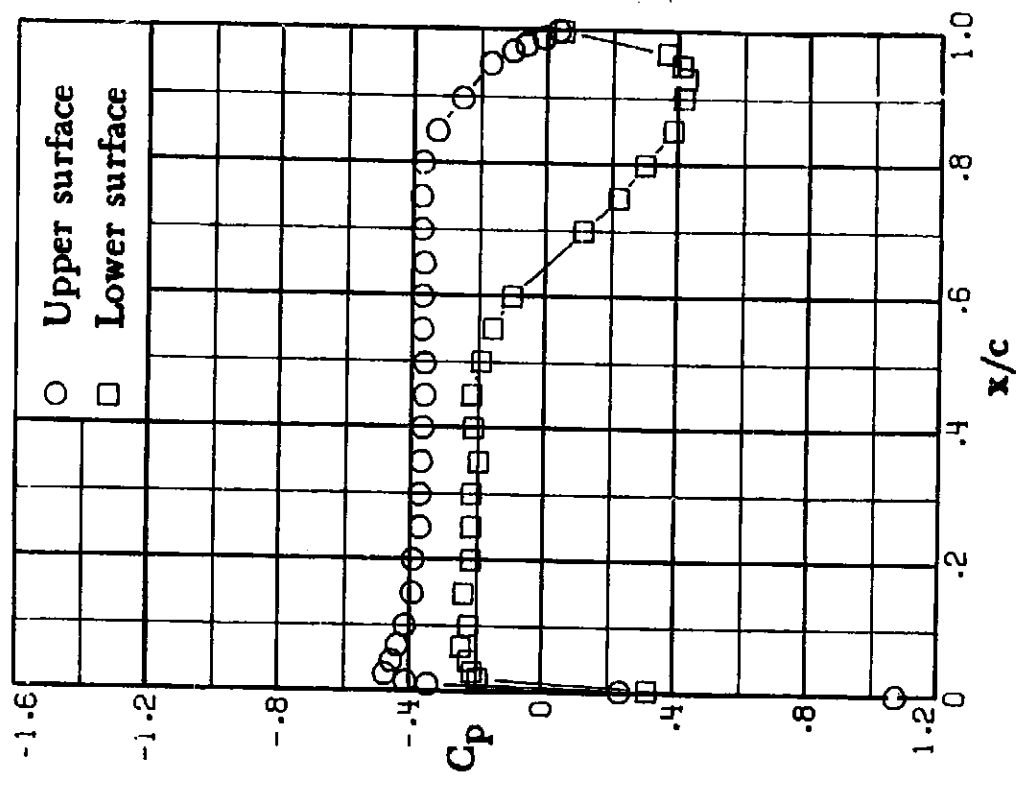


(c) $M = 0.50$; $c_n = 0.38$.

Figure II. - Continued.



(a) $M = 0.50$; $c_n = 0.21$.

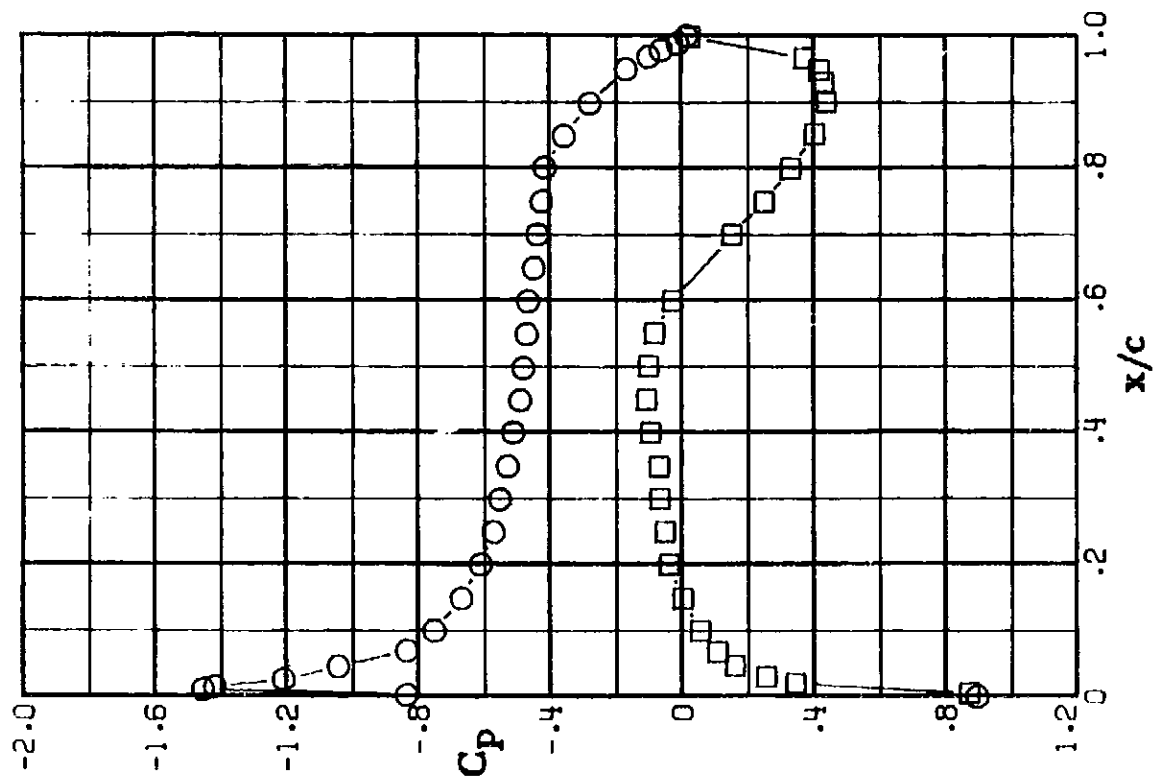


(b) $M = 0.50$; $c_n = 0.33$.

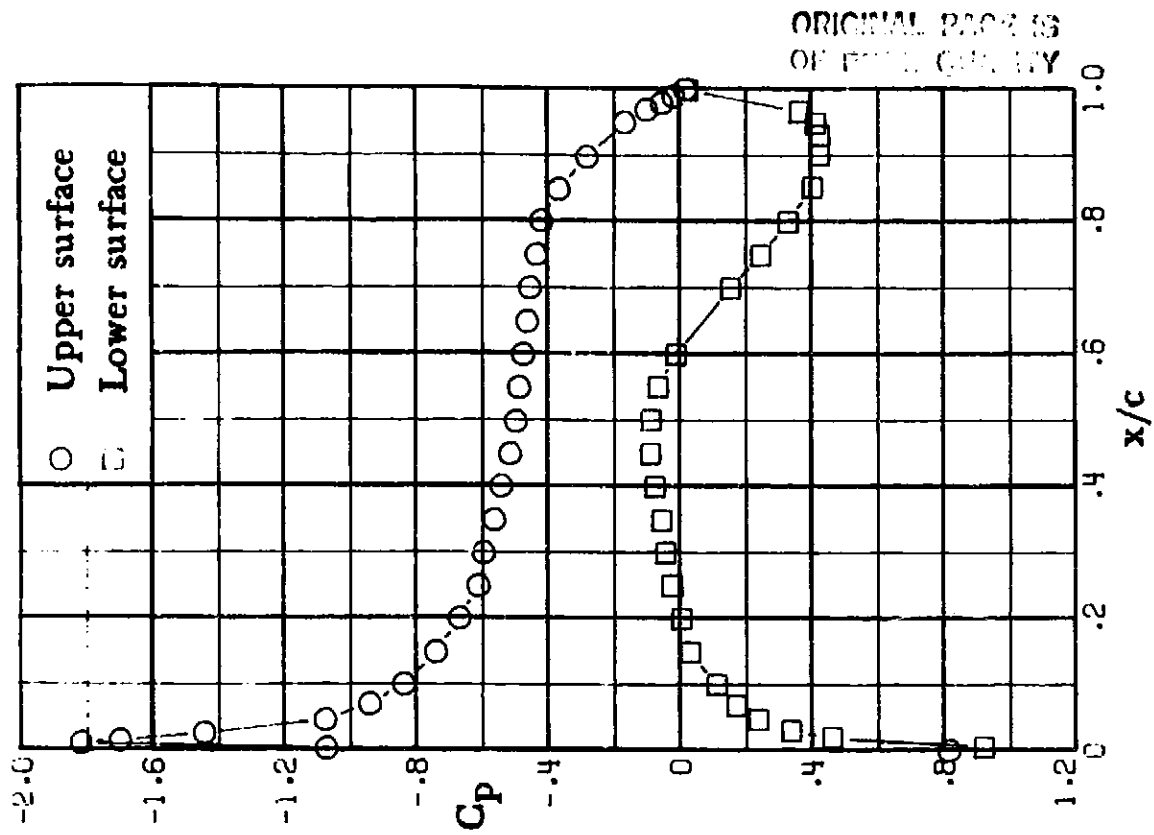
Figure 11.- Chordwise pressure coefficient vs. x/c for a 12 percent thick supercritical airfoil 33. $M = 0.50$.

CONFIDENTIAL

~~CONFIDENTIAL~~

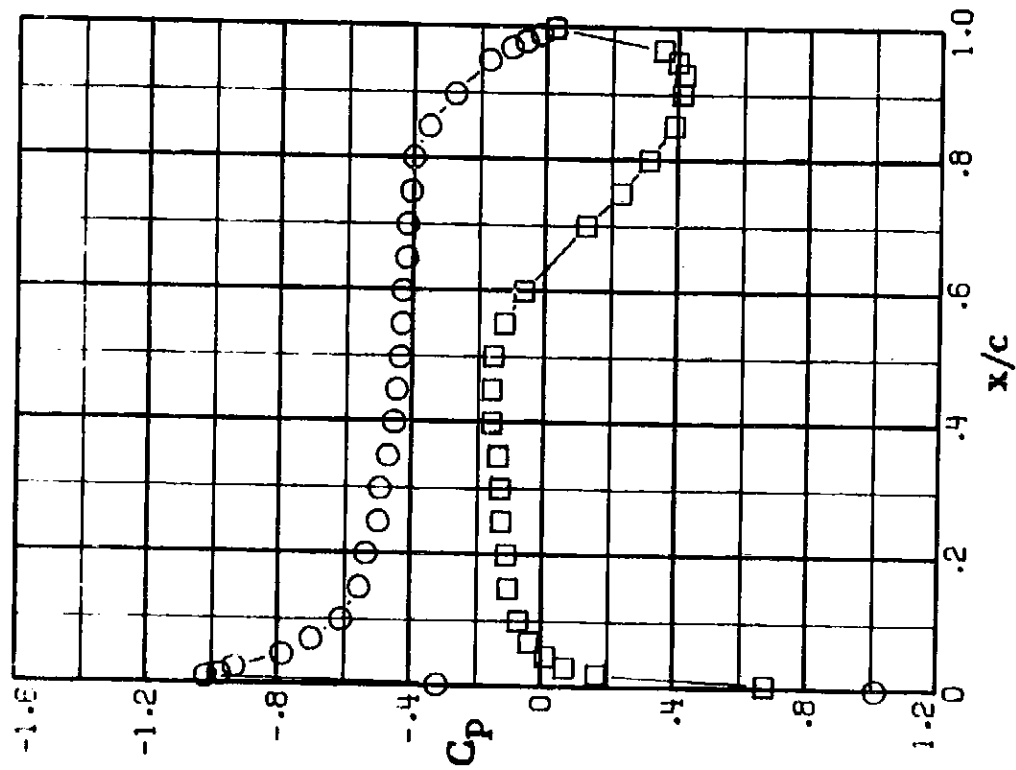


(g) $M = 0.50$; $c_n = 0.61$.

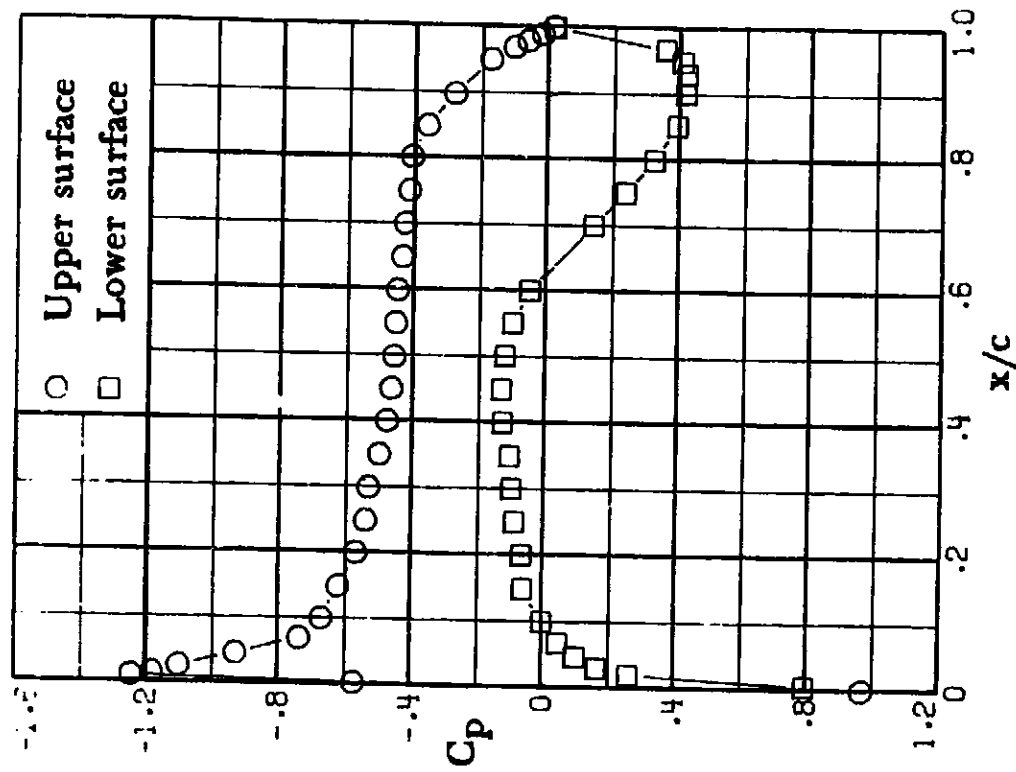


(h) $M = 0.50$; $c_n = 0.67$.

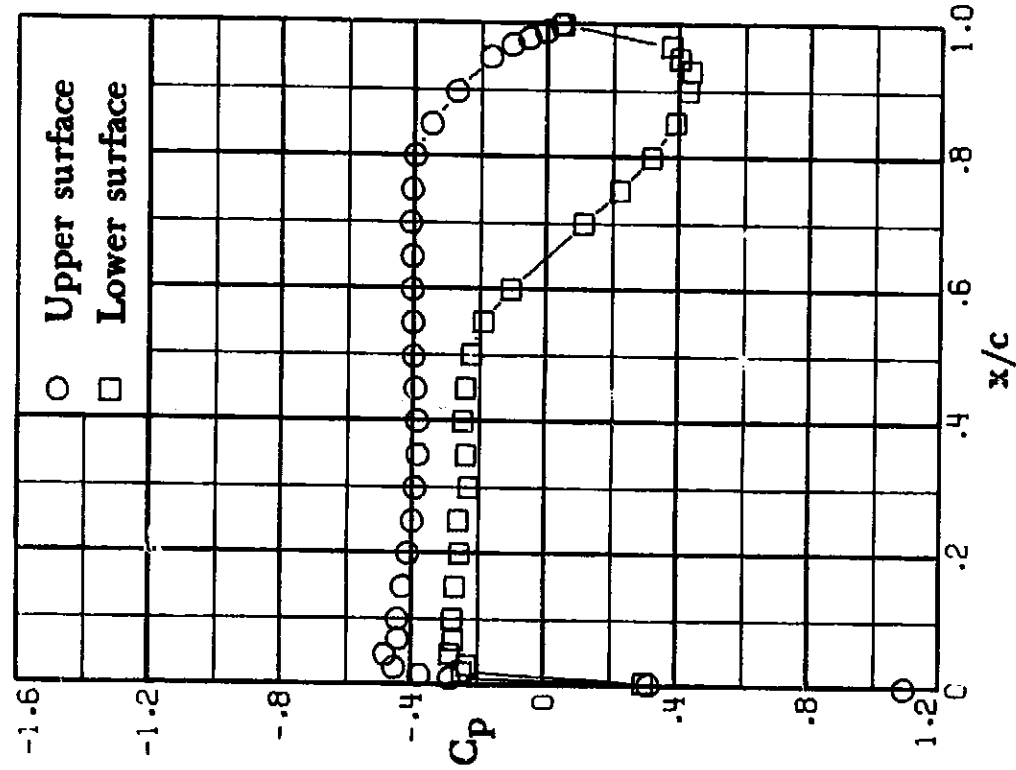
Figure II. - Continued.



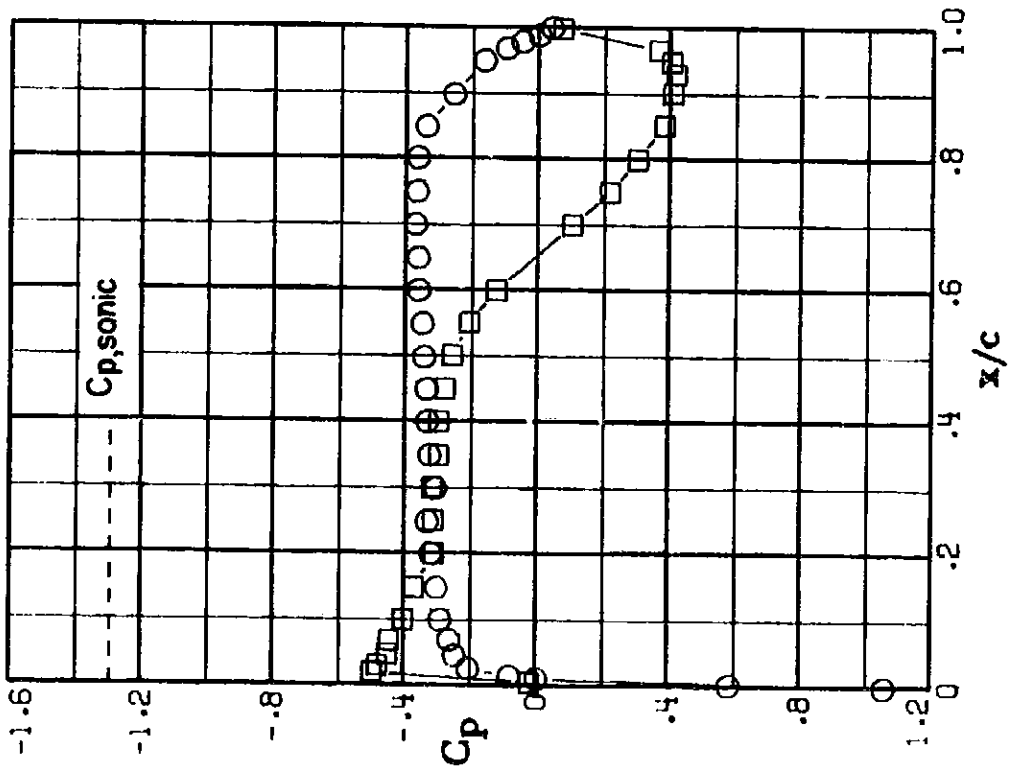
(e) $M = 0.50$; $c_n = 0.49$.



(f) $M = 0.50$; $c_n = 0.56$.

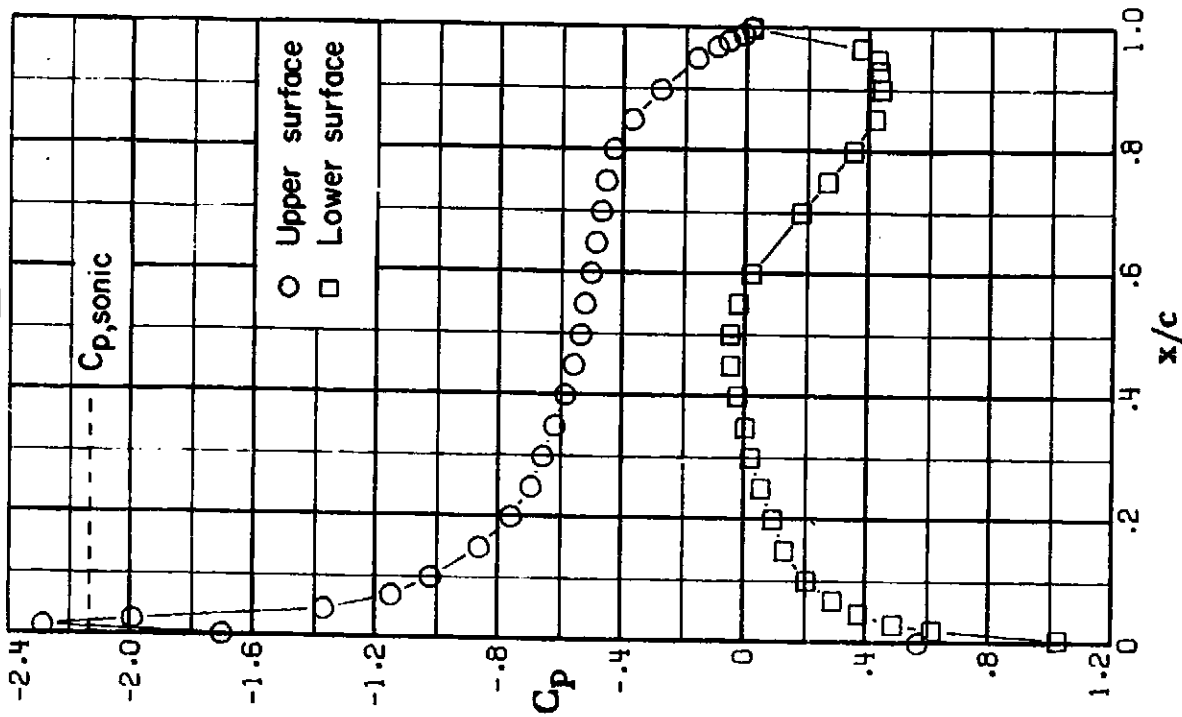


(a) $M = 0.60$; $c_n = 0.21$.



(b) $M = 0.60$; $c_n = 0.33$.

Figure 12.- Chordwise pressure distributions for 10-percent thick supercritical airfoil 33. $M = 0.60$.

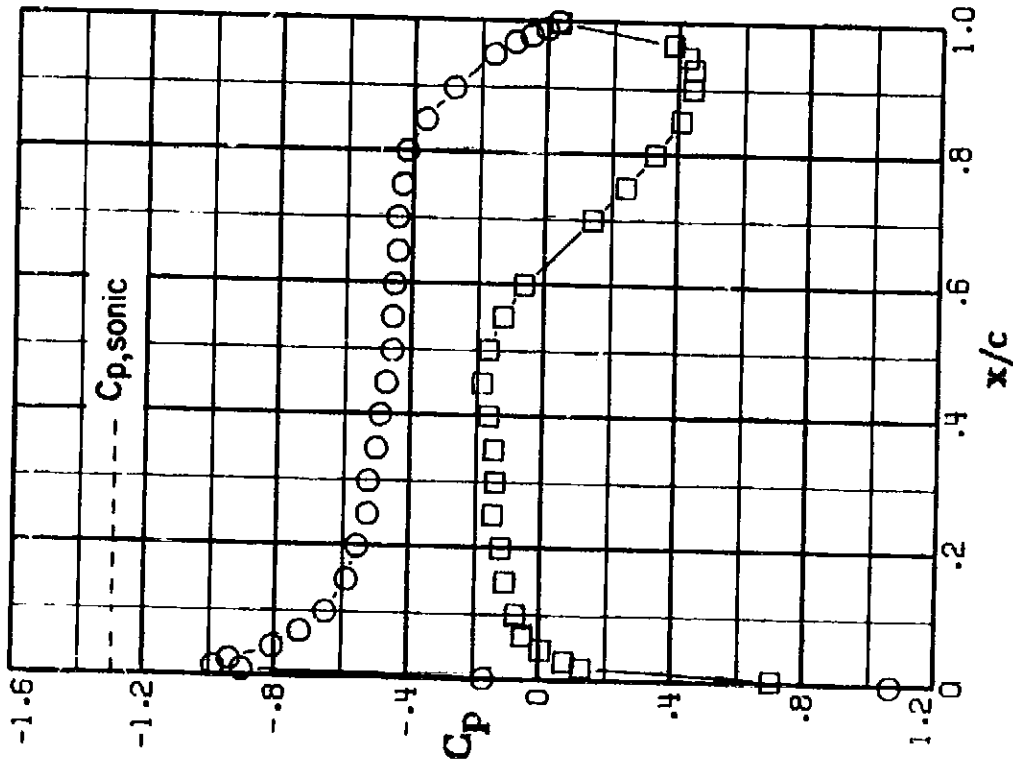


(i) $M = 0.50$; $c_n = 0.80$.

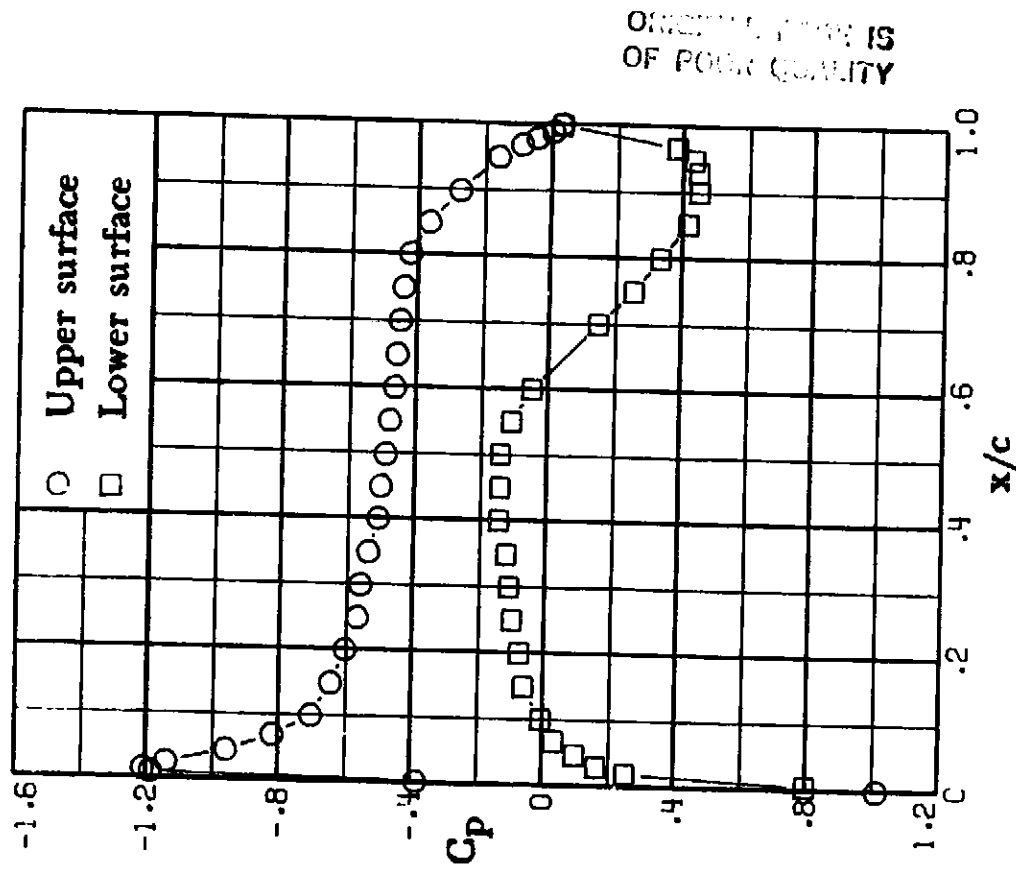
Figure II. - Concluded.

SHEETS

CONFIDENTIAL

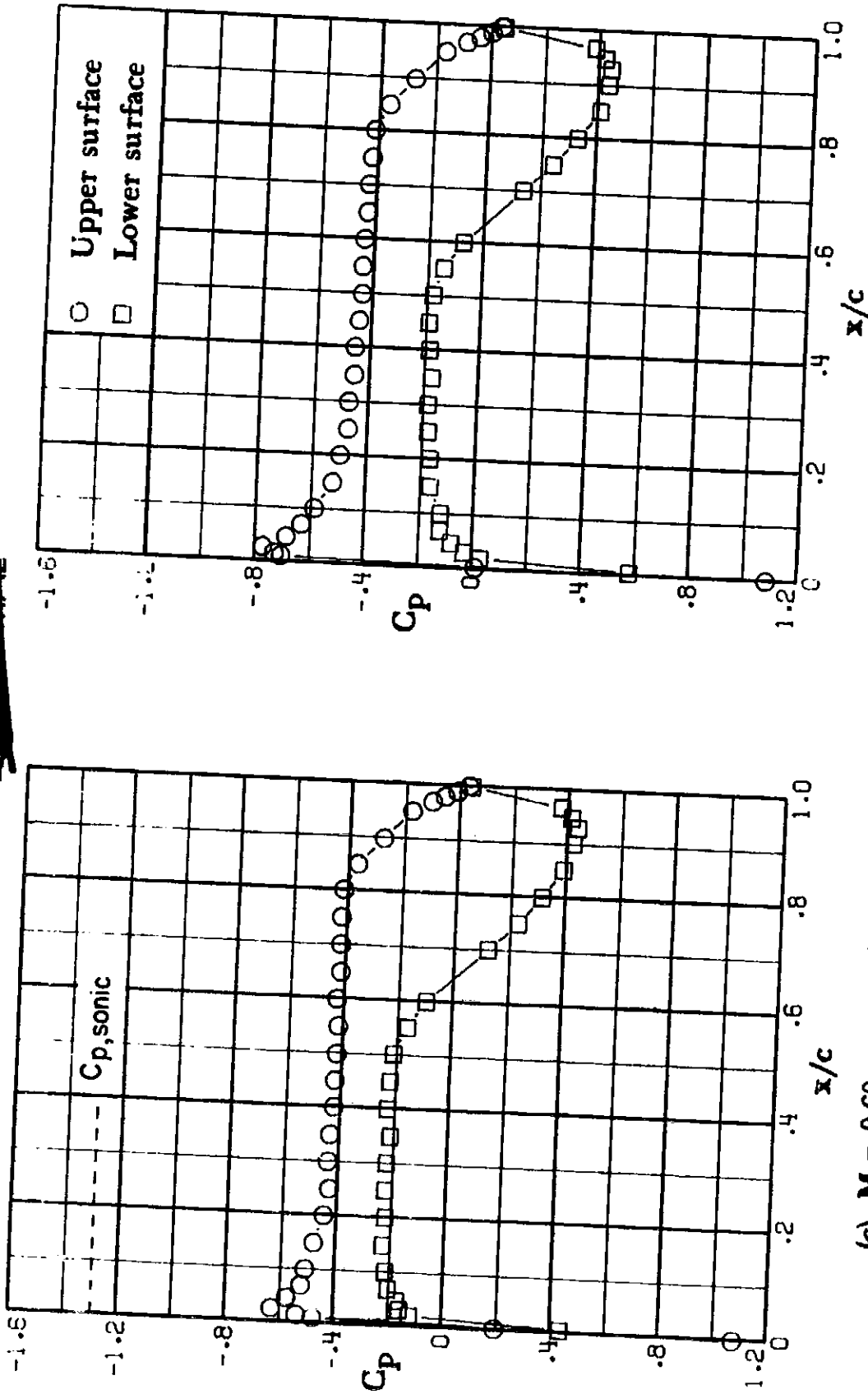


(e) $M = 0.60$; $c_n = 0.52$.



(f) $M = 0.60$; $c_n = 0.58$.

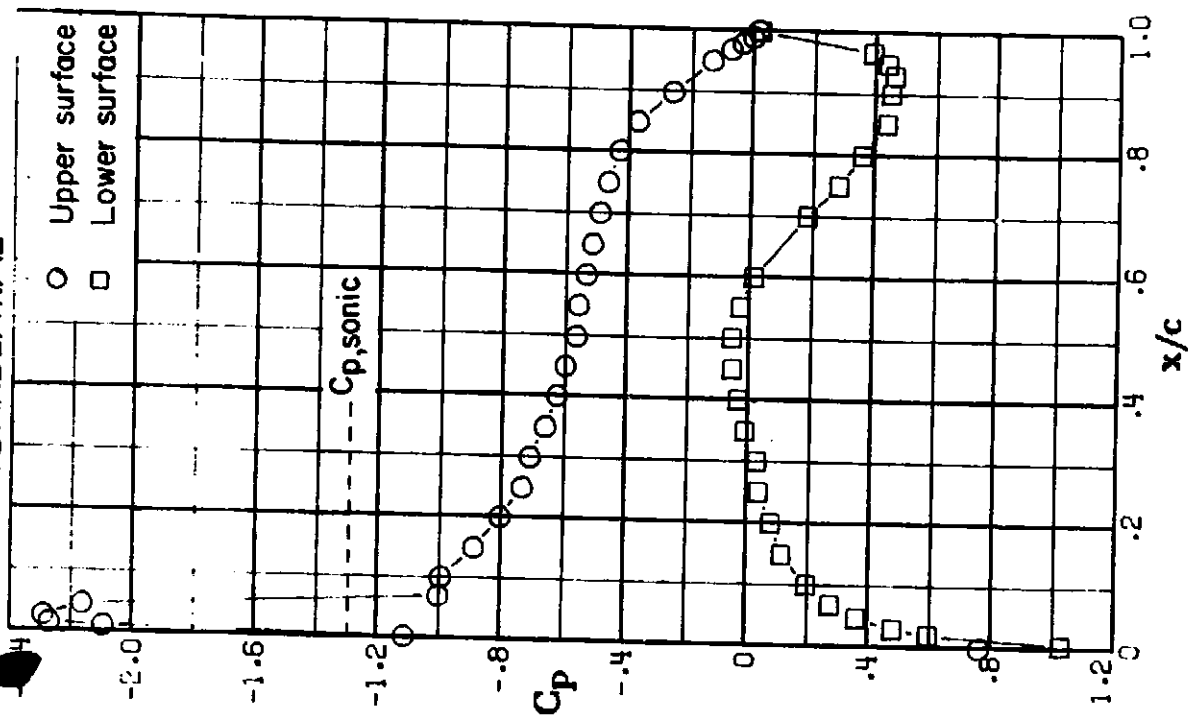
Figure 12. - Continued.



(c) $M = 0.60$; $c_n = 0.39$.

(d) $M = 0.60$; $c_n = 0.46$.

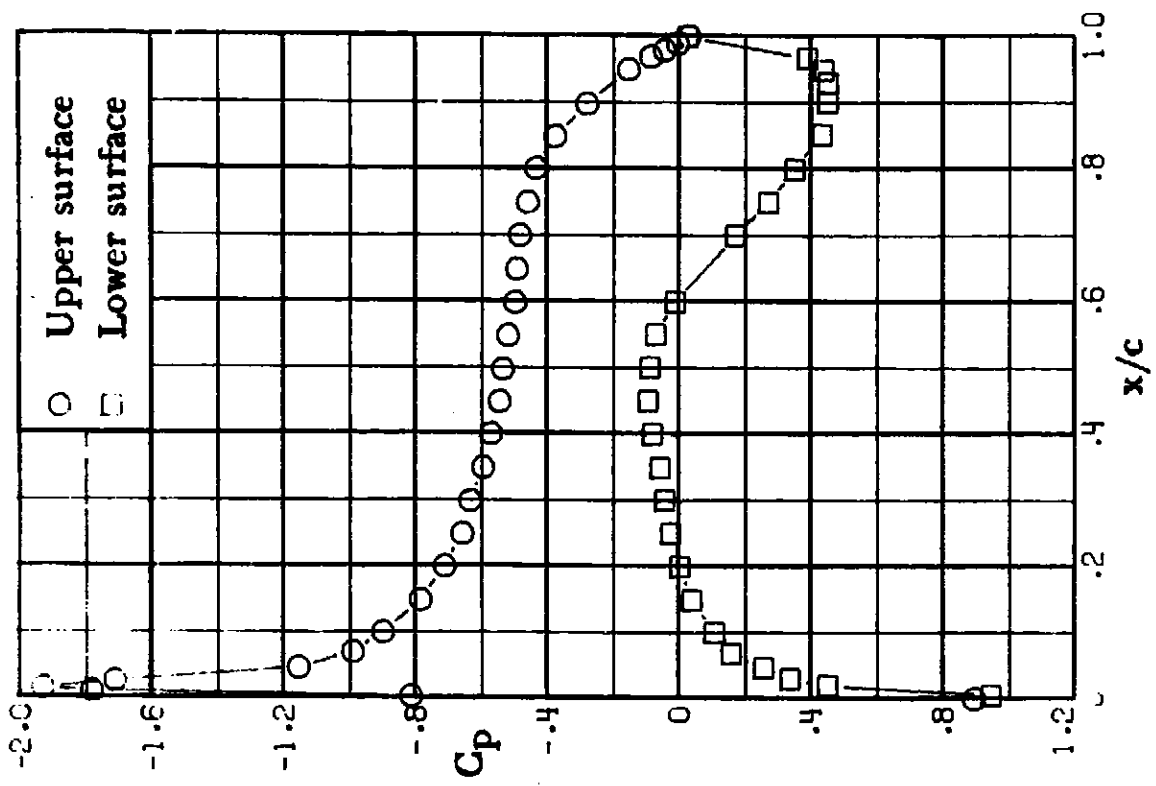
CONFIDENTIAL



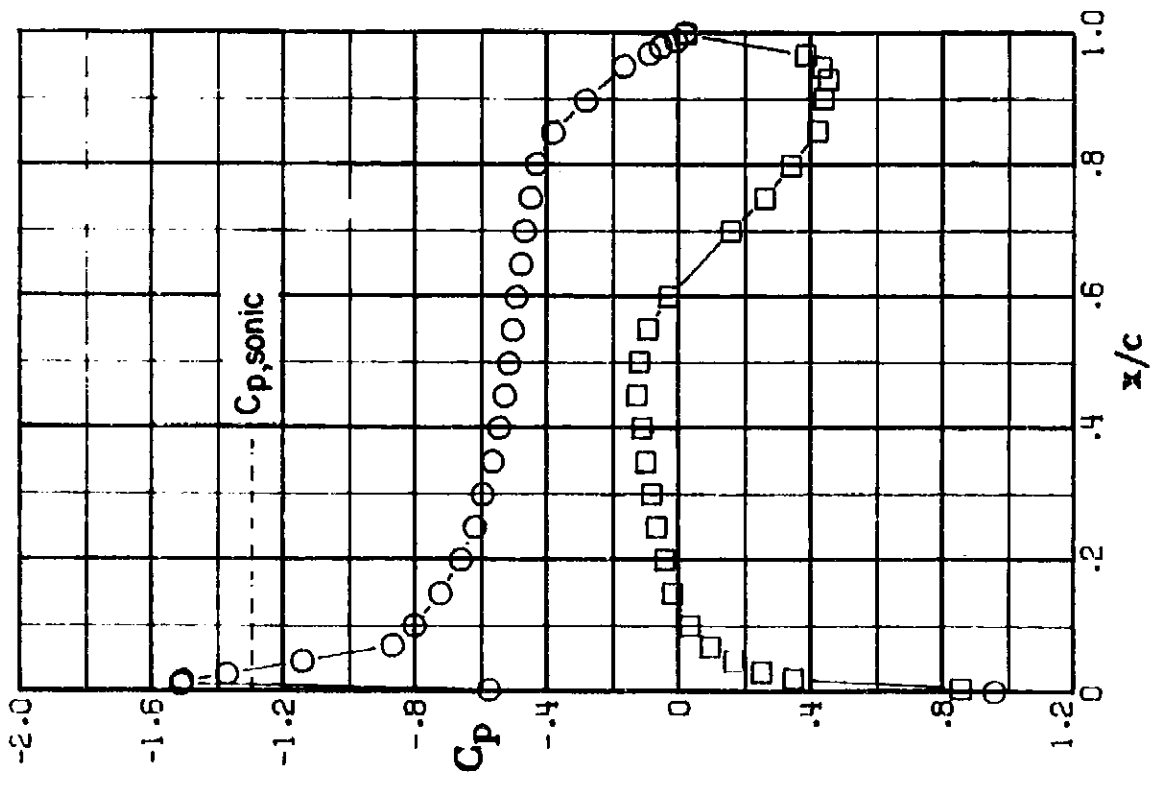
(i) $M = 0.60$; $c_n = 0.82$.

Figure 12. - Concluded.

ORIGINAL PAGE IS
OF POOR QUALITY



(h) $M = 0.60$; $c_n = 0.71$.

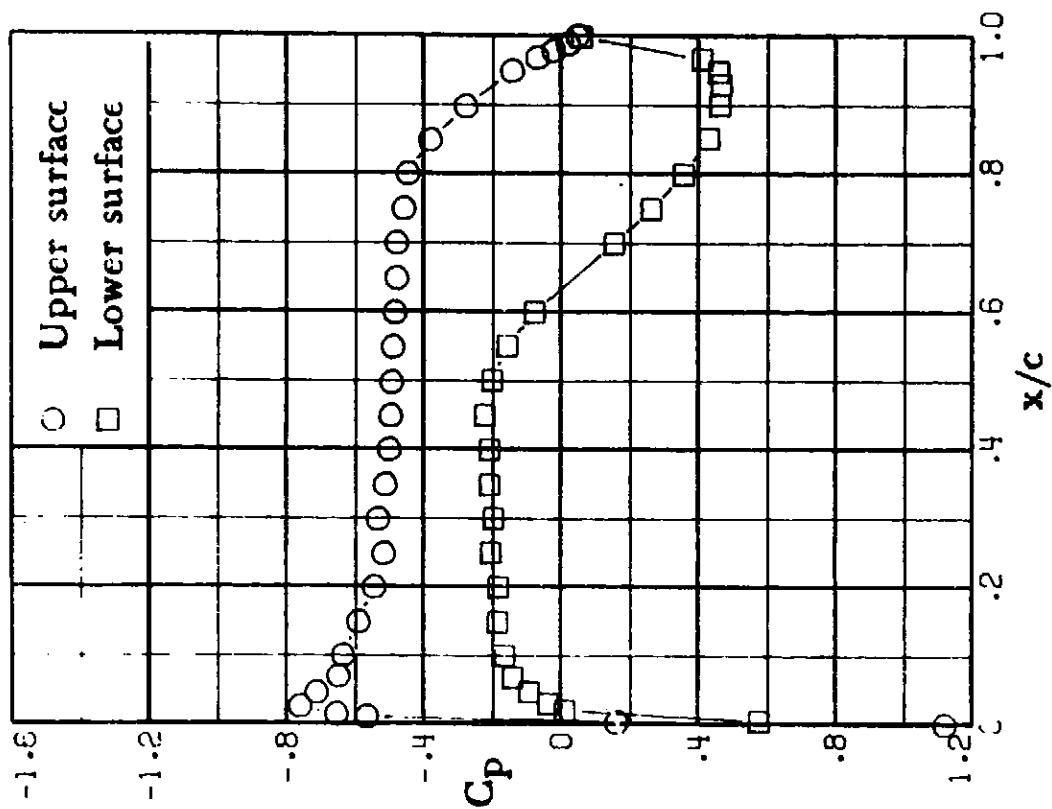


(g) $M = 0.60$; $c_n = 0.64$.

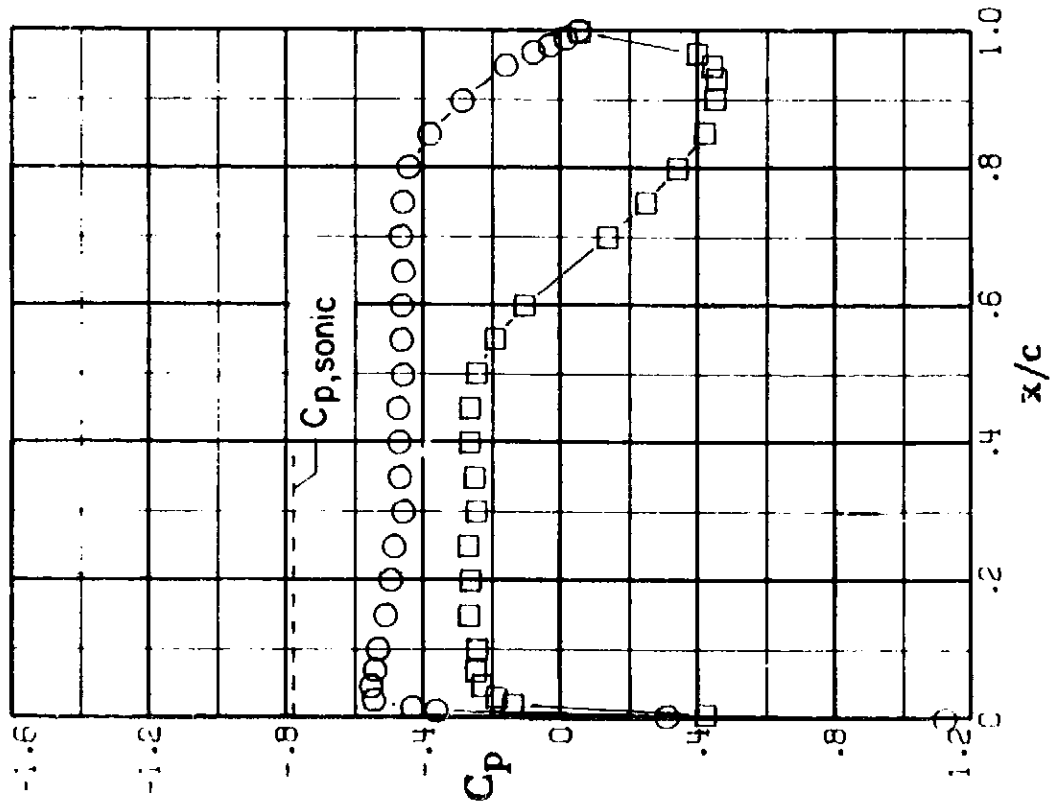
Figure 12.- Continued.

CONFIDENTIAL

ORIGINAL SOURCE OF POOR QUALITY

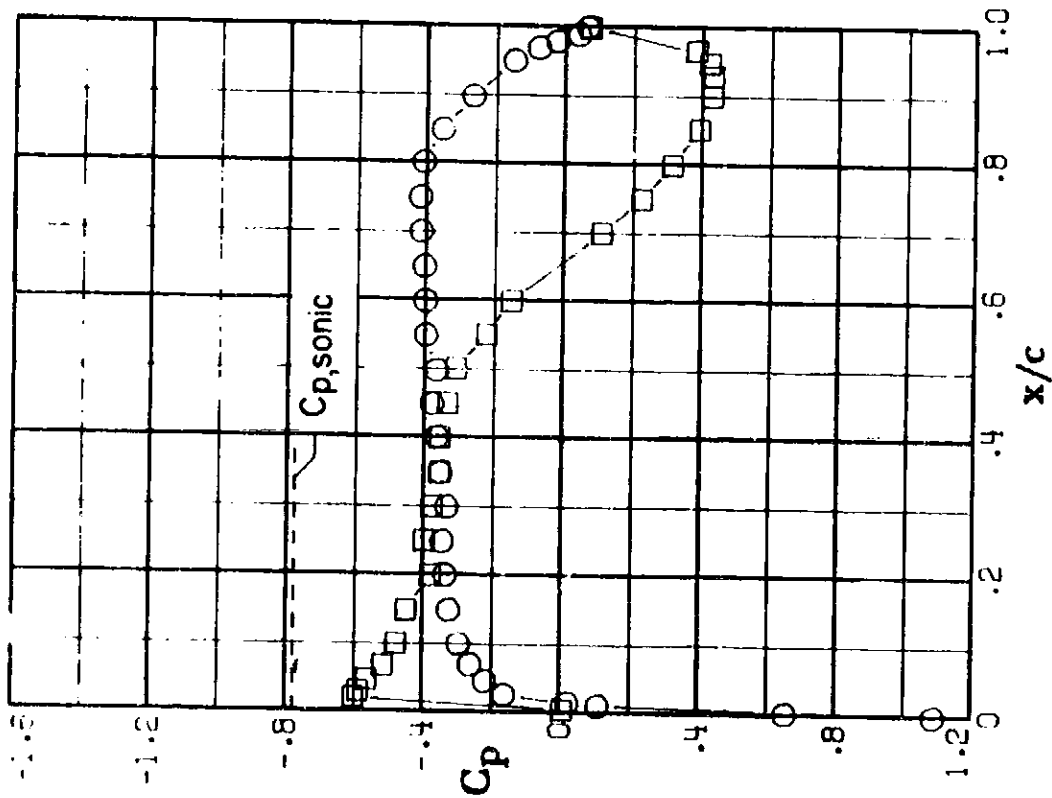


(d) $M = 0.70$; $c_n = 0.48$.

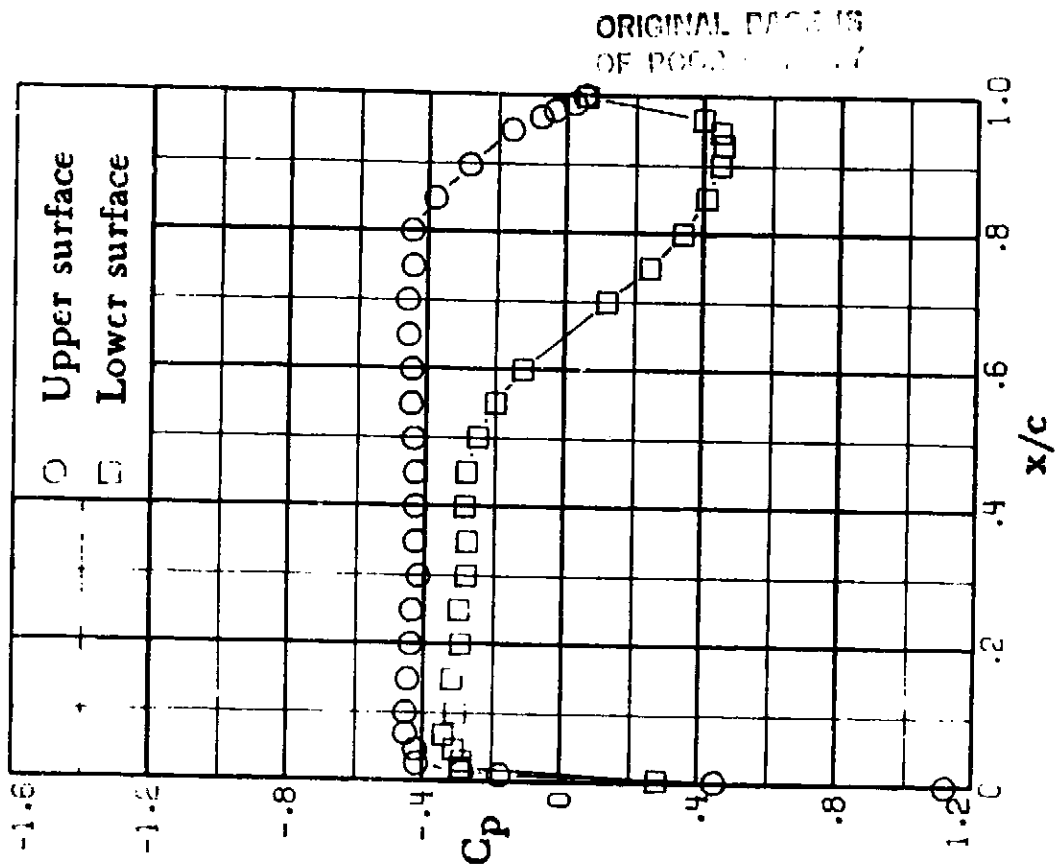


(c) $M = 0.70$; $c_n = 0.40$.

Figure 13. - Continued.



(a) $M = 0.70$; $c_n = 0.19$.



(b) $M = 0.70$; $c_n = 0.34$.

Figure 13. - Chordwise pressure distributions for 10-percent thick supercritical airfoil 33. $M = 0.70$.

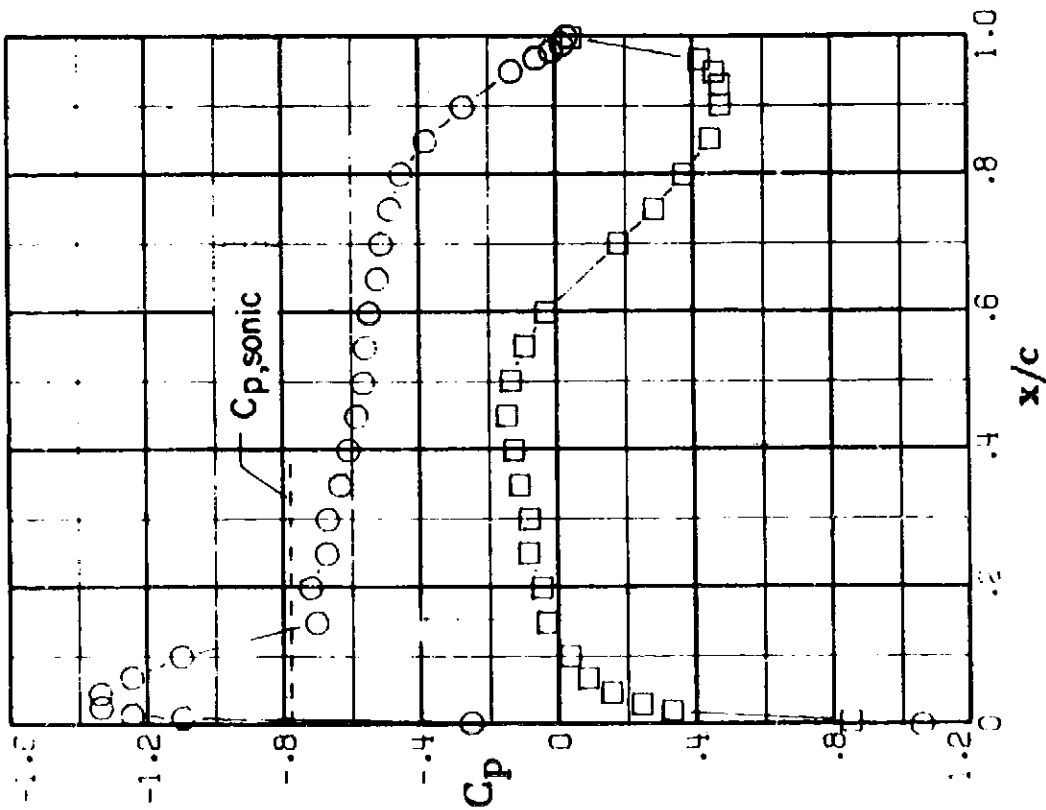
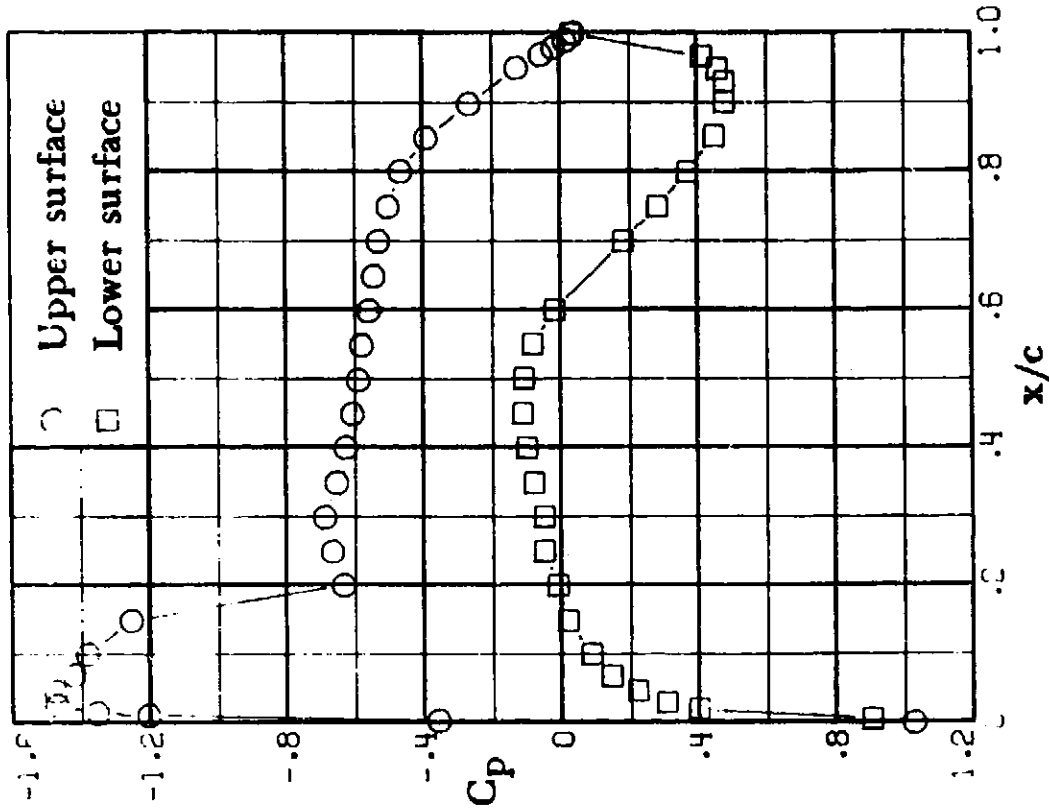
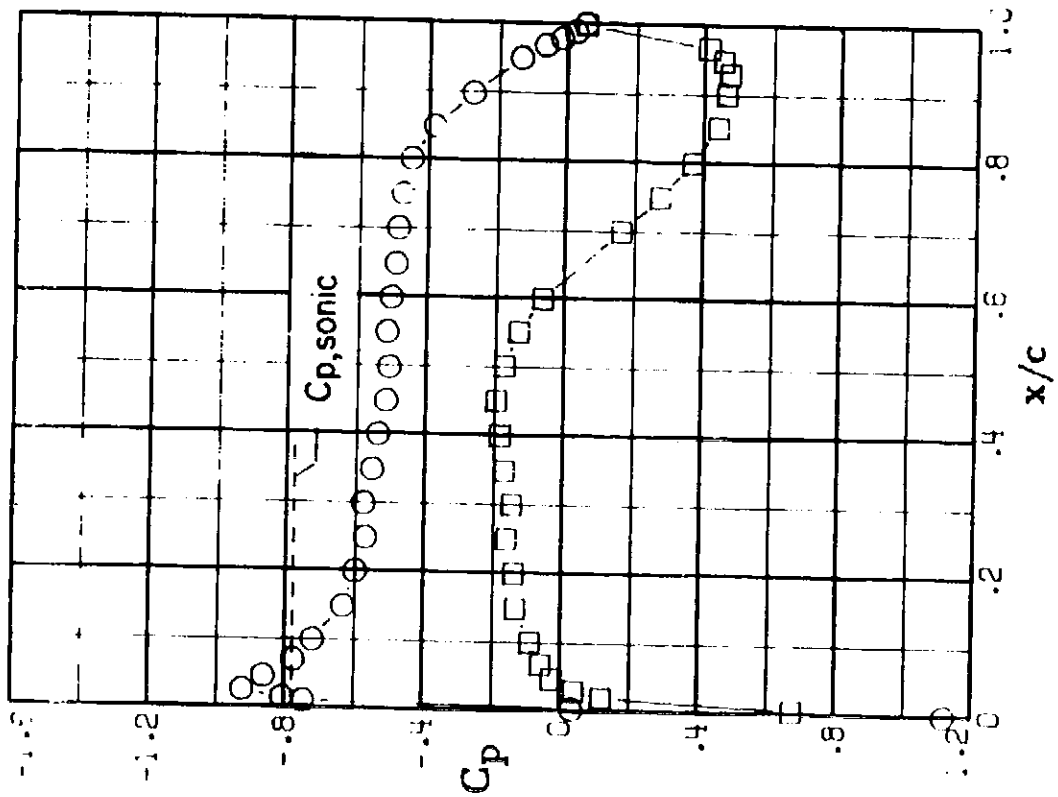
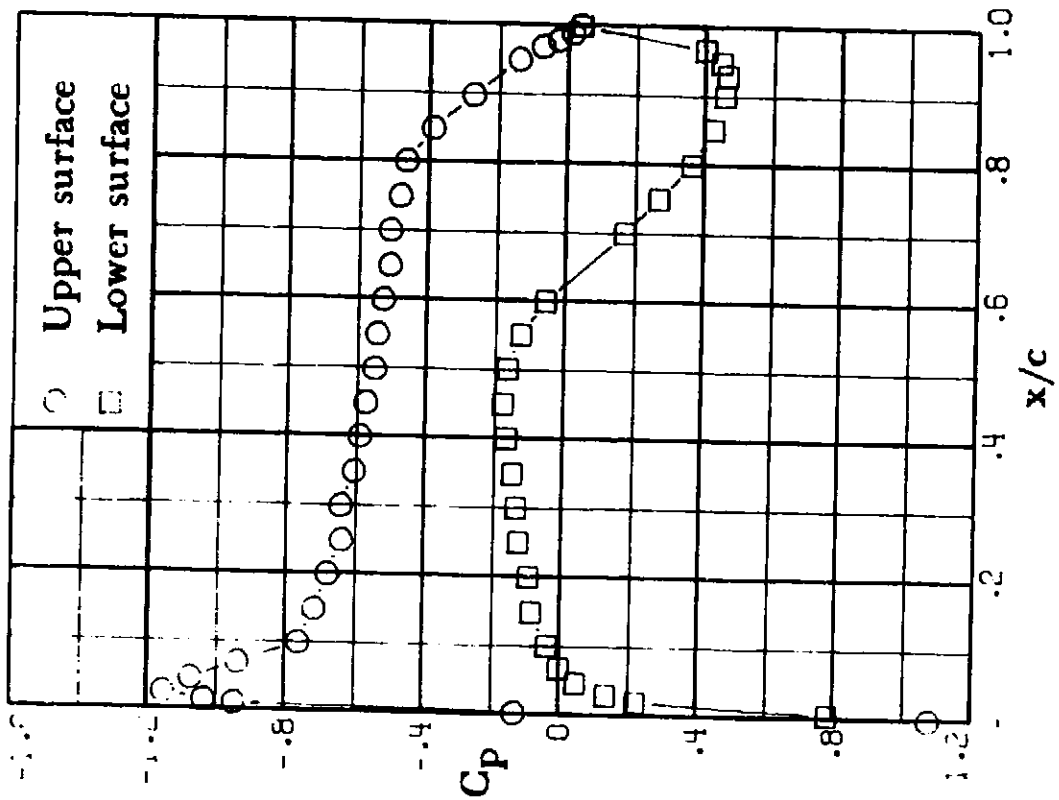


Figure 13. - Continued.



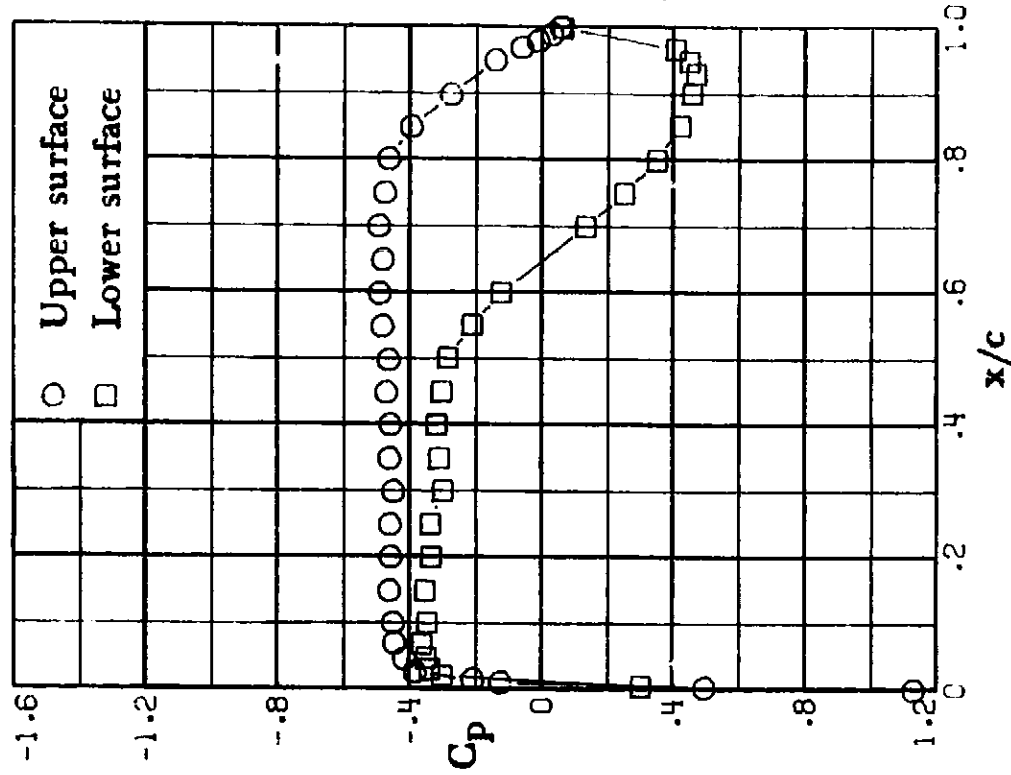
(e) $M = 0.70$; $c_n = 0.555$.



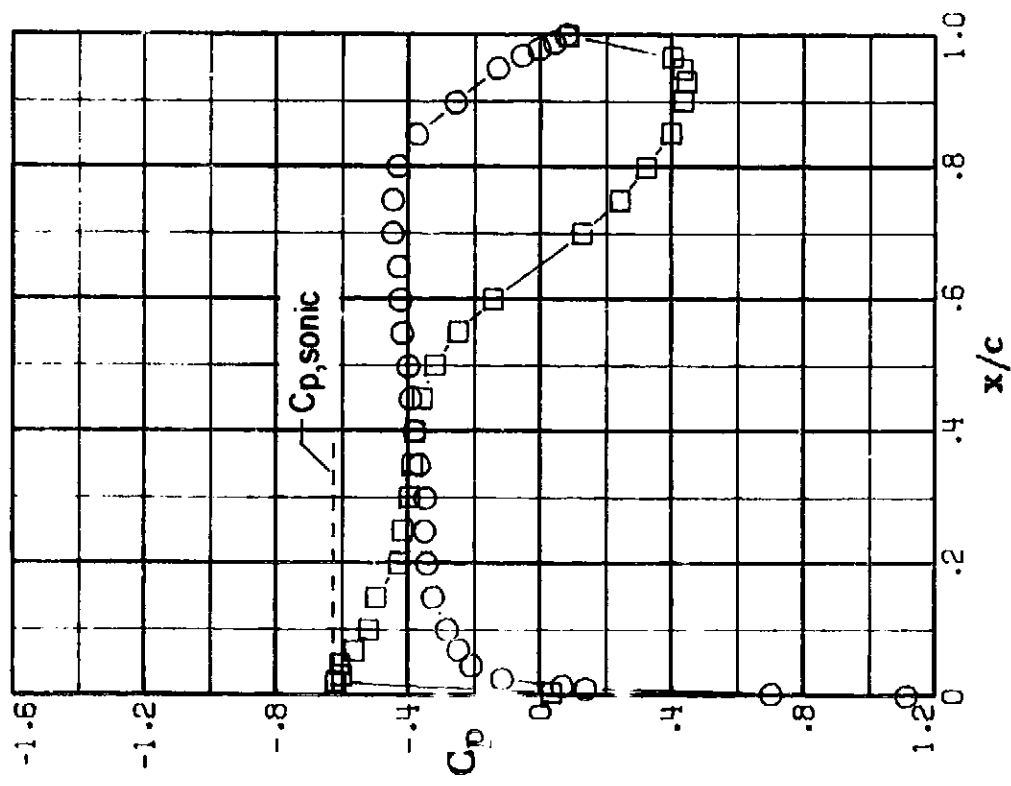
(f) $M = 0.70$; $c_n = 0.62$.

Figure 13. - Continued.

ORIGINAL PAGE IS
OF POOR QUALITY

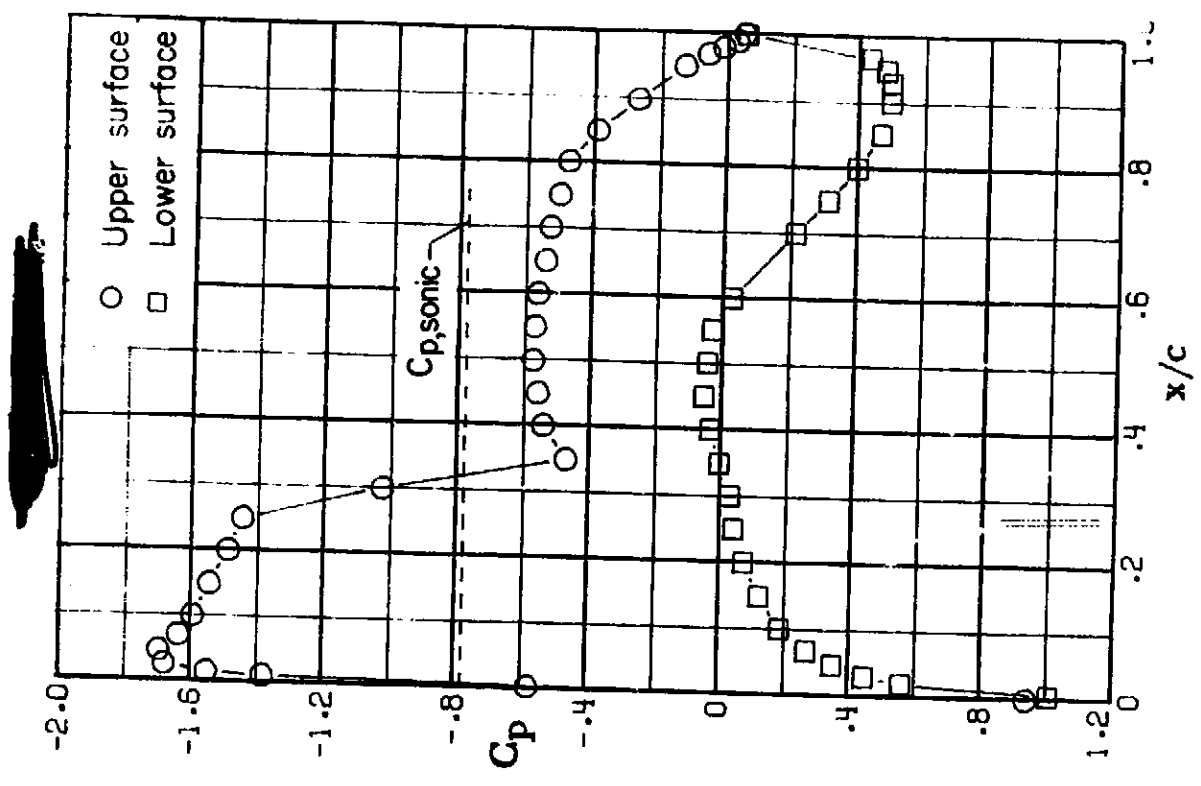


(a) $M = 0.74$; $c_n = 0.19$.



(b) $M = 0.74$; $c_n = 0.34$.

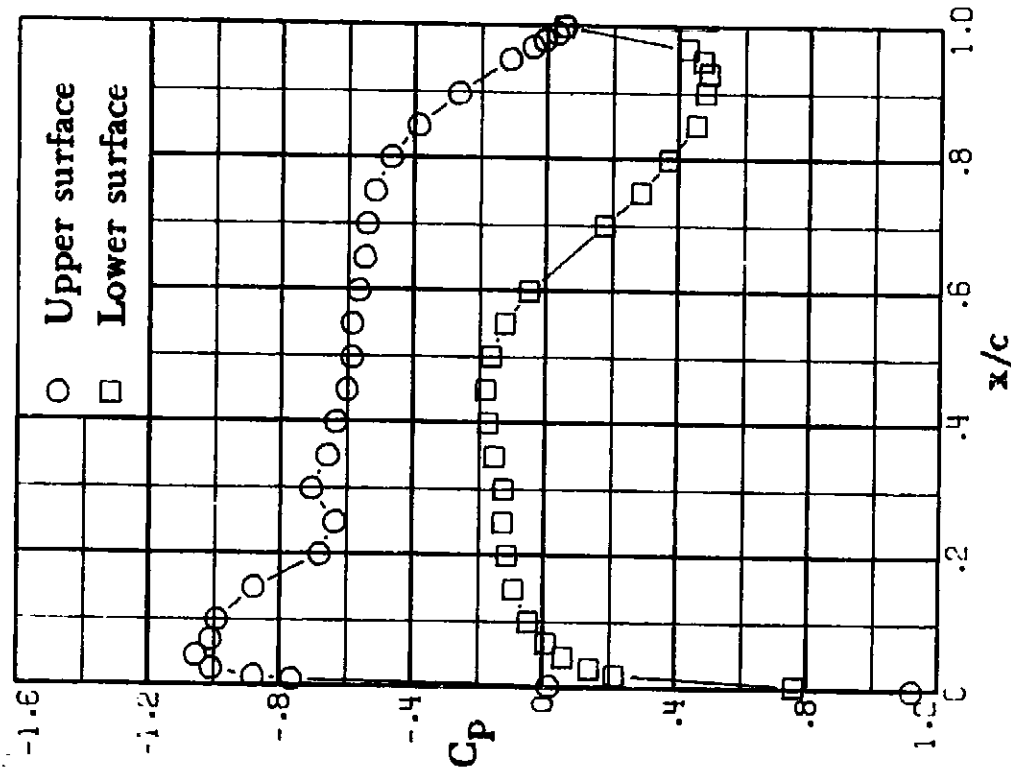
Figure i4. - Chordwise pressure distributions for 10-percent thick supercritical airfoil 33. $M = 0.74$.



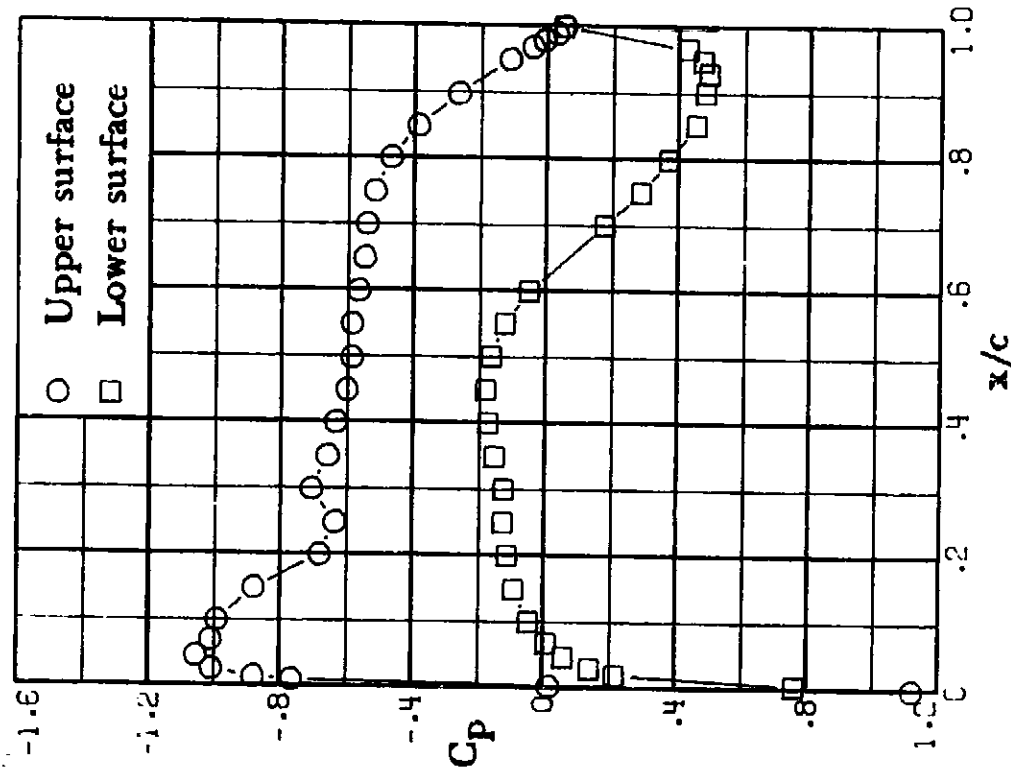
(4) $M = 0.70$; $c_n = 0.96$.

Figure 13. - Concluded.
 CONFIDENTIAL

ORIGINAL PAGE IS
OF POOR QUALITY

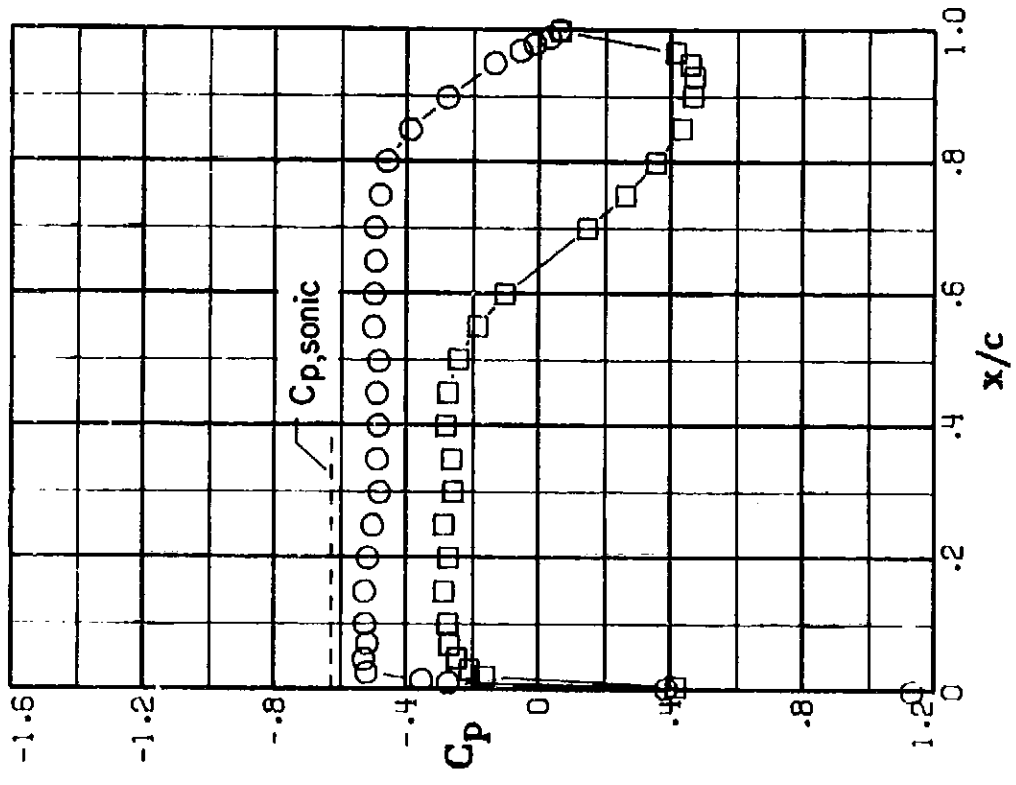


(e) $M = 0.74$; $c_n = 0.57$.

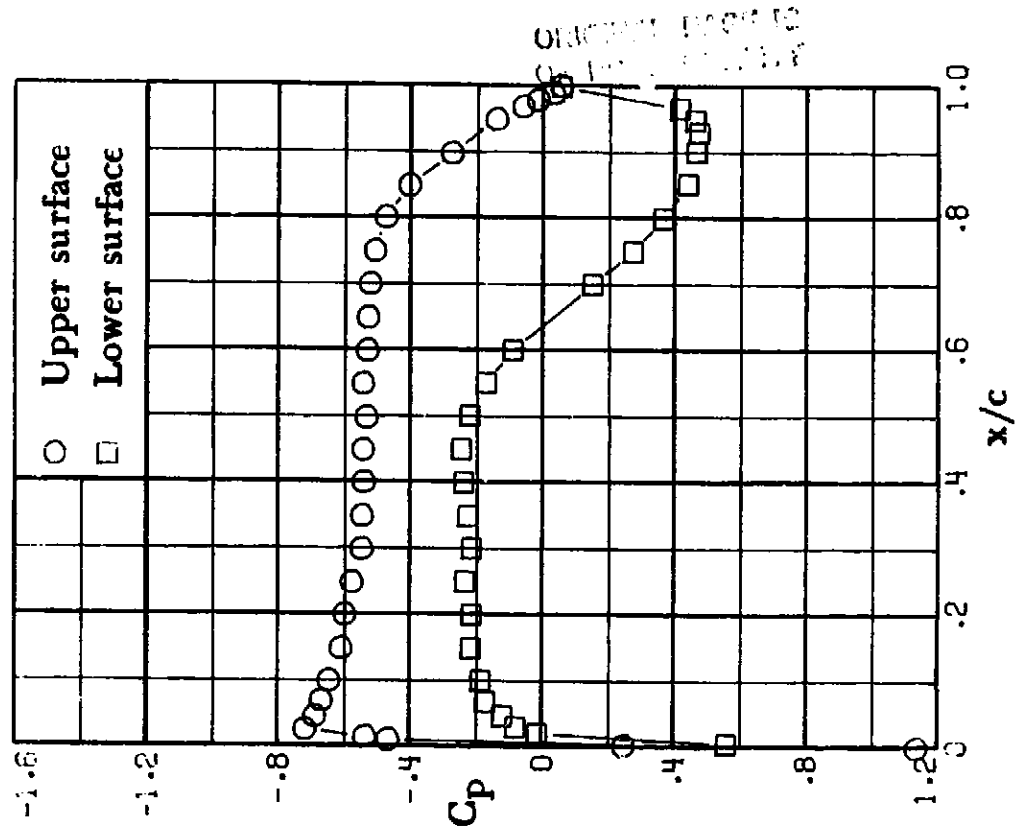


(f) $M = 0.74$; $c_n = 0.65$.

Figure 14. - Continued.



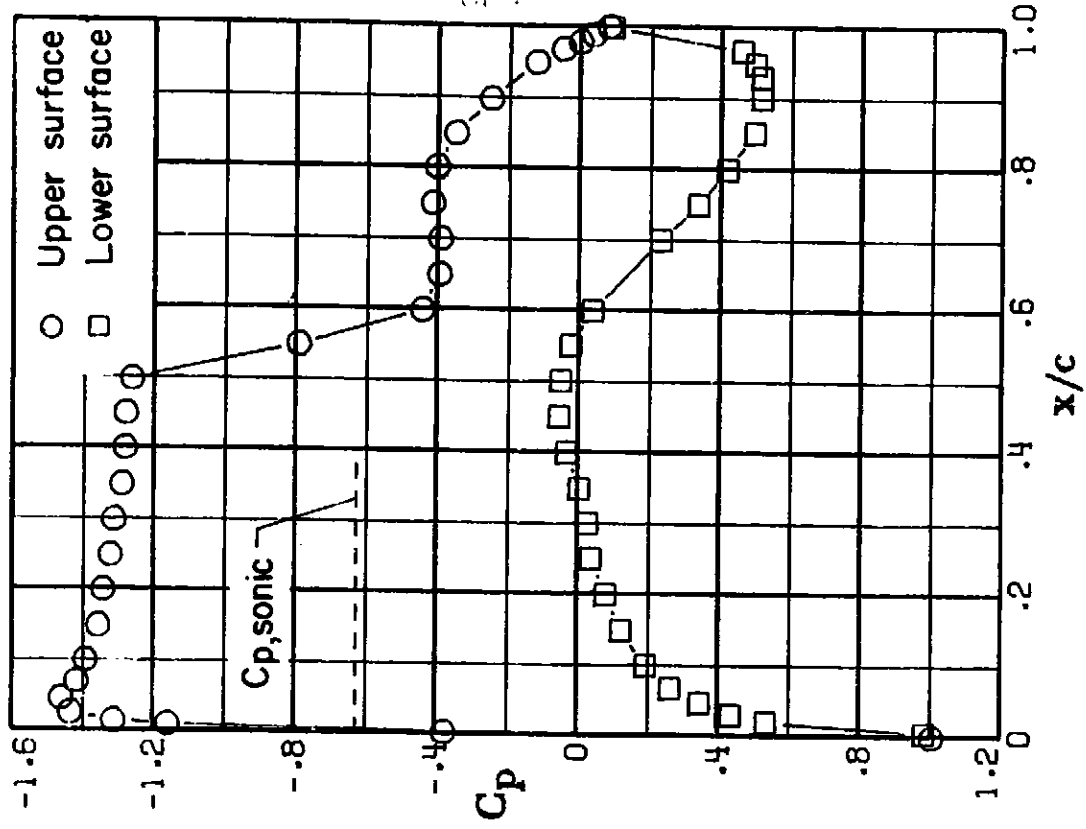
(c) $M = 0.74$; $c_n = 0.41$.



(d) $M = 0.74$; $c_n = 0.50$.

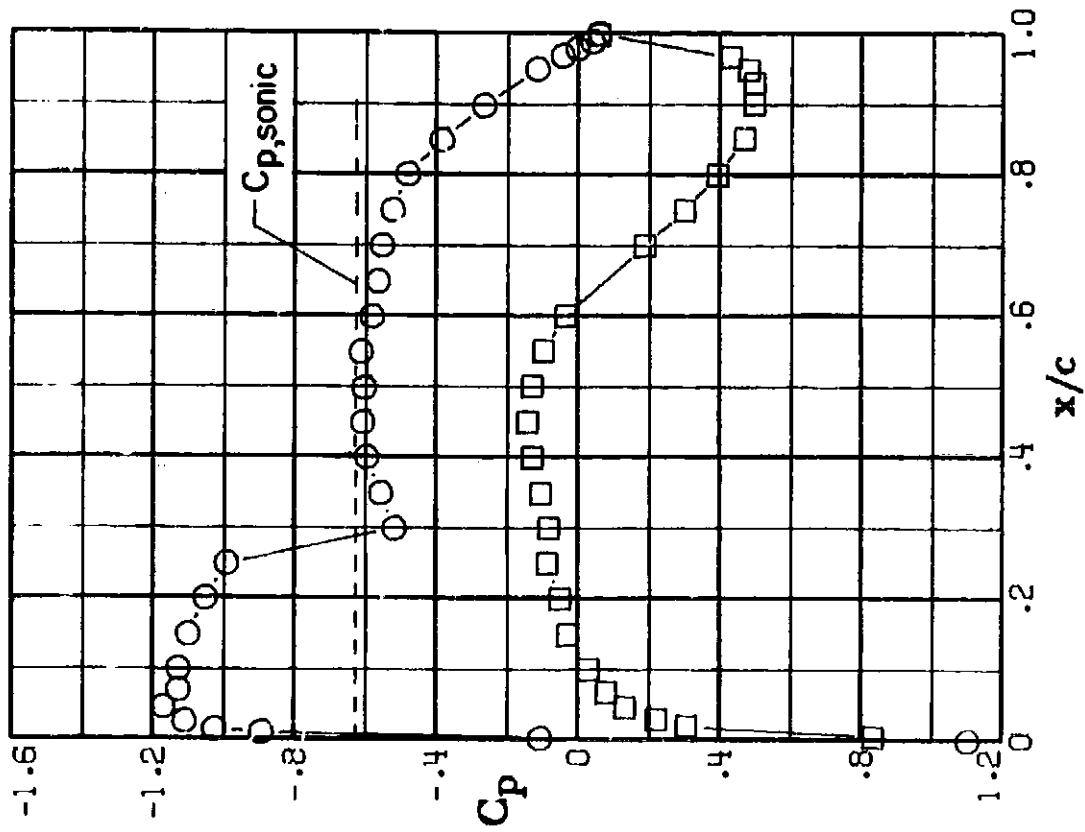
Figure 14. - Continued.

[REDACTED]

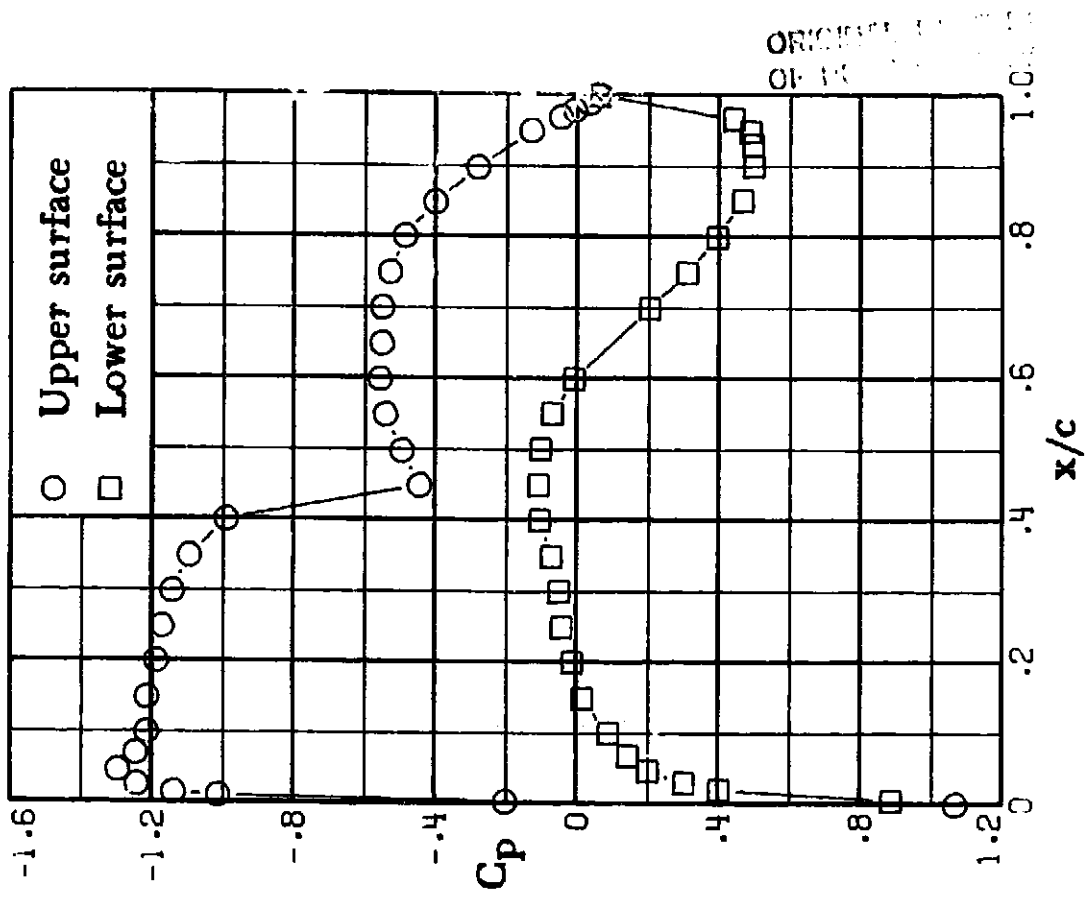


(i) $M = 0.74$; $c_{\Omega} = 1.06$.

Figure 14. - Concluded.



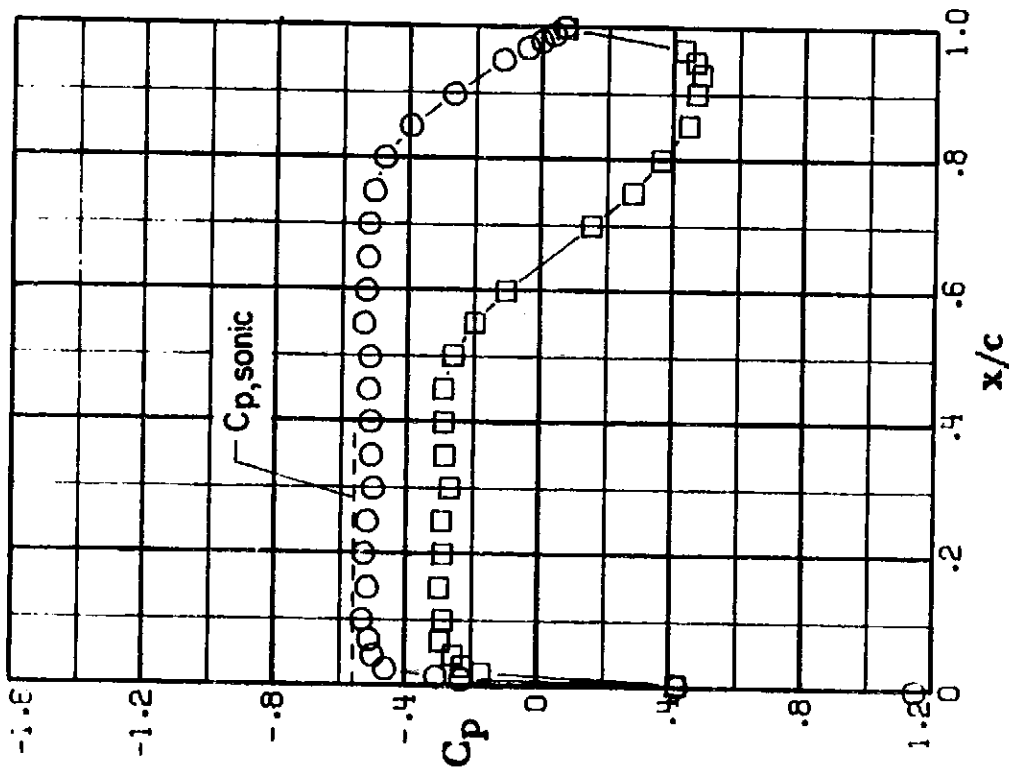
(g) $M = 0.74$; $c_n = 0.74$.



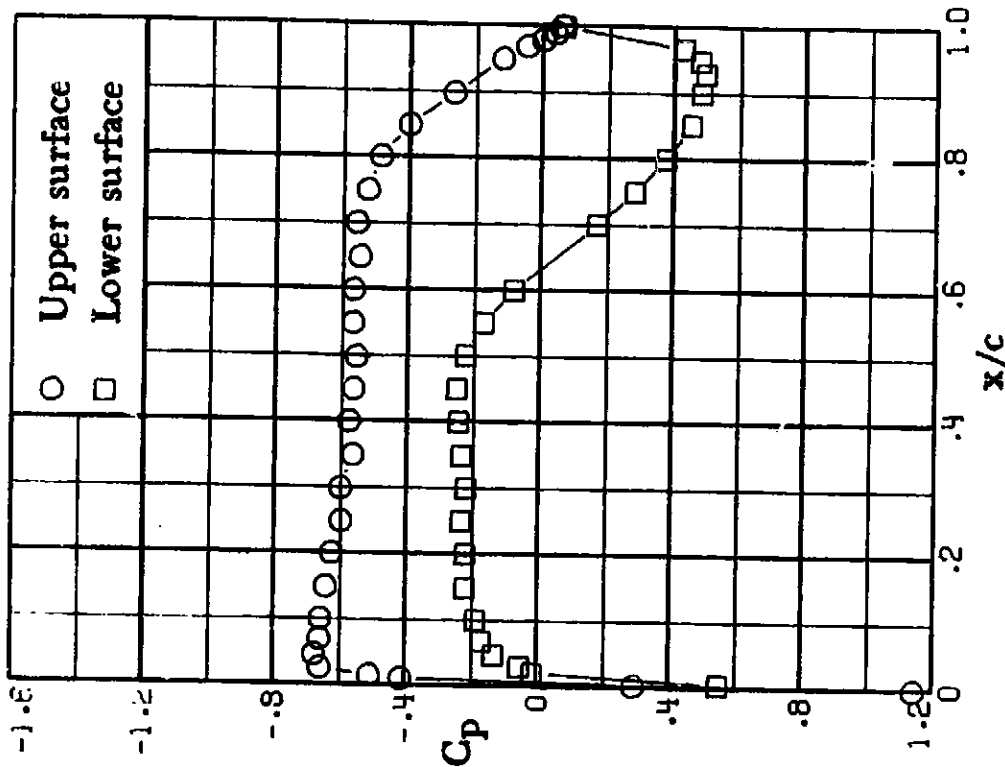
(h) $M = 0.74$; $c_n = 0.86$.

Figure 14. - Continued.

~~CONFIDENTIAL~~



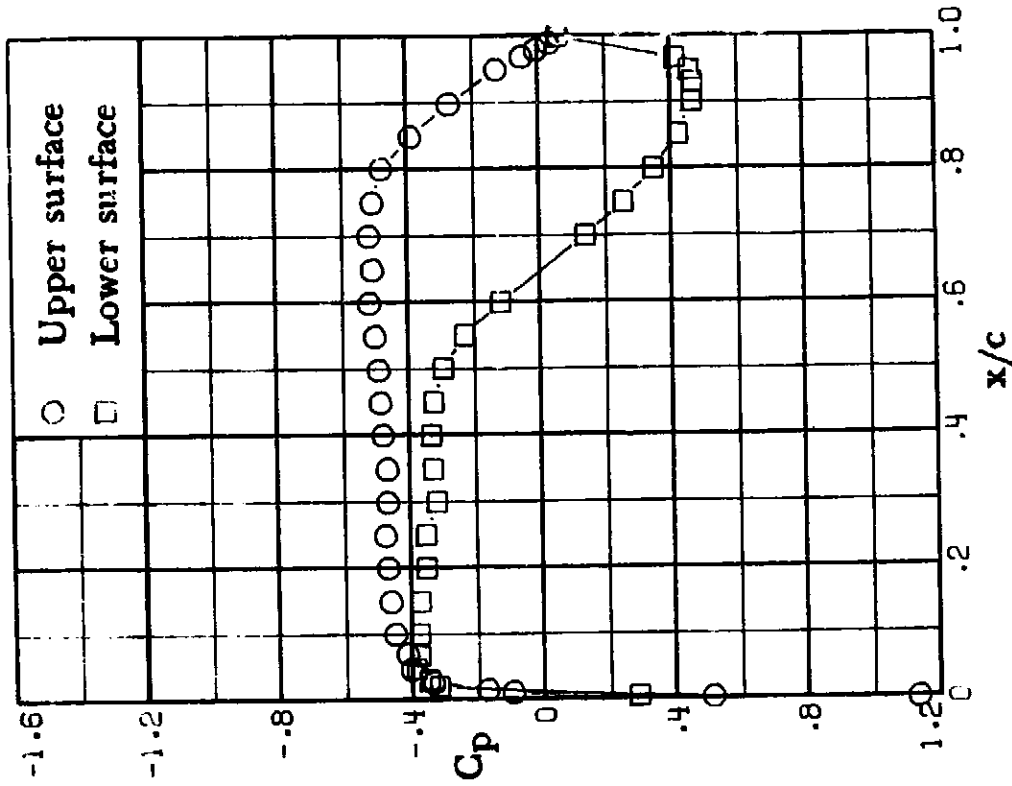
(c) $M = 0.76$; $c_n = 0.41$.



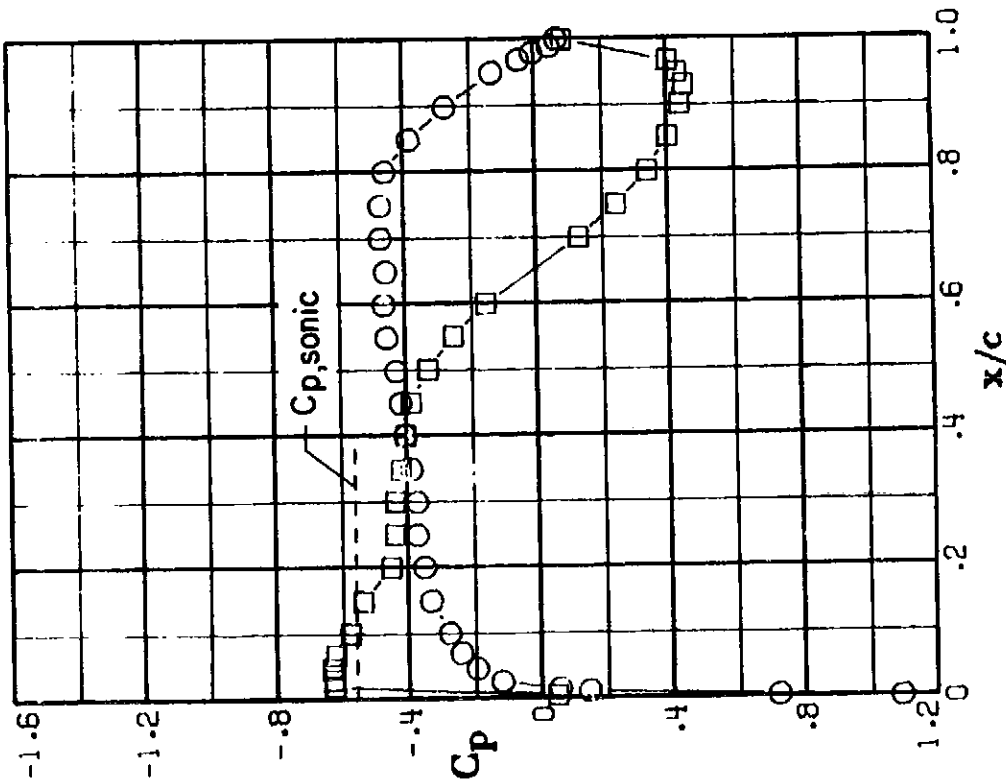
(d) $M = 0.76$; $c_n = 0.52$.

Figure 15. - Continued.

ORIGINAL PAGE IS
OF POOR QUALITY

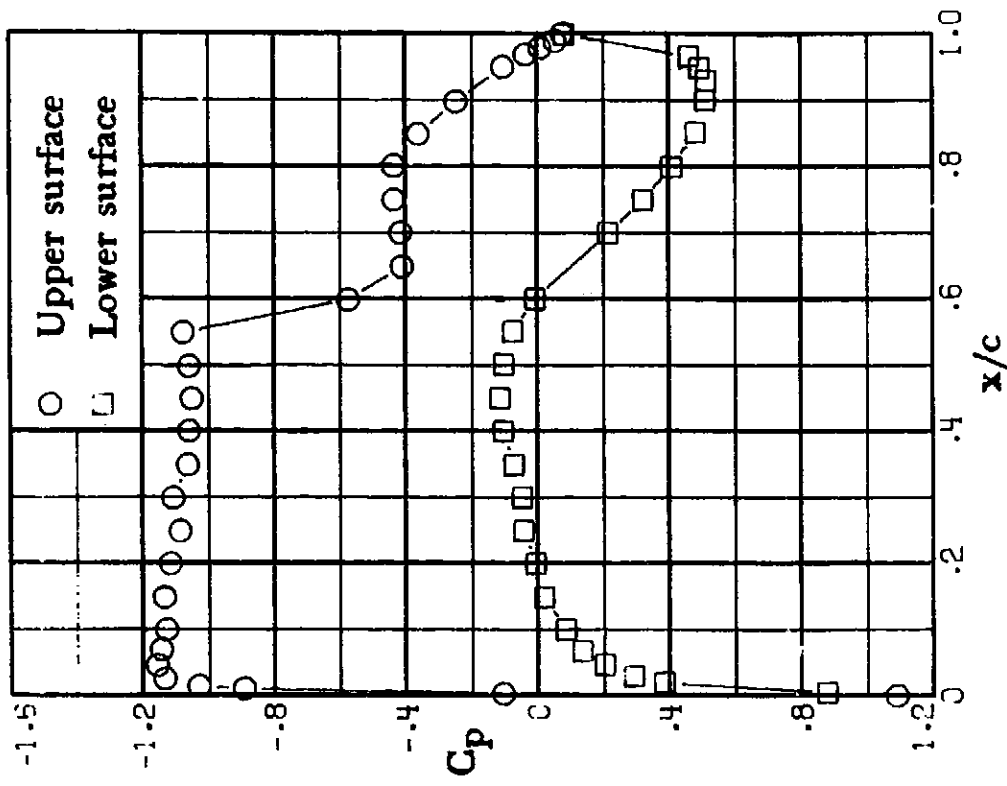


(b) $M = 0.76$; $c_n = 0.34$.

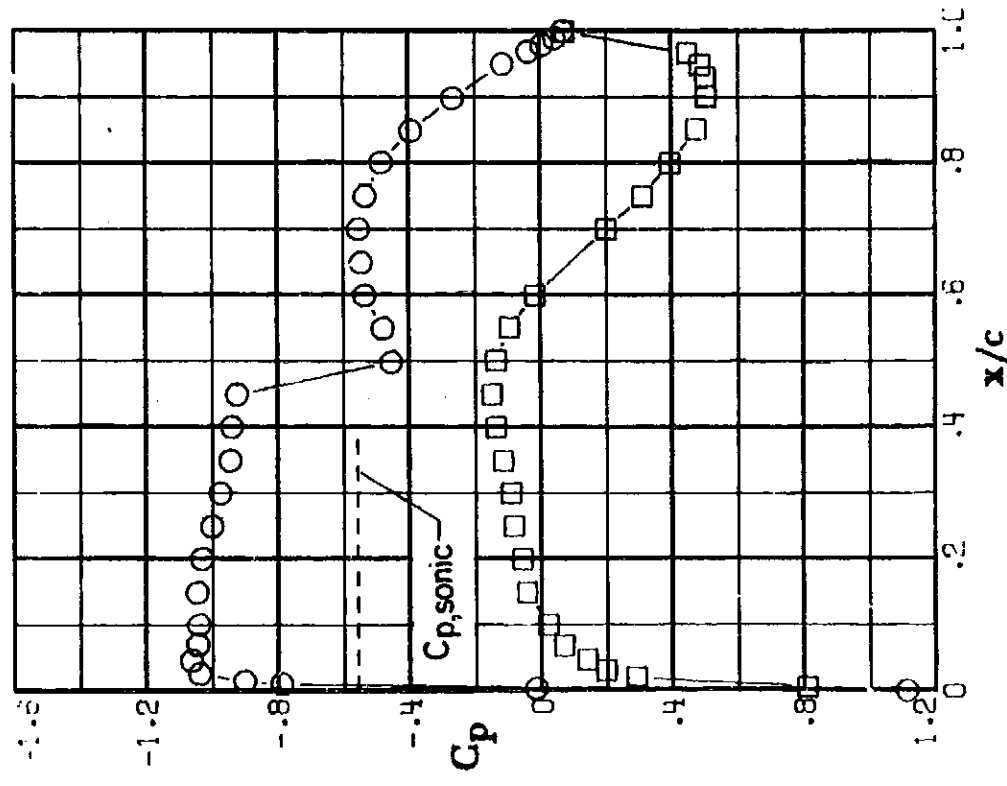


(a) $M = 0.76$; $c_n = 0.19$.

Figure 15.- Chordwise pressure distributions for 10-percent thick supercritical airfoil 33. $M = 0.76$.

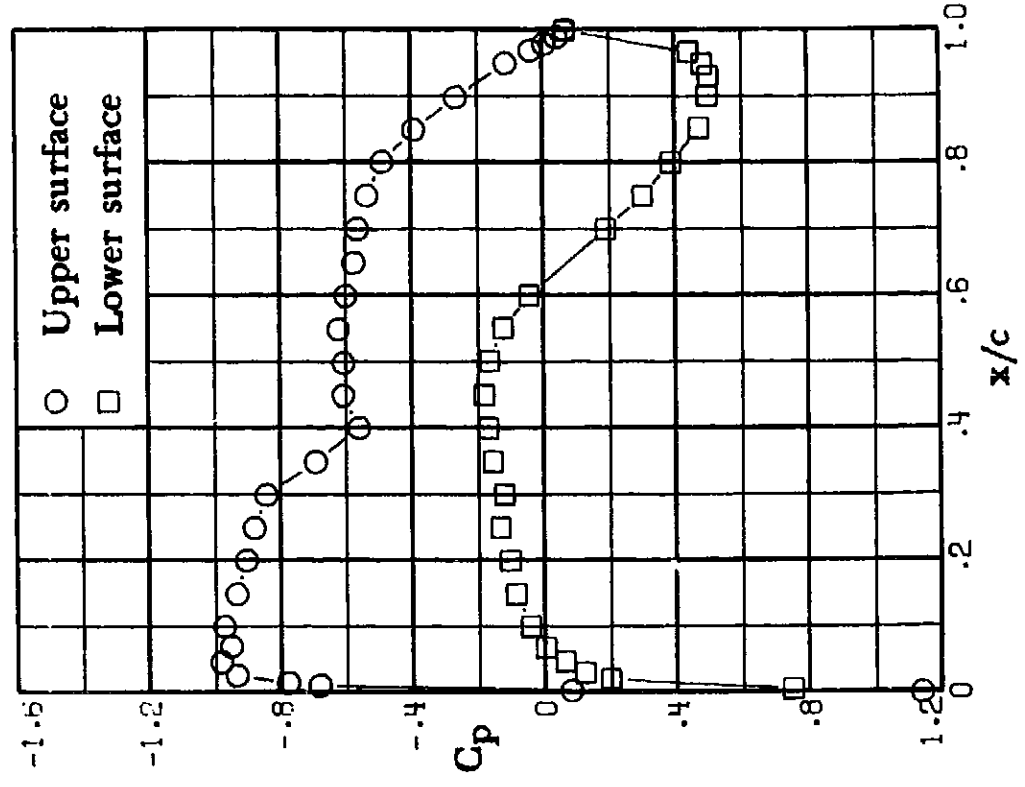


(h) $M = 0.76$; $c_n = 0.90$.

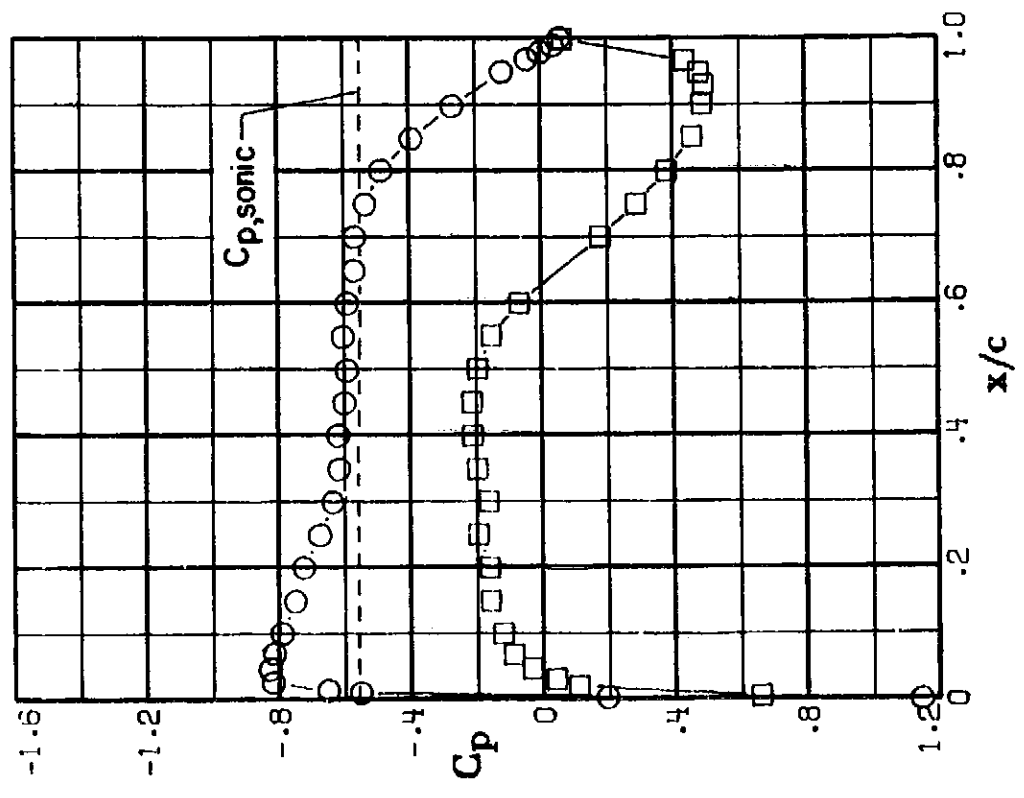


(g) $M = 0.76$; $c_n = 0.78$.

Figure 15. - Continued.

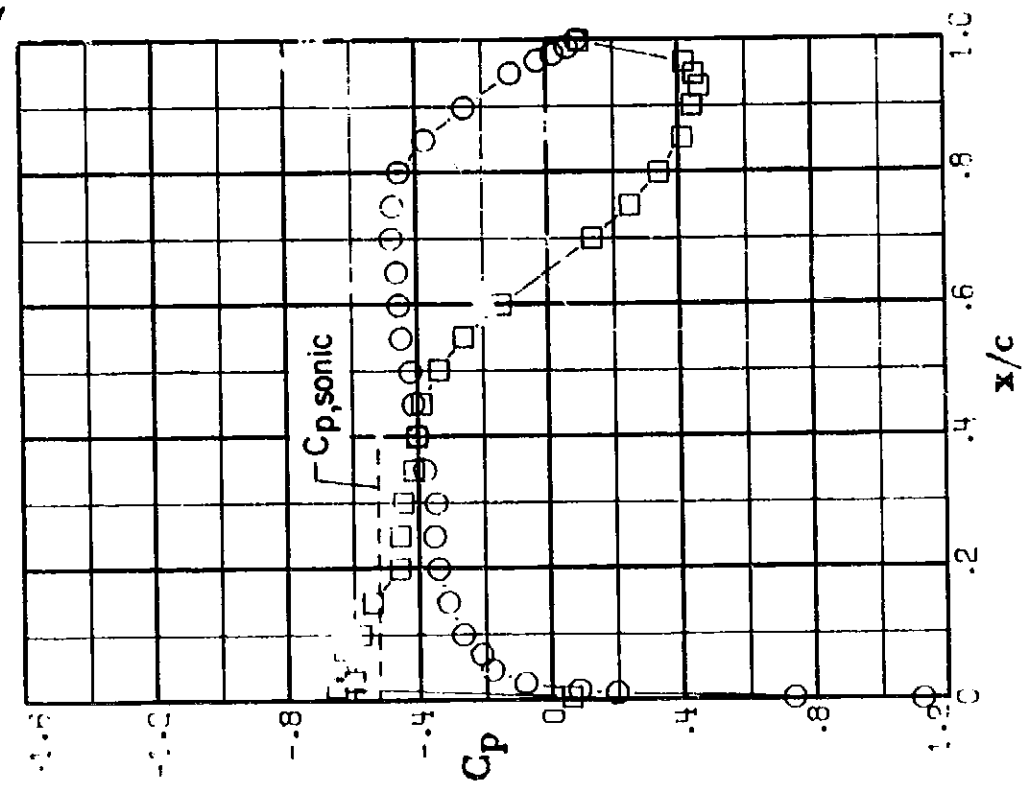


(f) $M = 0.76$; $c_n = 0.69$.

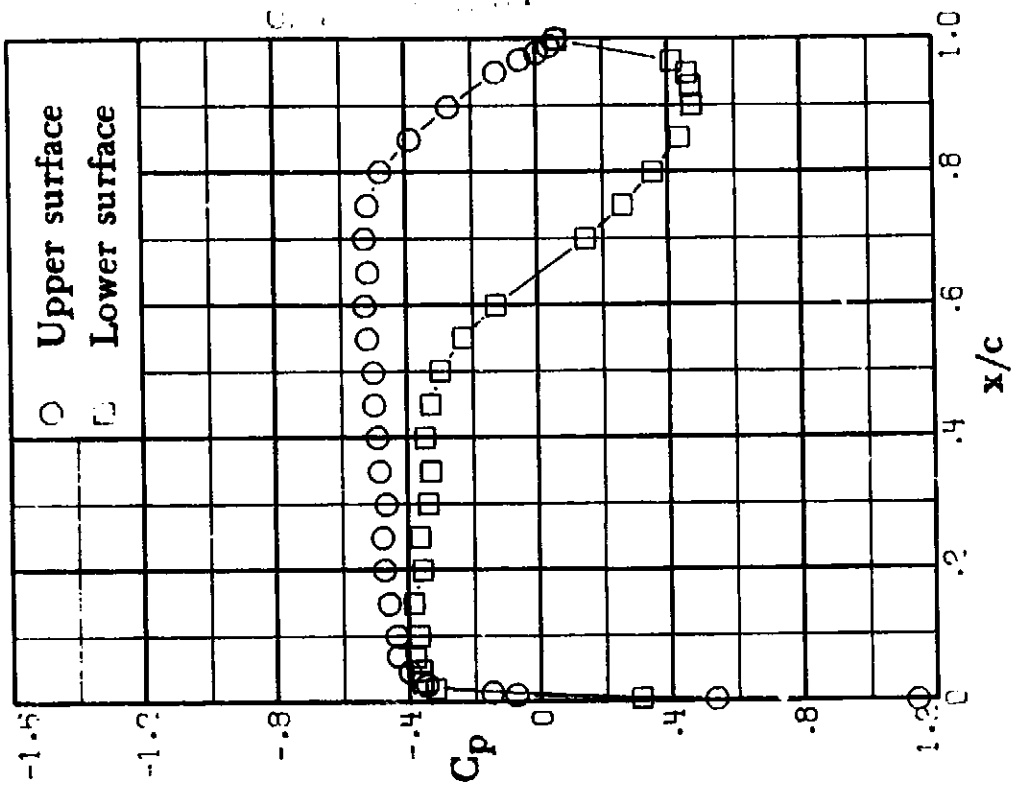


(e) $M = 0.76$; $c_n = 0.59$.

Figure 15. - Continued.

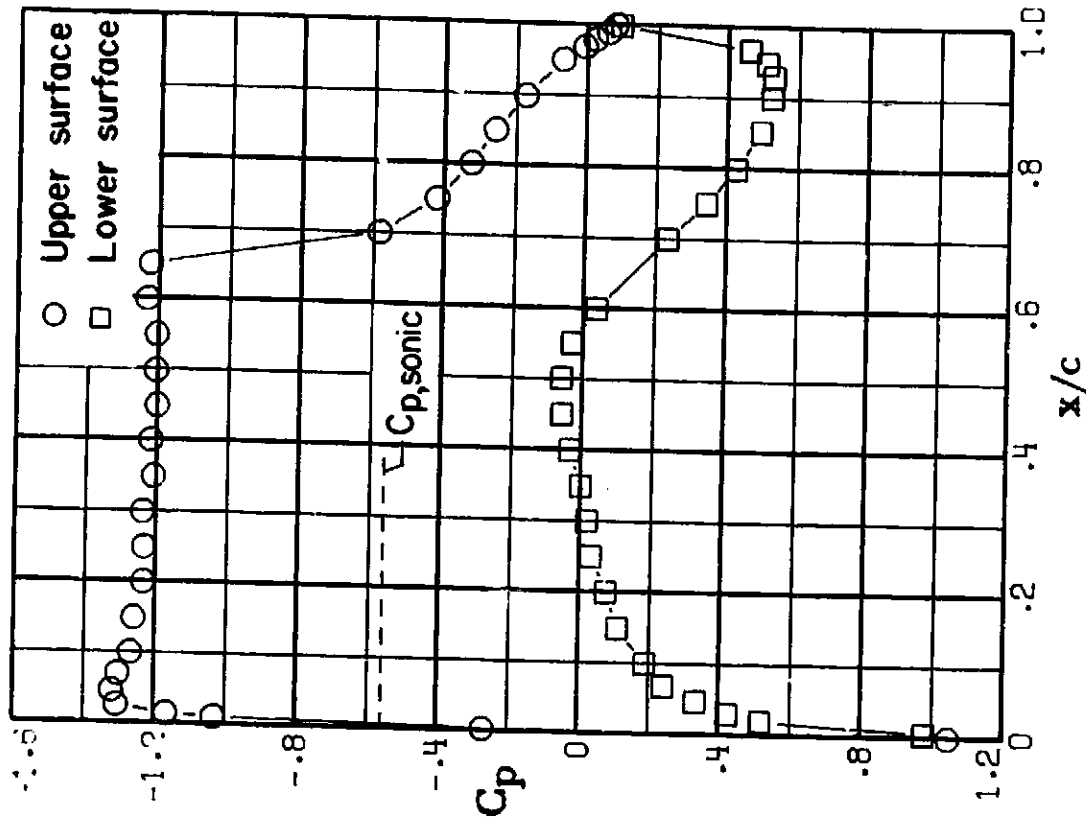


(a) $M = 0.77$; $c_n = 0.18$.



(b) $M = 0.77$; $c_n = 0.94$.

Figure 16. - Chordwise pressure distributions for 10-percent thick supercritical airfoil 33. $M = 0.77$.

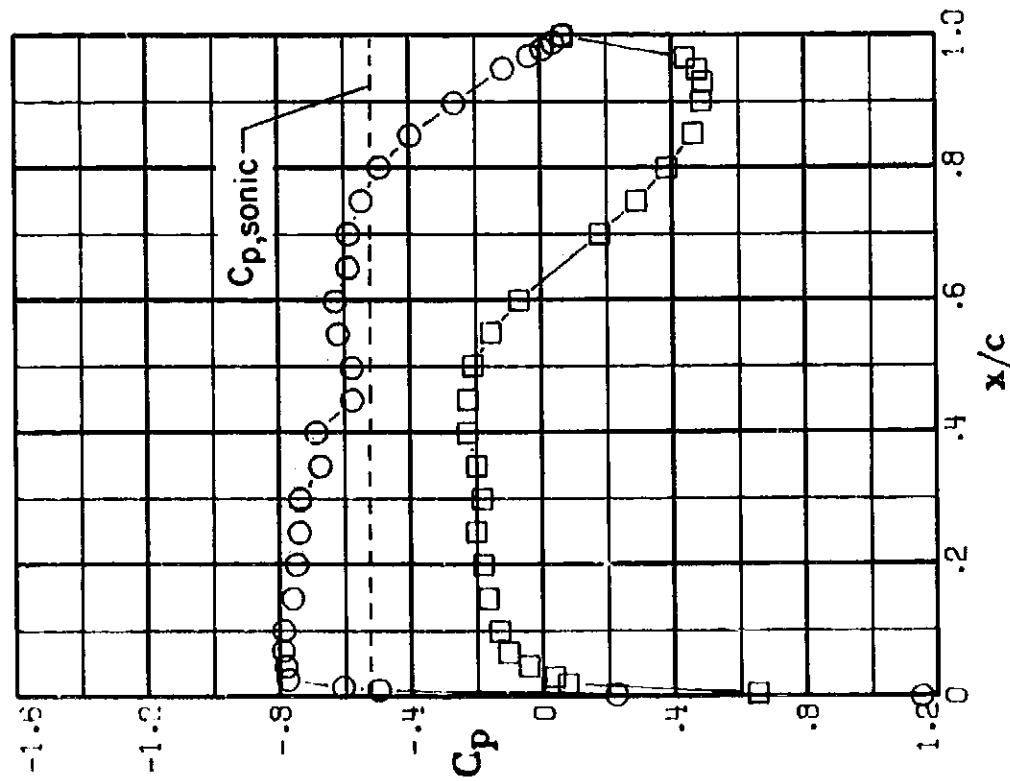


(i) $M = 0.76$; $c_n = 1.10$.

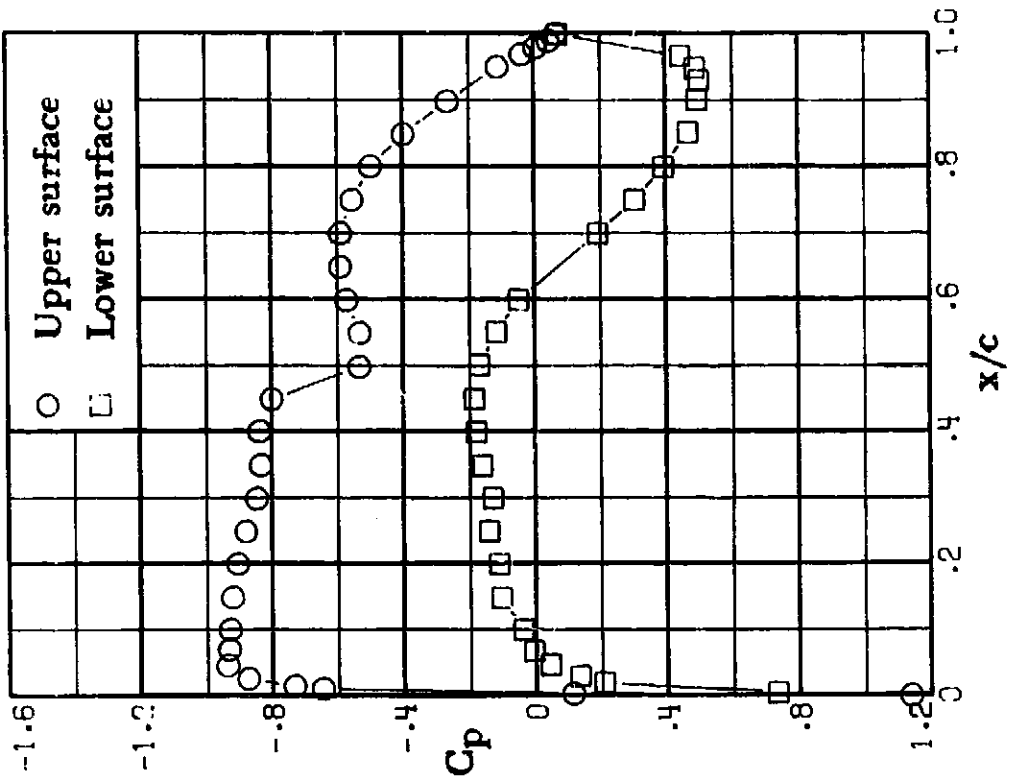
Figure 15. - Concluded.

SHEET 2

CONFIDENTIAL

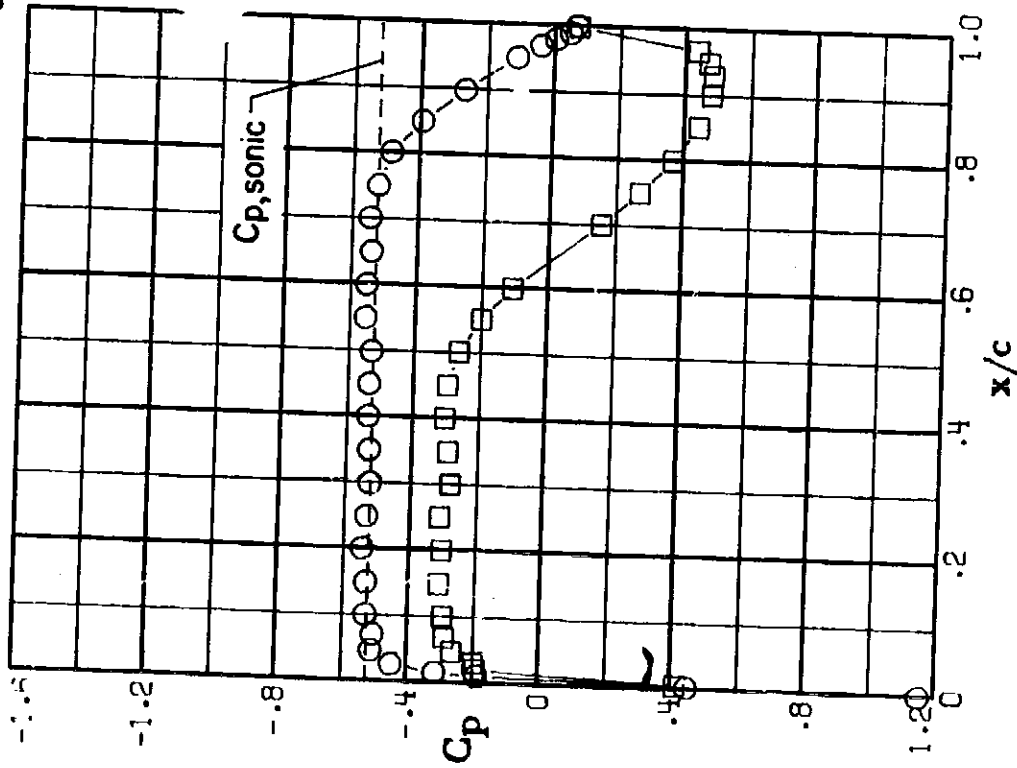


(e) $M = 0.77$; $c_n = 0.60$.

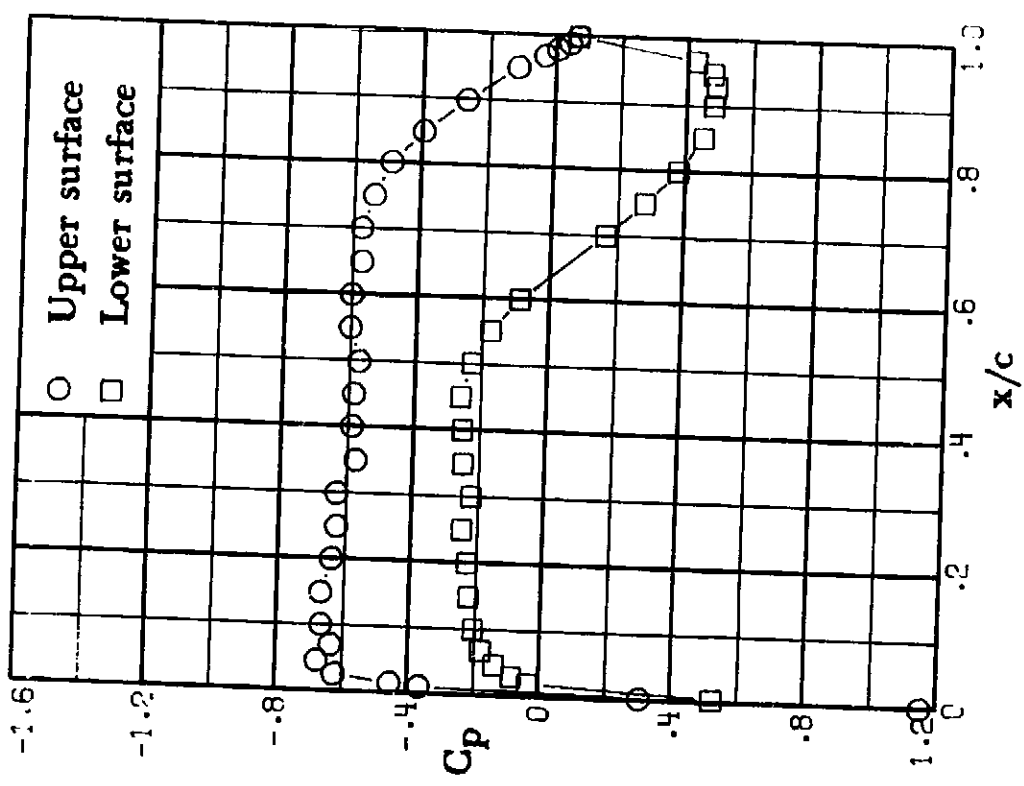


(f) $M = 0.77$; $c_n = 0.71$.

Figure 16. - Continued.

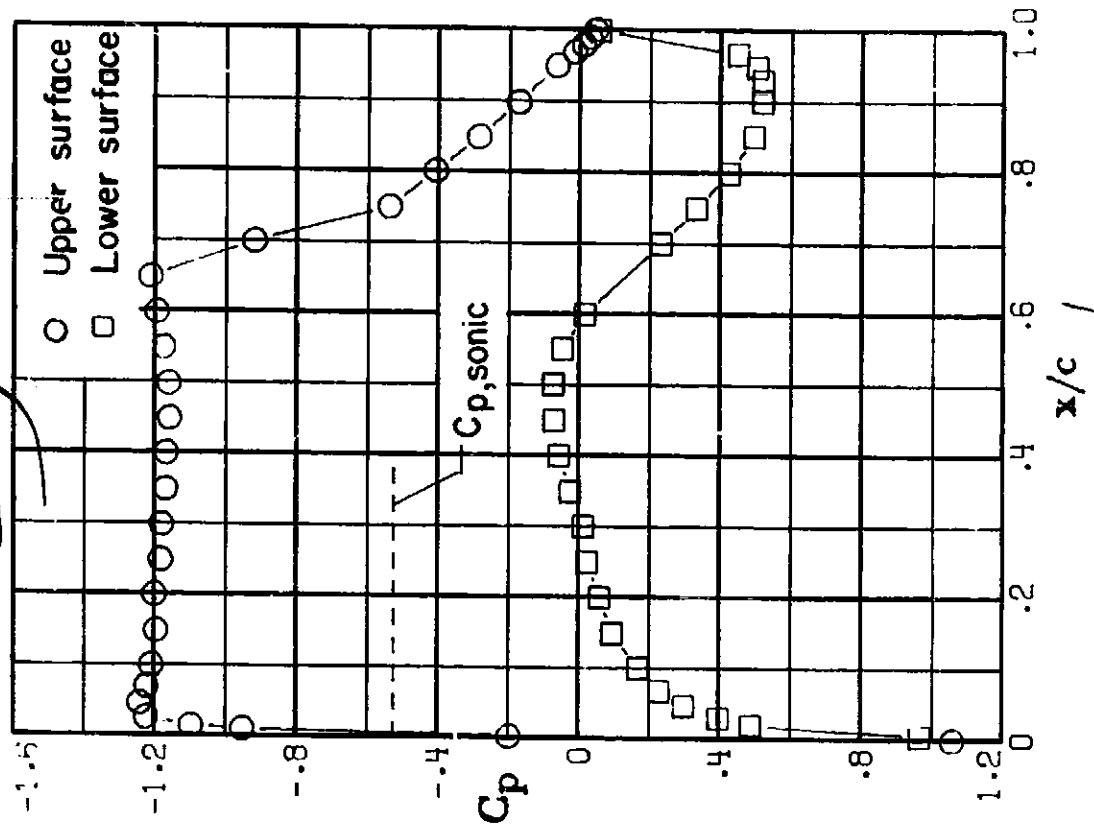


(c) $M = 0.77$; $c_n = 0.42$.



(d) $M = 0.77$; $c_n = 0.52$.

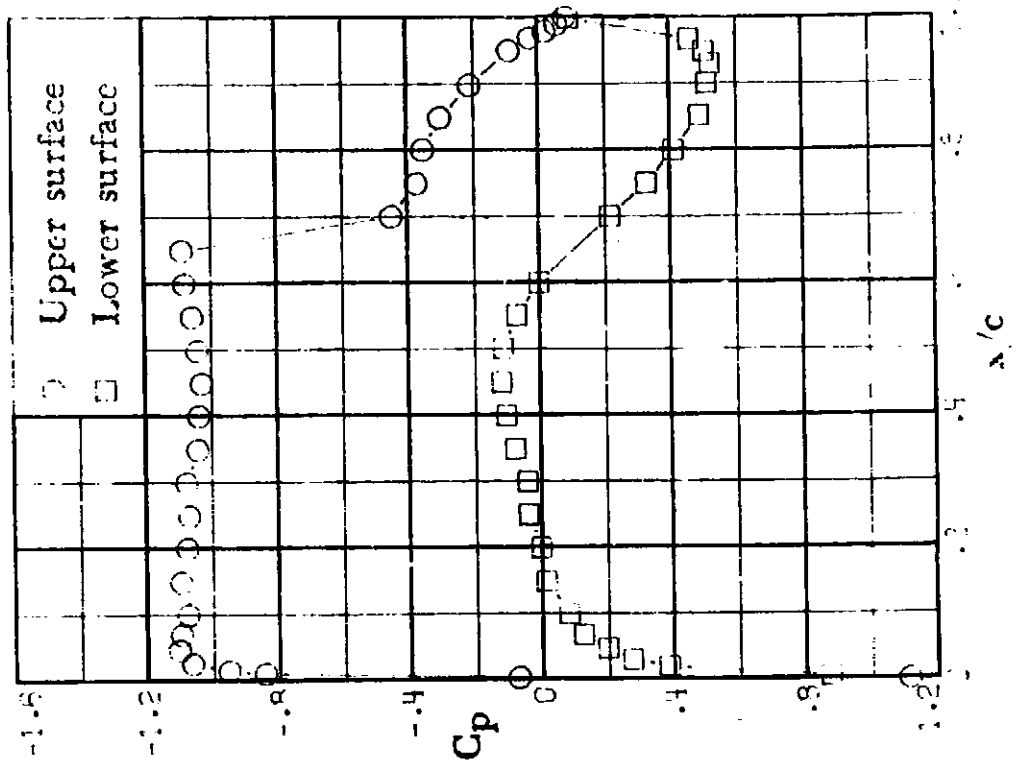
Figure 16. - Continued.



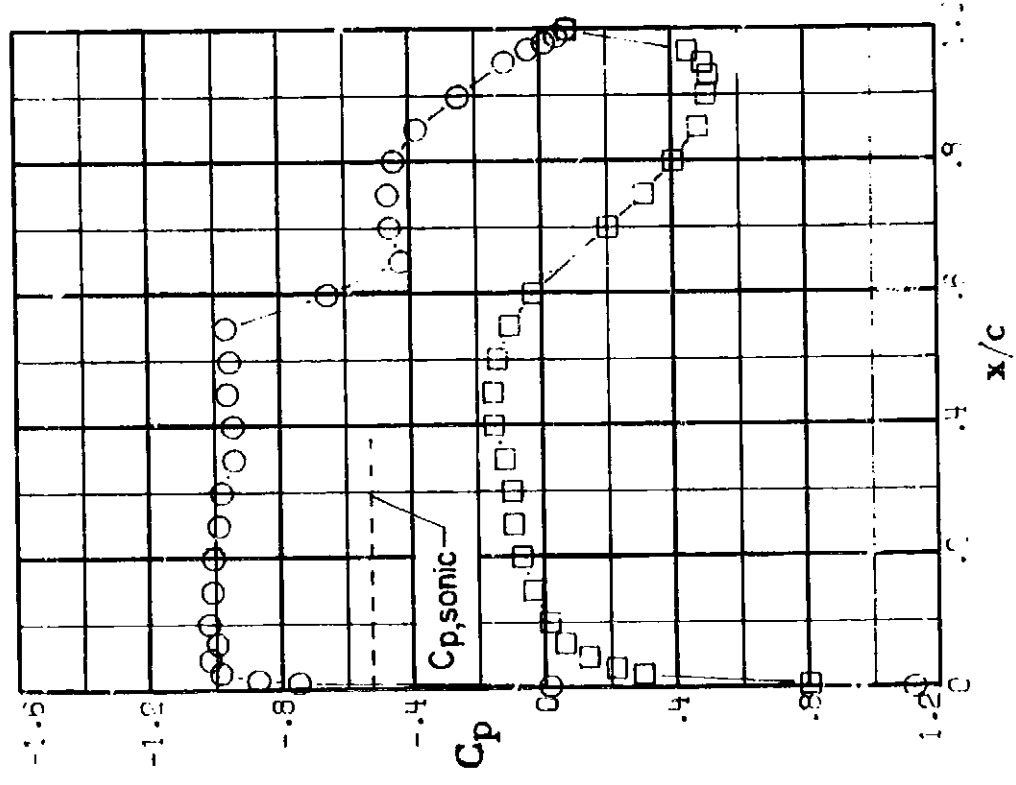
(i) $M = 0.77$; $c_n = 1.09$.

Figure 16. - Concluded.

NEW YORK UNIVERSITY
OFFICE OF AERONAUTICS

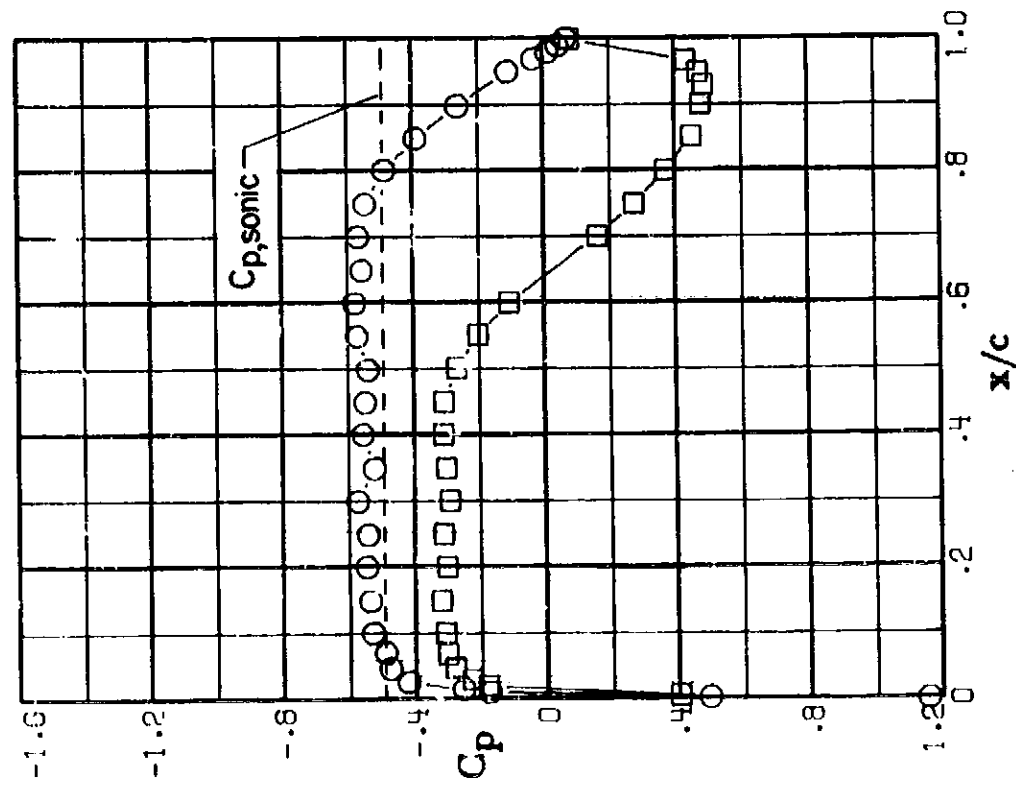


(h) $M = 0.77$ $c_n = 0.93$.

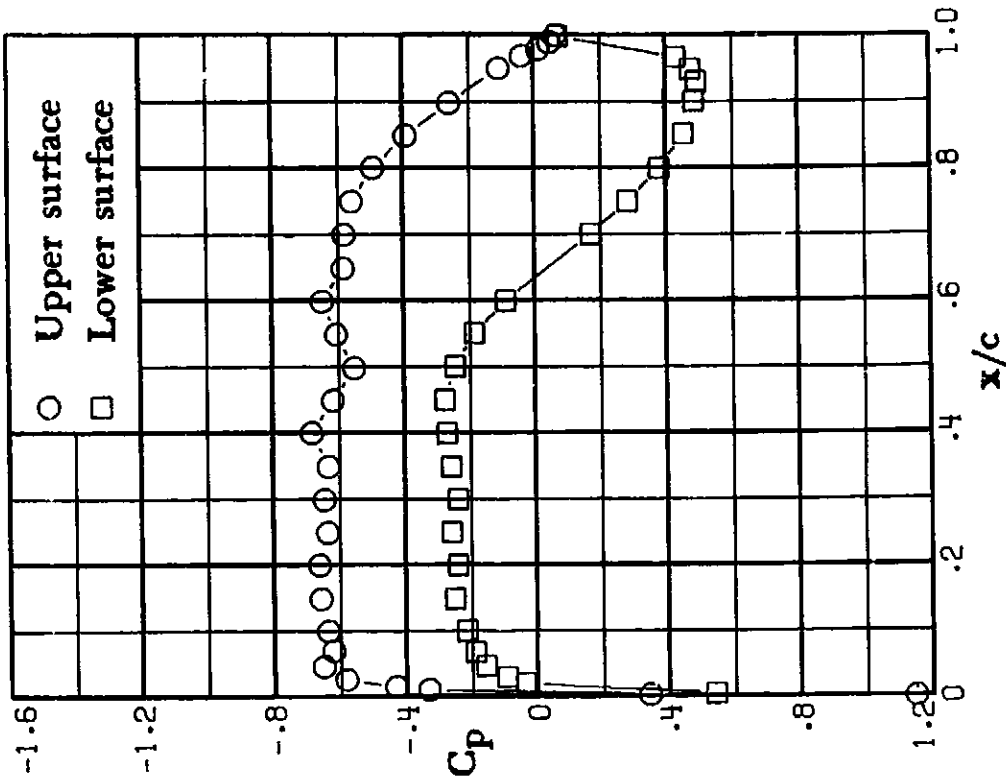


(g) $M = 0.77$ $c_n = 0.81$.

Figure 16. - Continued.

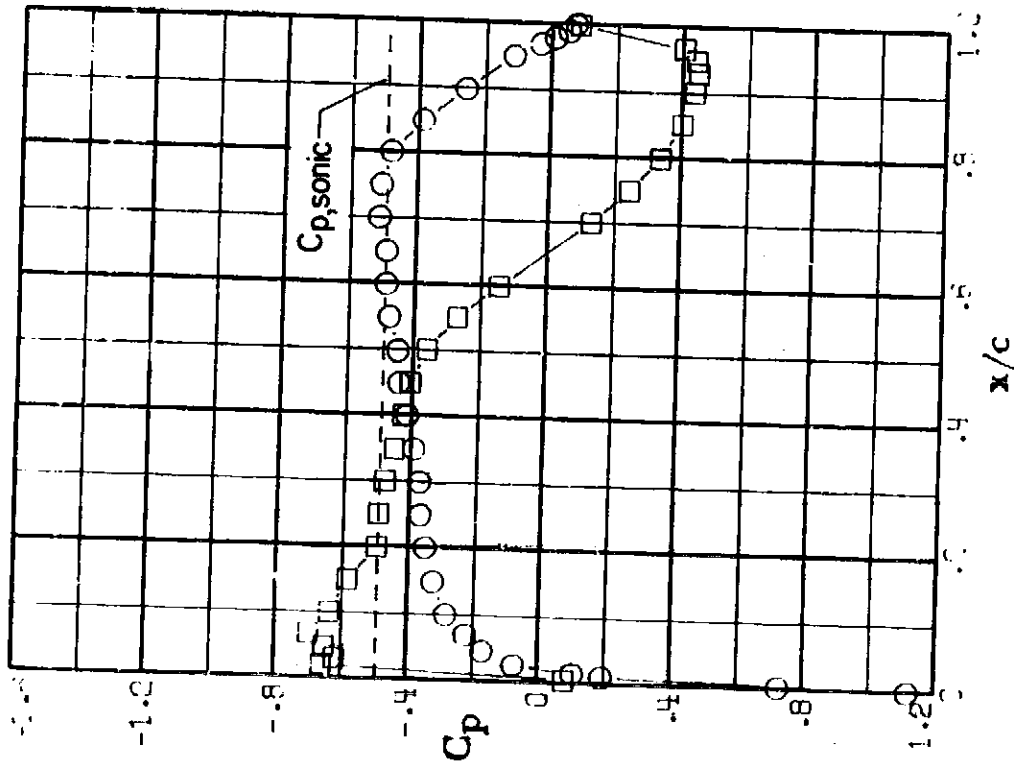


(c) $M = 0.78$; $c_n = 0.42$.

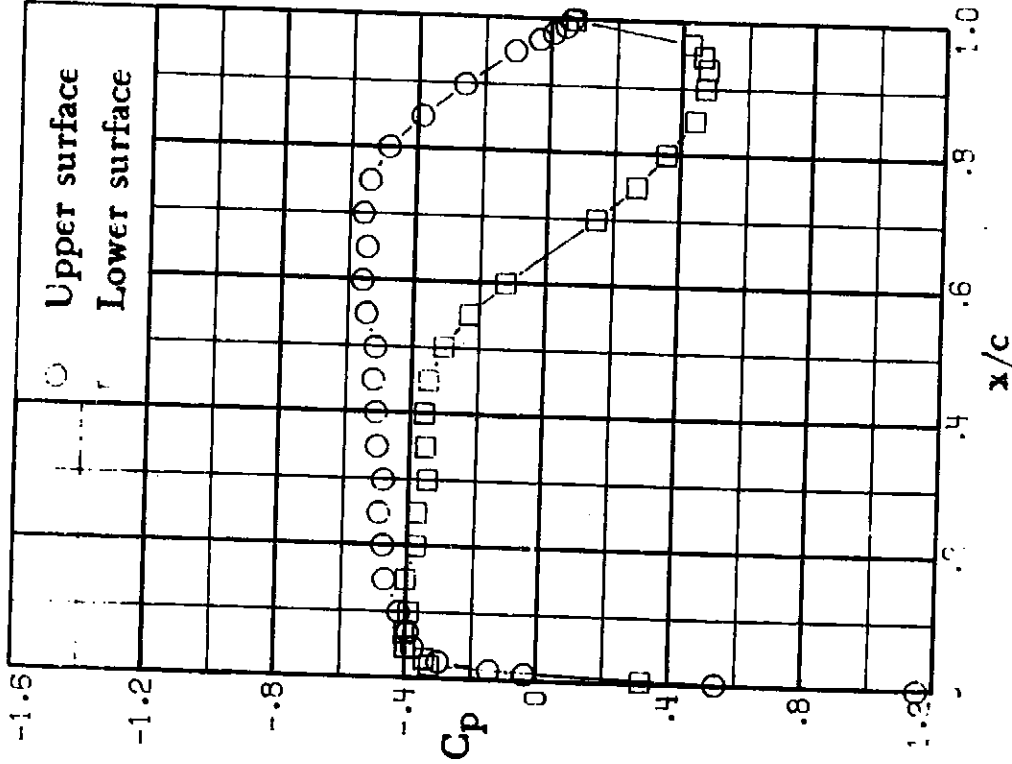


(d) $M = 0.78$; $c_n = 0.52$.

Figure 17. - Continued.



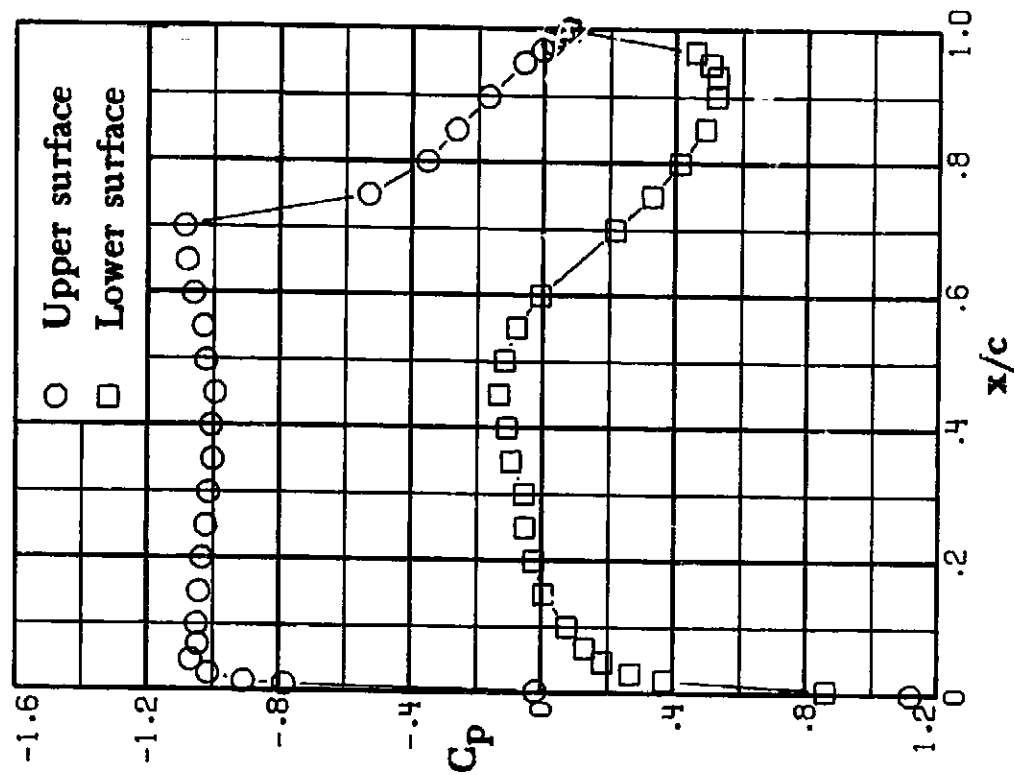
(a) $M = 0.78$; $c_n = 0.18$.



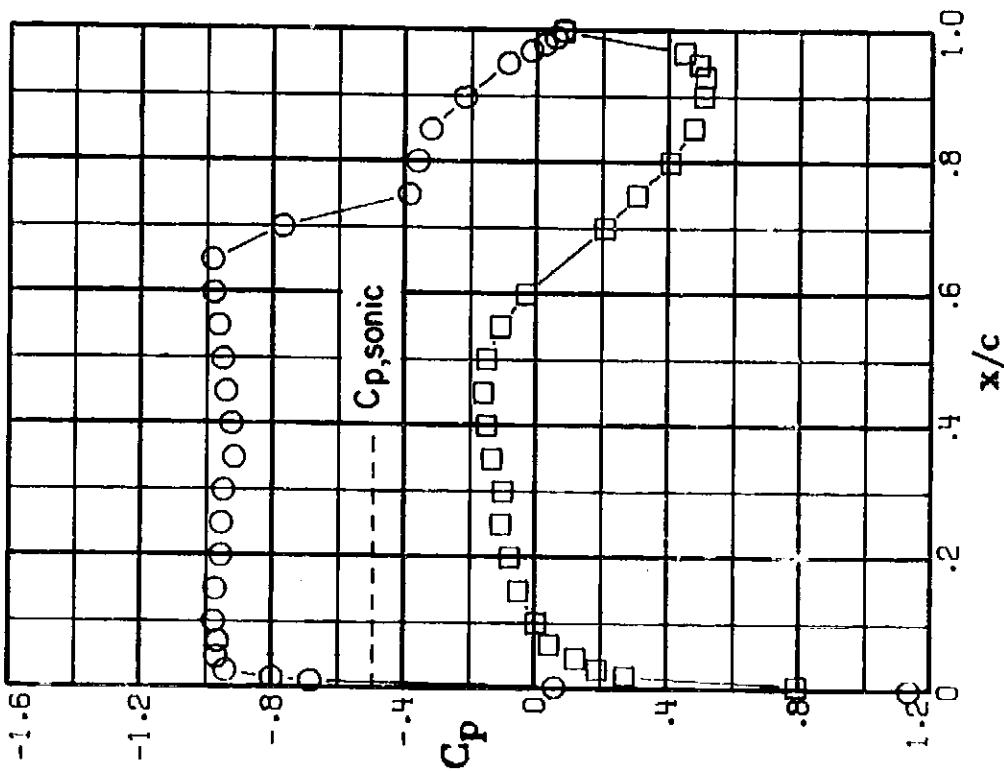
(b) $M = 0.78$; $c_n = 0.35$.

Figure 17.- Chordwise pressure distributions for 10-percent thick supercritical airfoil 33. $M = 0.78$.

ORIGINAL PAGE IS
OF POOR QUALITY



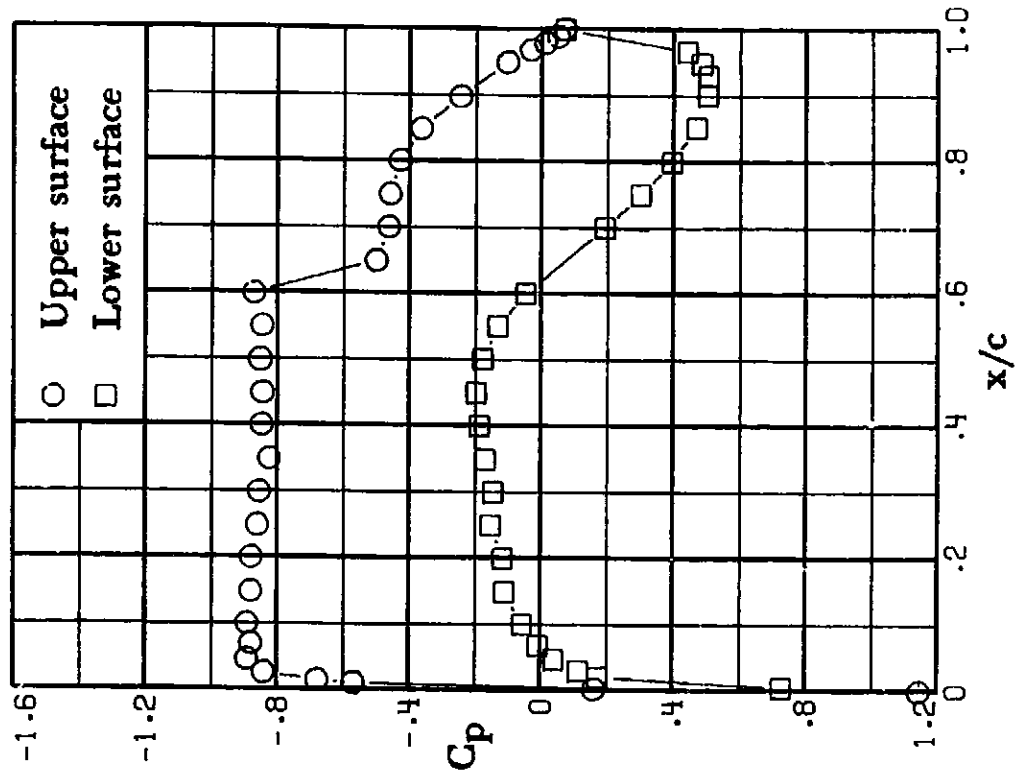
(h) $M = 0.78$; $c_n = 0.94$.



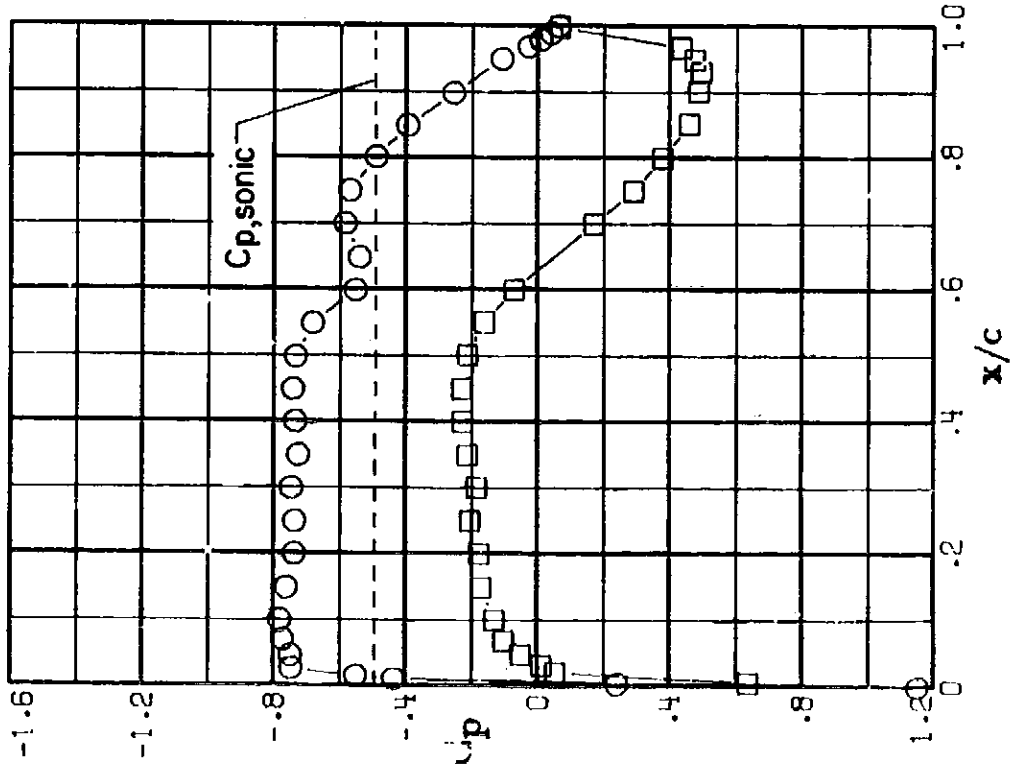
(g) $M = 0.78$; $c_n = 0.84$.

Figure 17. - Concluded.

ORIGINAL QUALITY
OF PAPER GUARANTEED



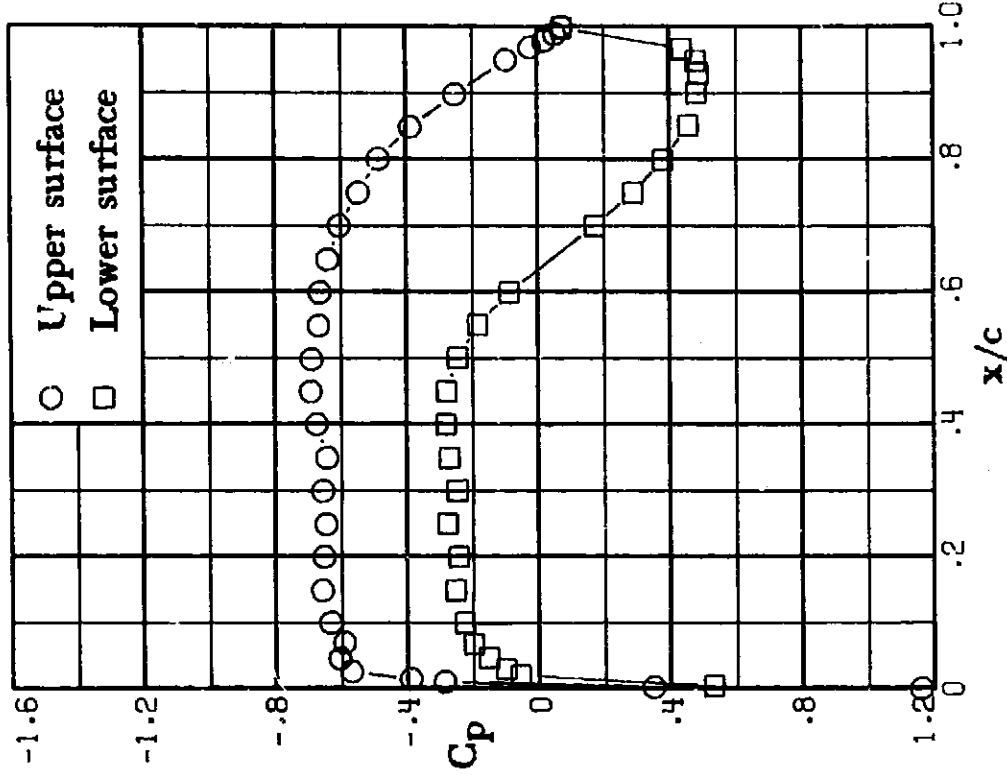
(f) $M = 0.78$; $c_n = 0.72$.



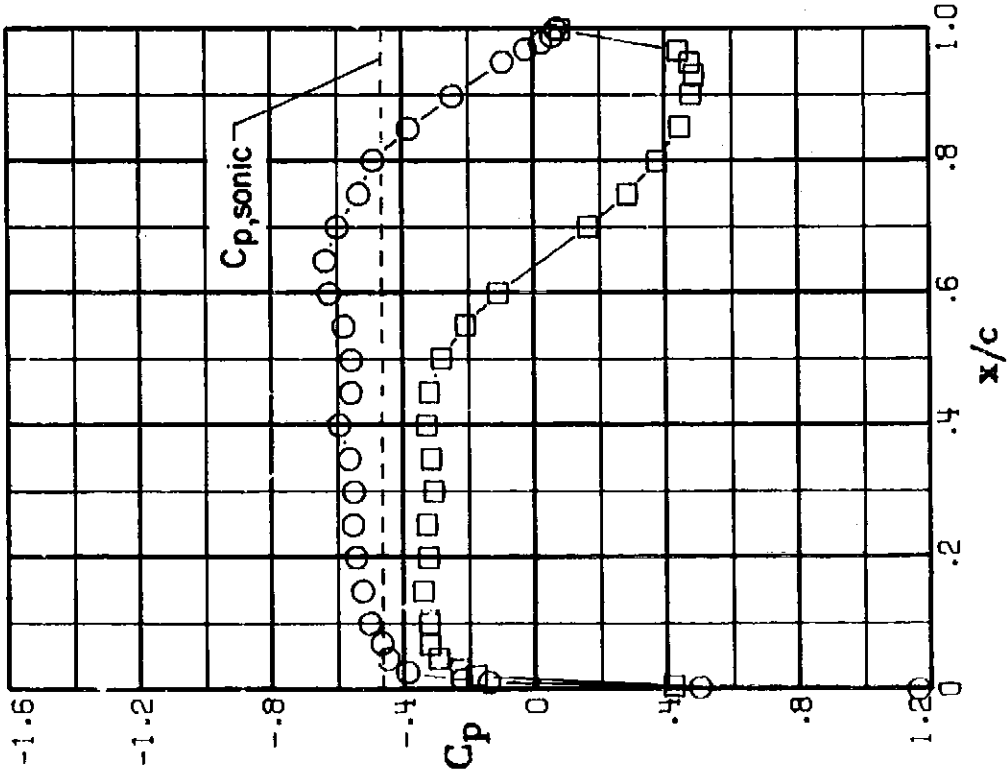
(e) $M = 0.78$; $c_n = 0.62$.

Figure 17. - Continued.

ORIGINAL PAGE IS
OF THIS QUALITY

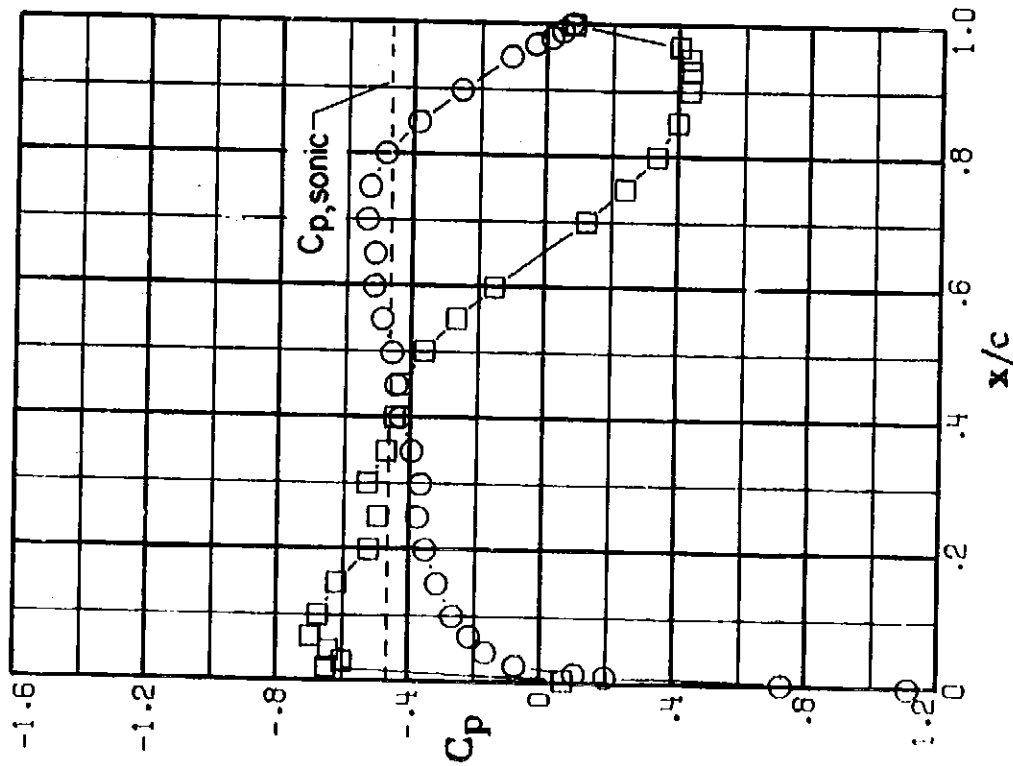


(d) $M = 0.79$; $c_n = 0.54$.

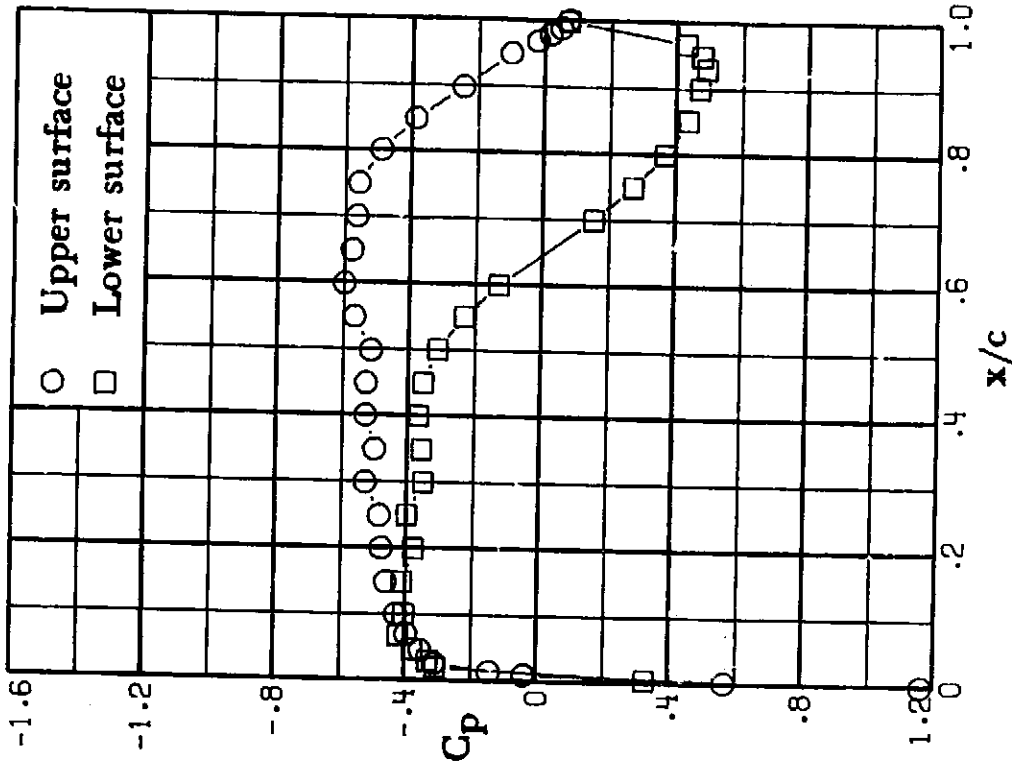


(c) $M = 0.79$; $c_n = 0.42$.

Figure 18. - Continued.



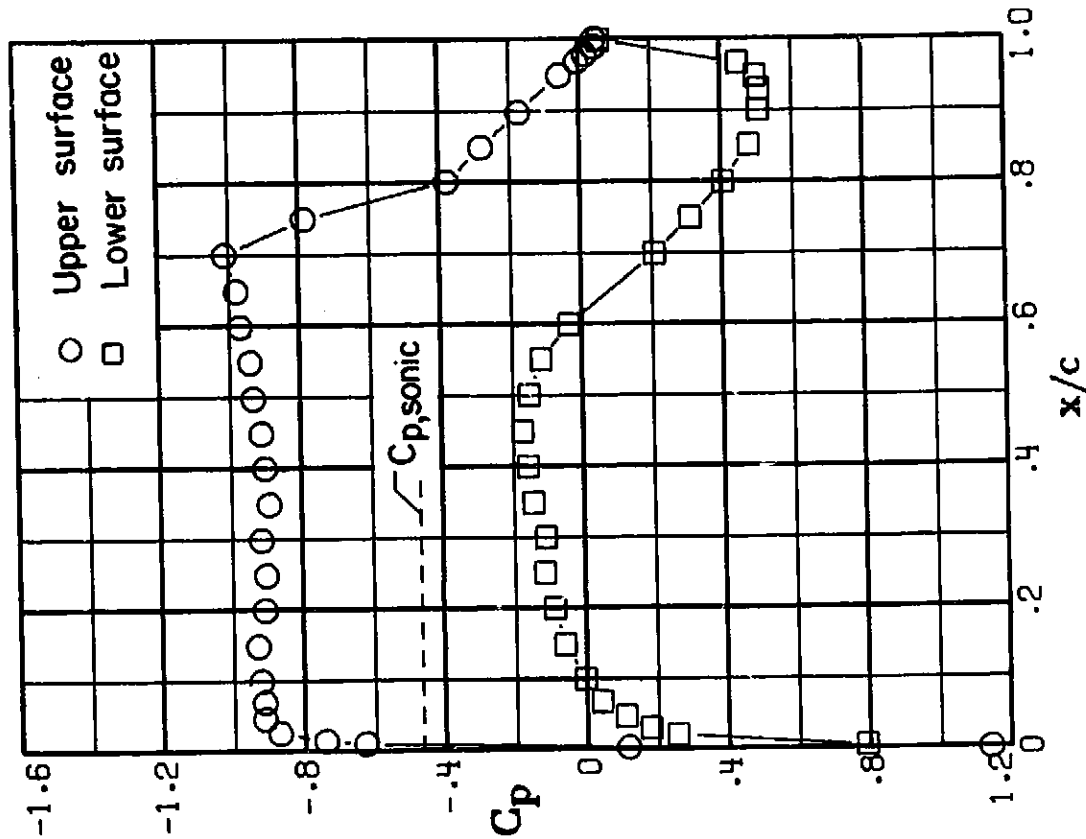
(a) $M = 0.79$; $c_n = 0.18$.



(b) $M = 0.79$; $c_n = 0.35$.

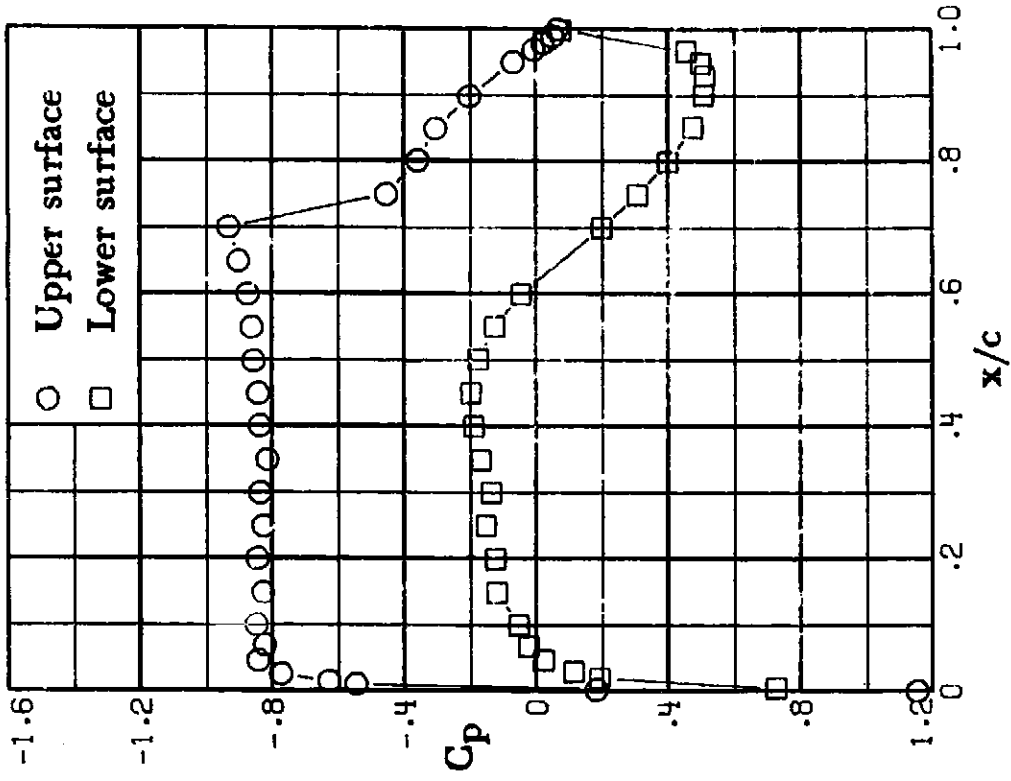
Figure 18. - Chordwise pressure distributions for 10-percent thick supercritical airfoil 33. $M = 0.79$.

CONFIDENTIAL

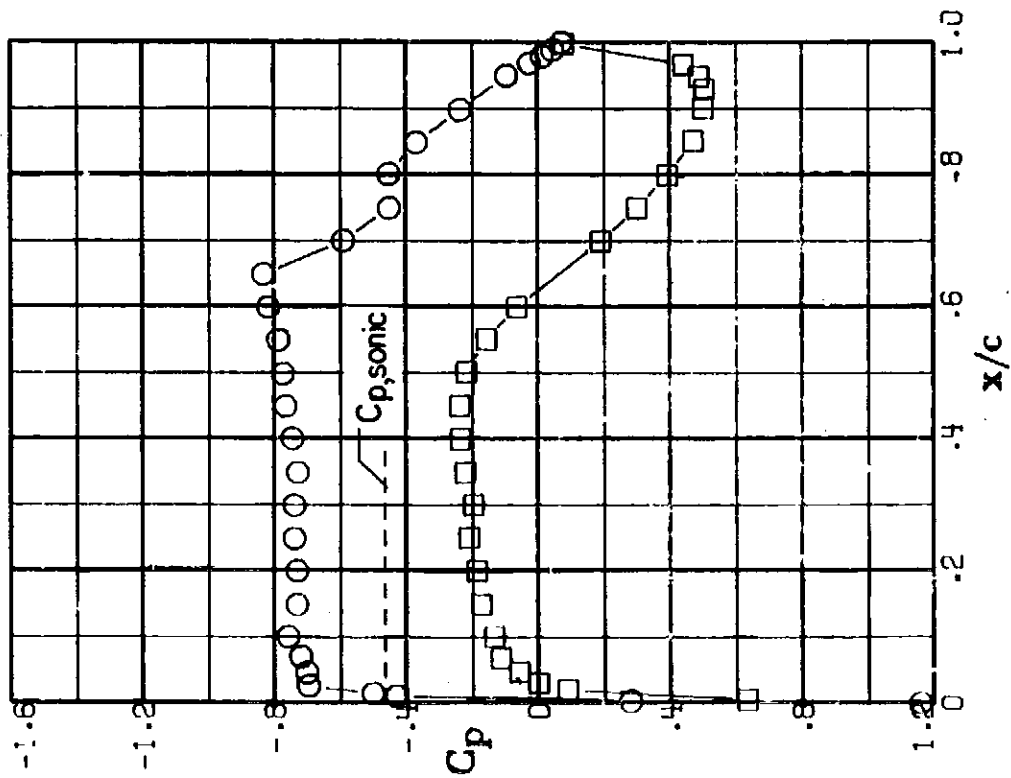


(g) $M = 0.79$; $c_n = 0.84$.

Figure 18. - Concluded.



(e) $M = 0.79$; $c_n = 0.64$.



(f) $M = 0.79$; $c_n = 0.74$.

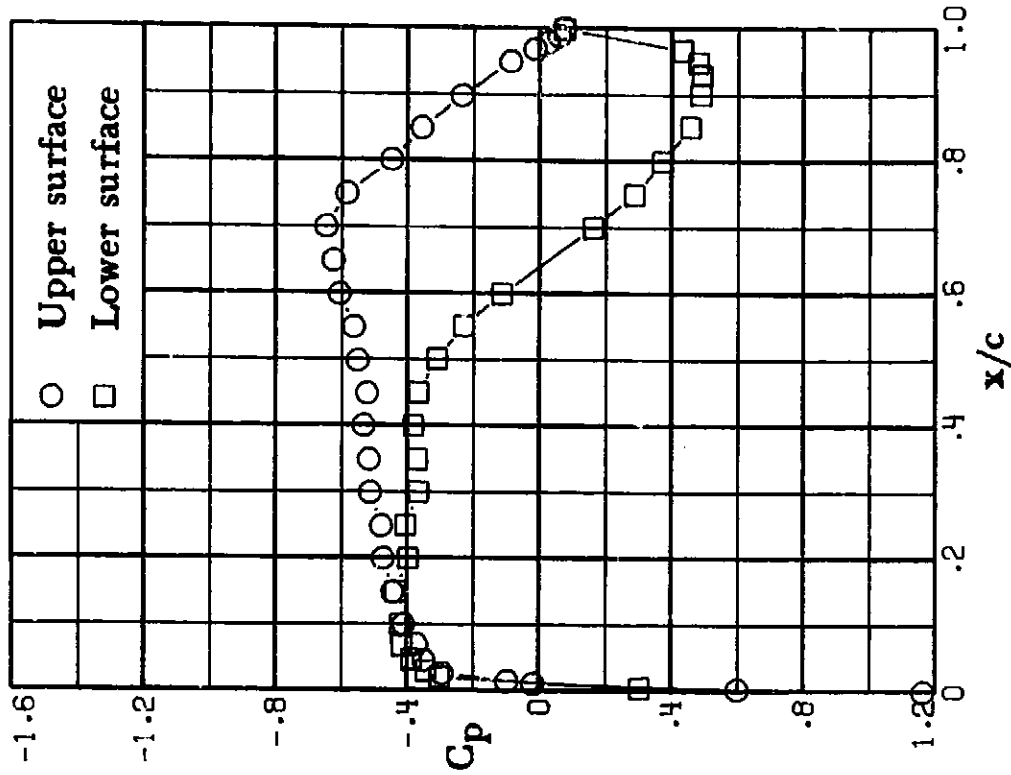
Figure 18. - Continued.

SHUTTLE

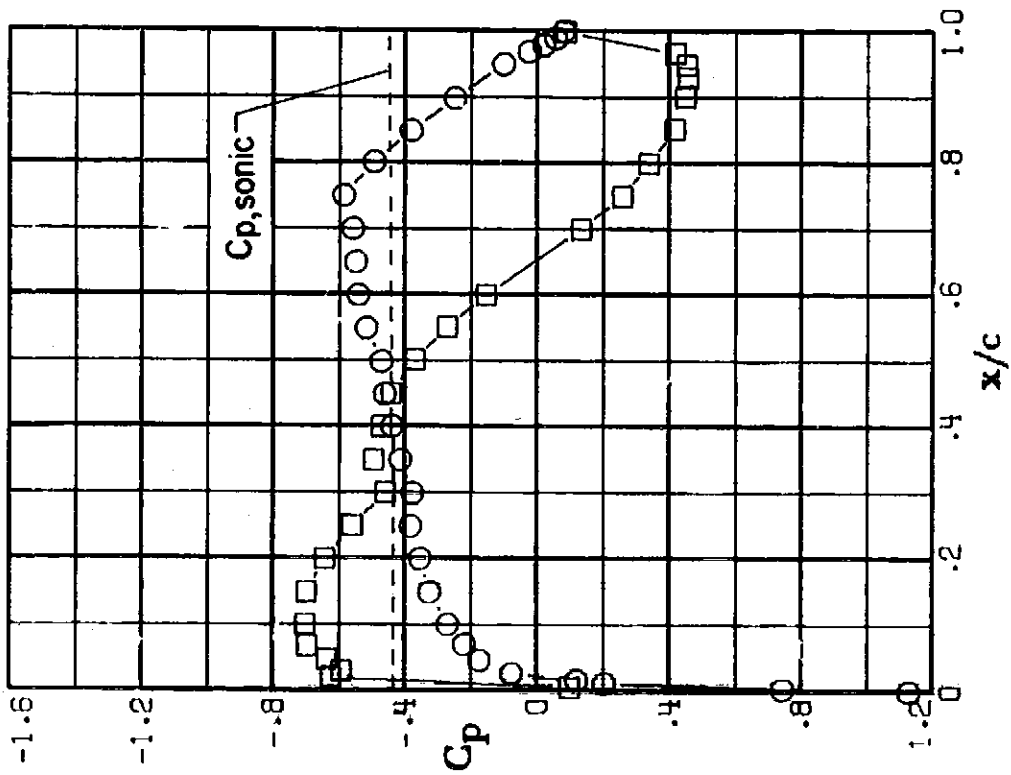
CONFIDENTIAL

CONFIDENTIAL

ORIGINAL REVISIONS
OF FIGURE 19

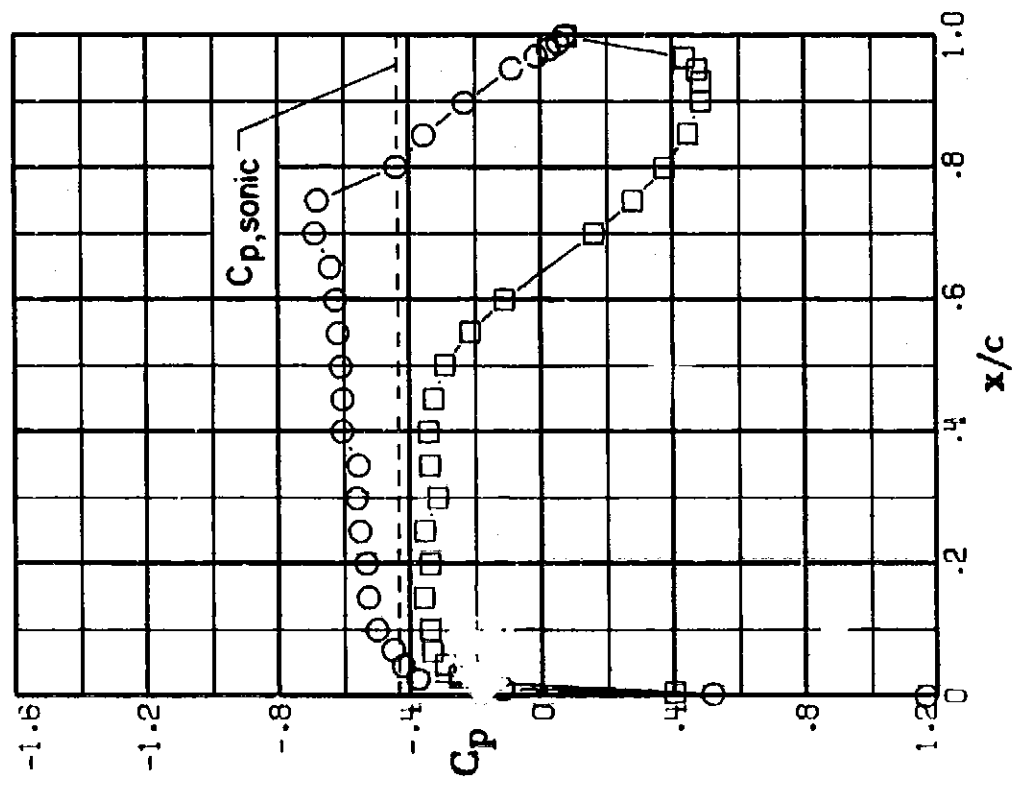


(a) $M = 0.80$; $c_n = 0.18$.

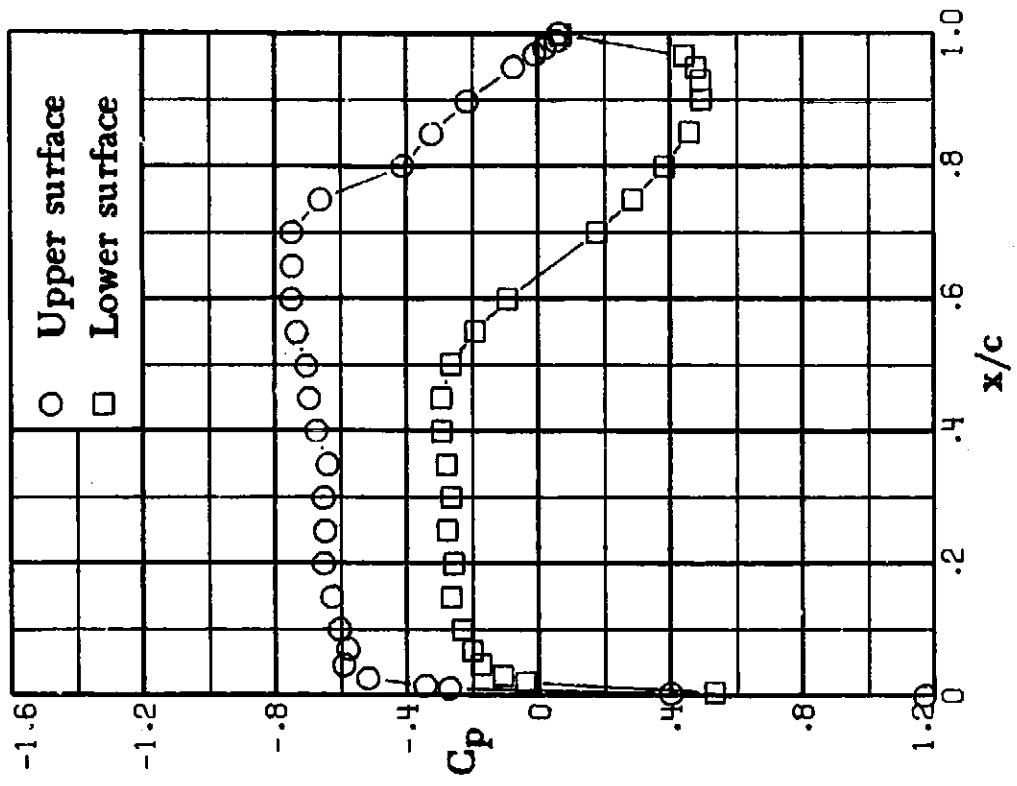


(b) $M = 0.80$; $c_n = 0.35$.

Figure 19. - Chordwise pressure distributions for 10-percent thick supercritical airfoil 33. $M = 0.80$.



(c) $M = 0.80$; $c_n = 0.43$.



(d) $M = 0.80$; $c_n = 0.54$.

Figure 19. - Continued.

SHEET 74C

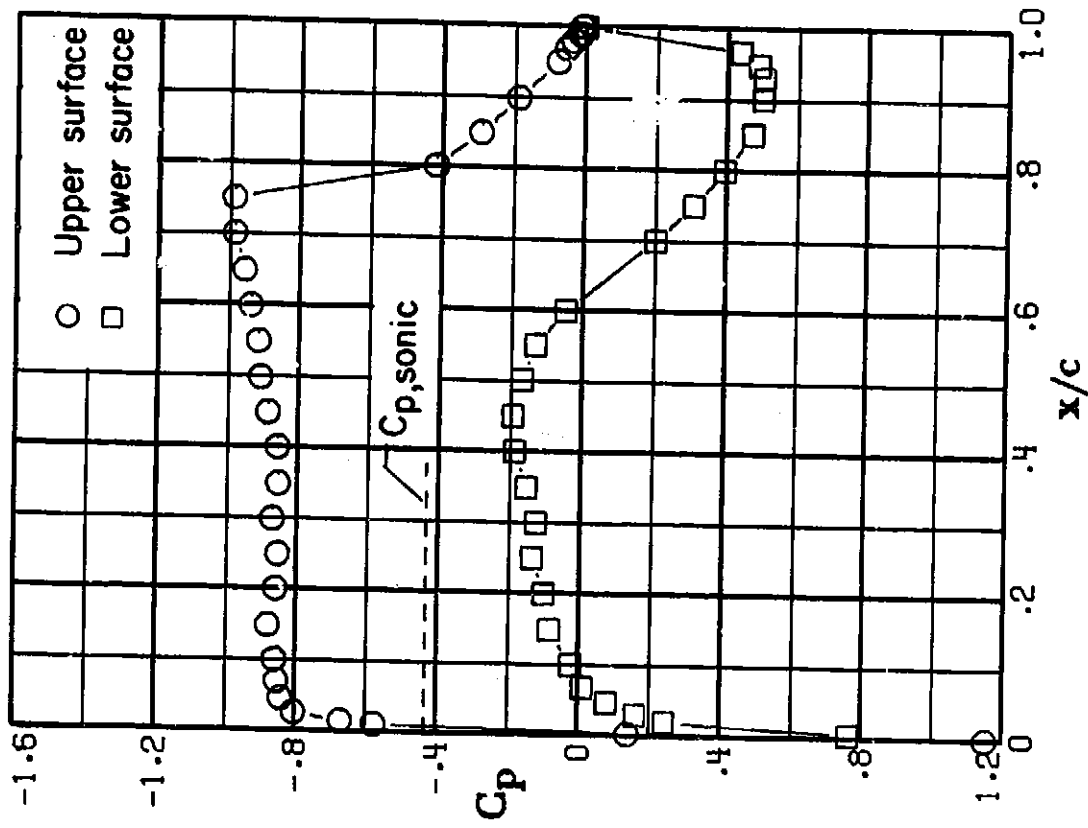
RESEARCH AIRCRAFT

WIND TUNNEL

1954

ORIGINAL FILED IN
OF POOR QUALITY

CONFIDENTIAL



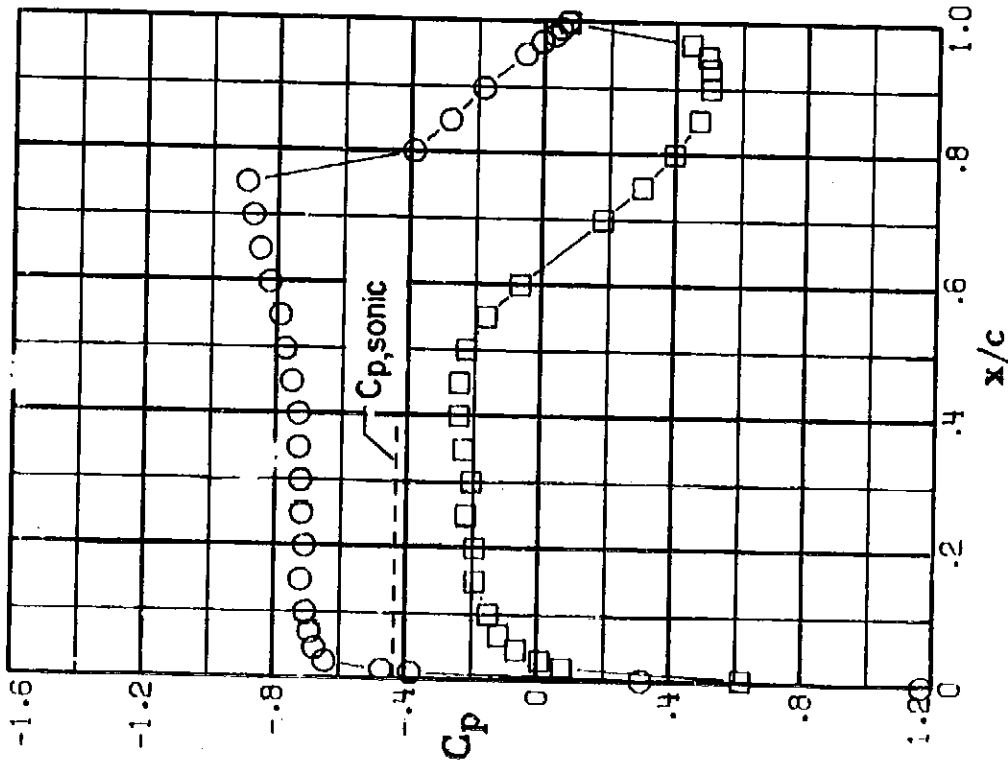
(g) $M = 0.80$; $c_n = 0.81$.

Figure 19. - Concluded.

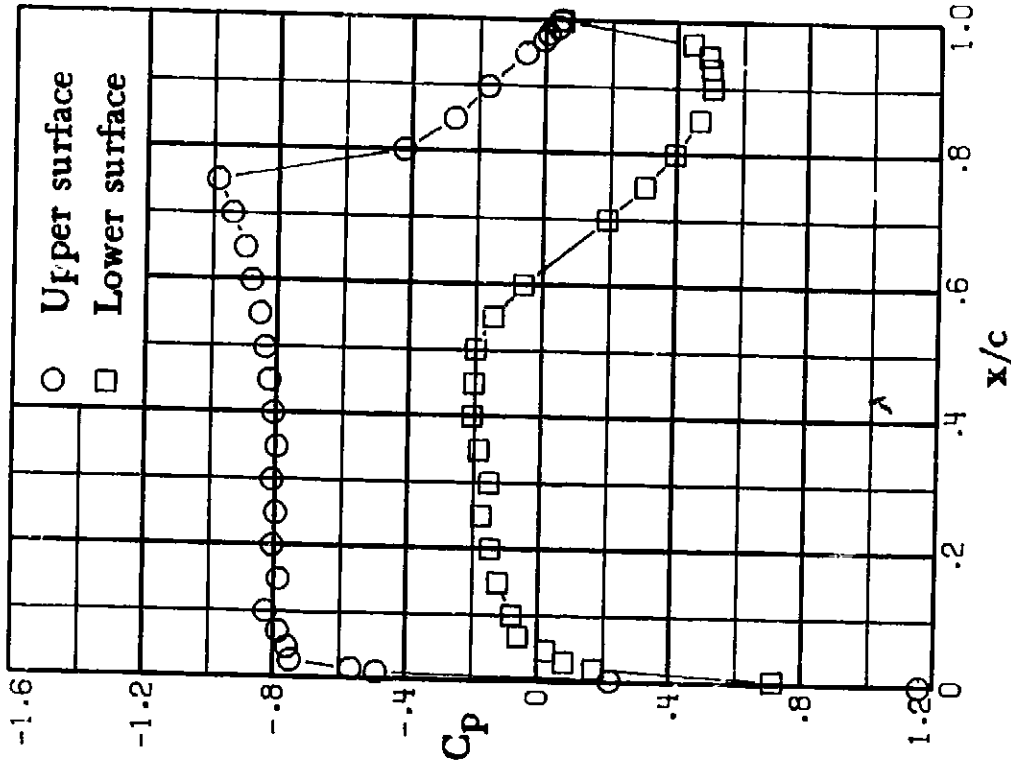
SHEET 42



CONFIDENTIAL

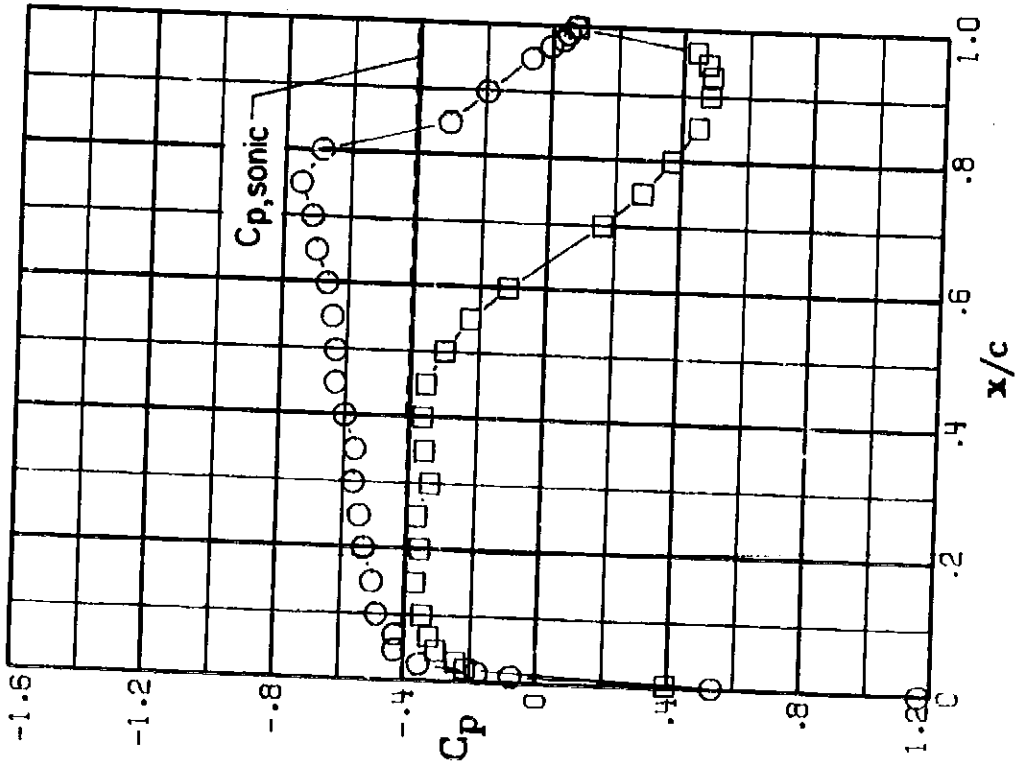


(e) $M = 0.80$; $c_n = 0.65$.

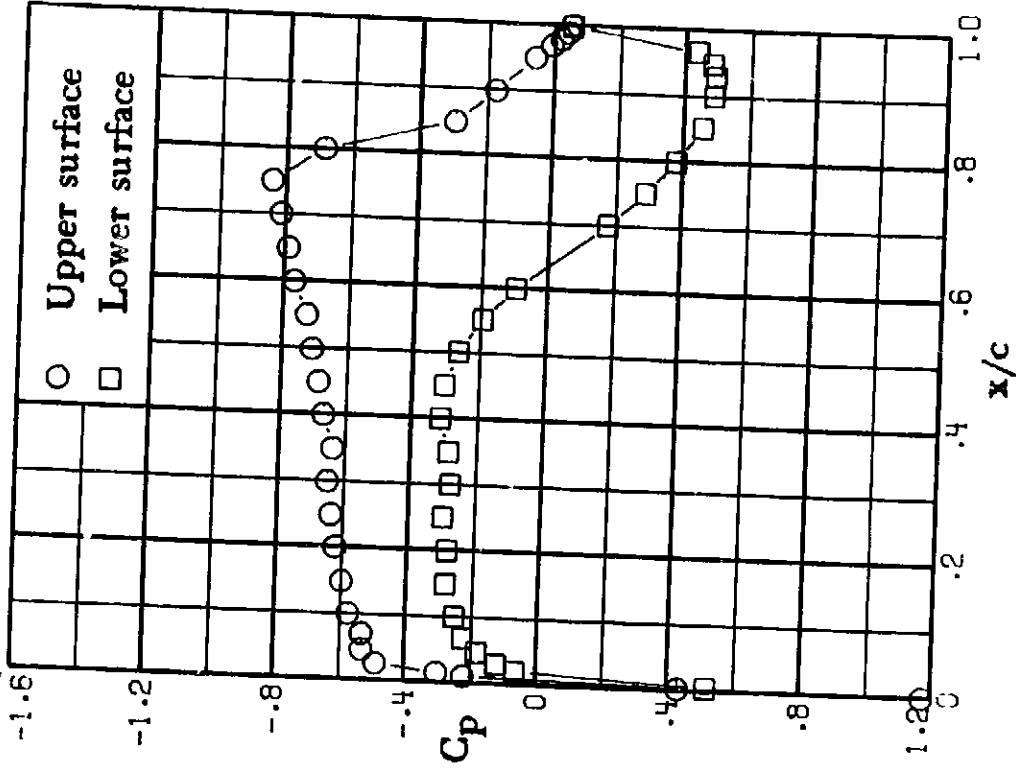


(f) $M = 0.80$; $c_n = 0.74$.

Figure 19. - Continued.

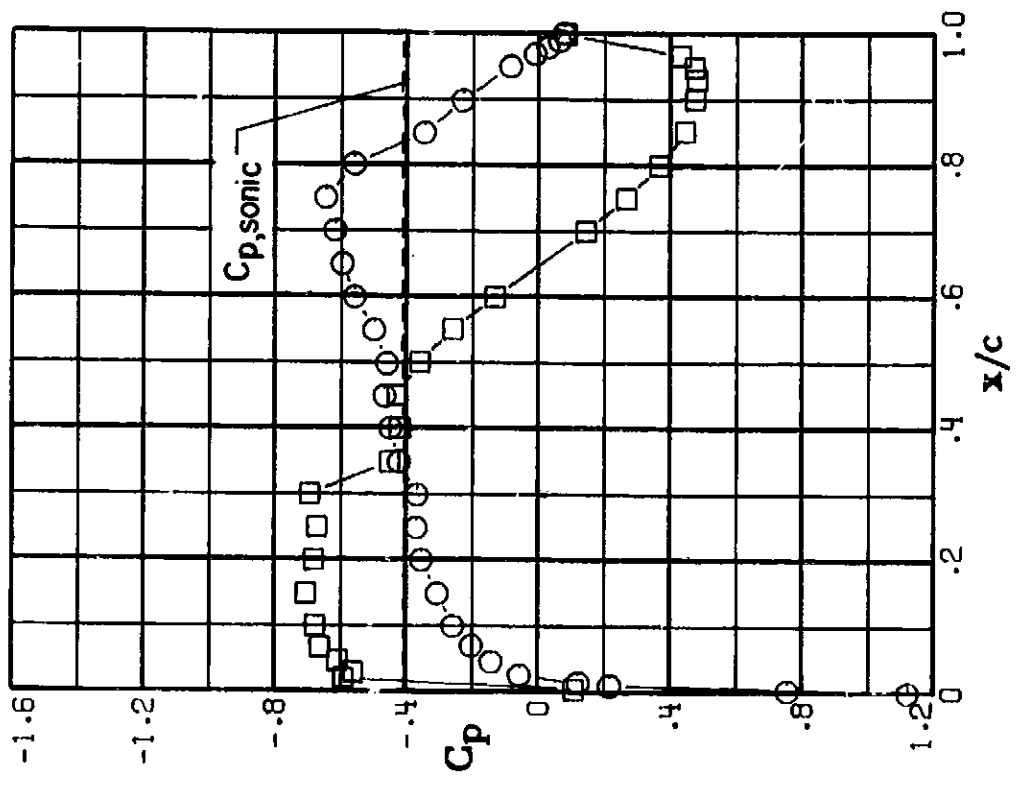


(c) $M = 0.81$; $c_n = 0.44$.

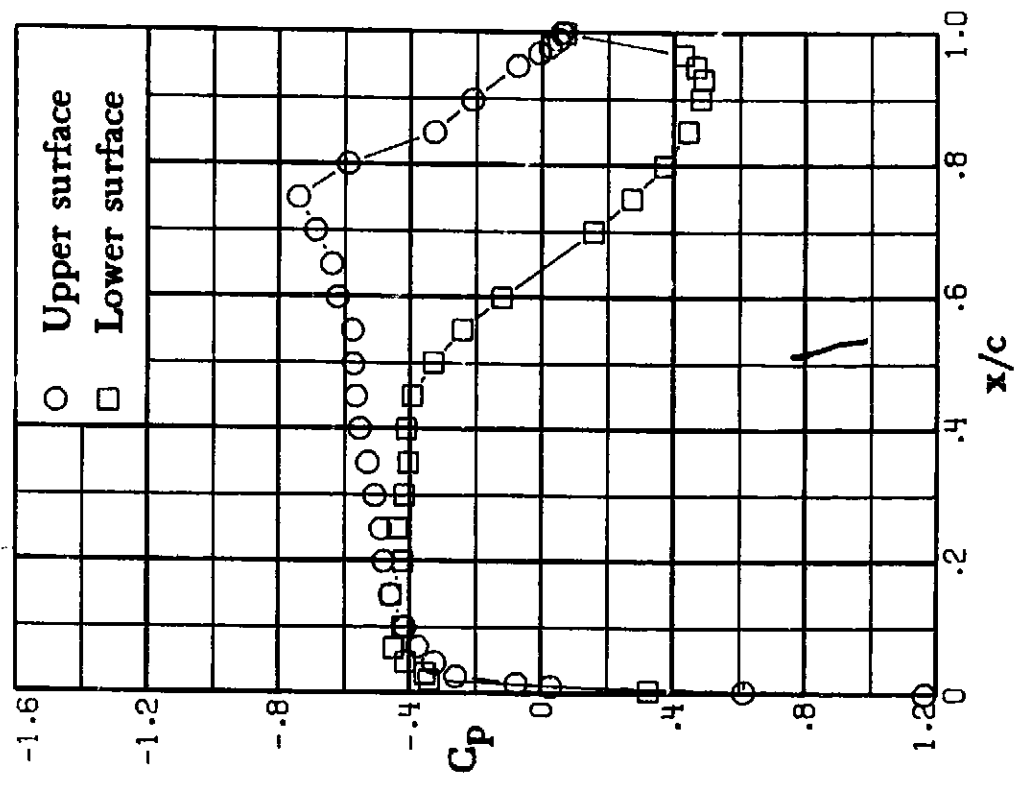


(d) $M = 0.81$; $c_n = 0.55$.

Figure 20. - Continued.

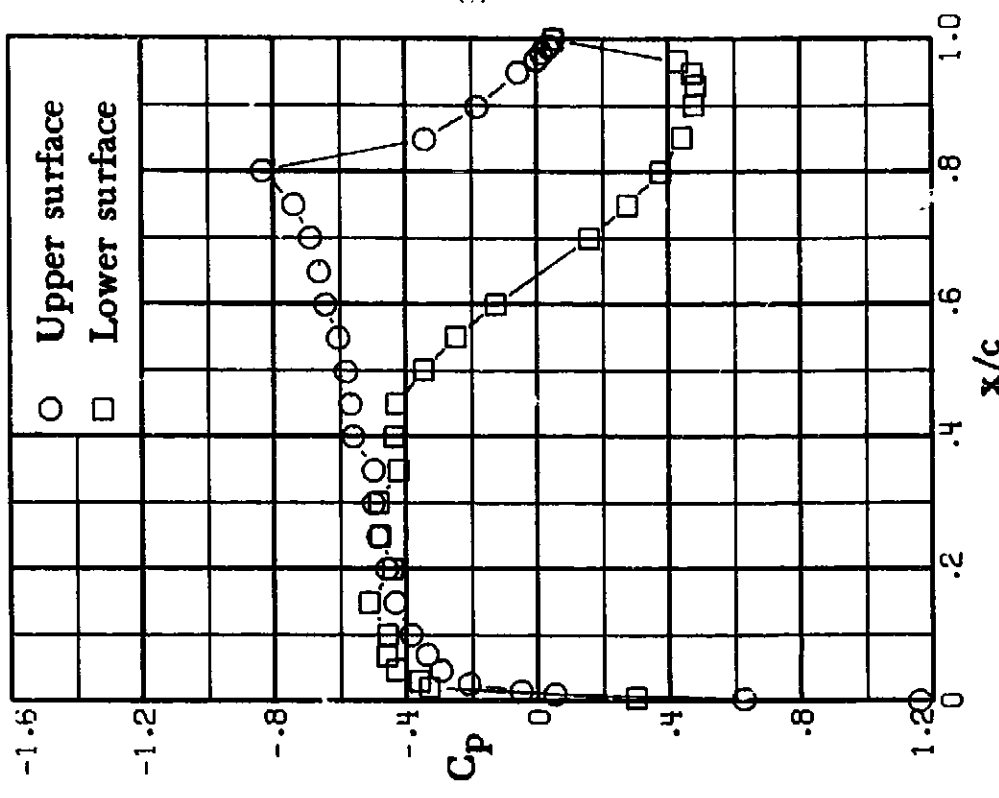


(a) $M = 0.81$; $c_n = 0.18$.

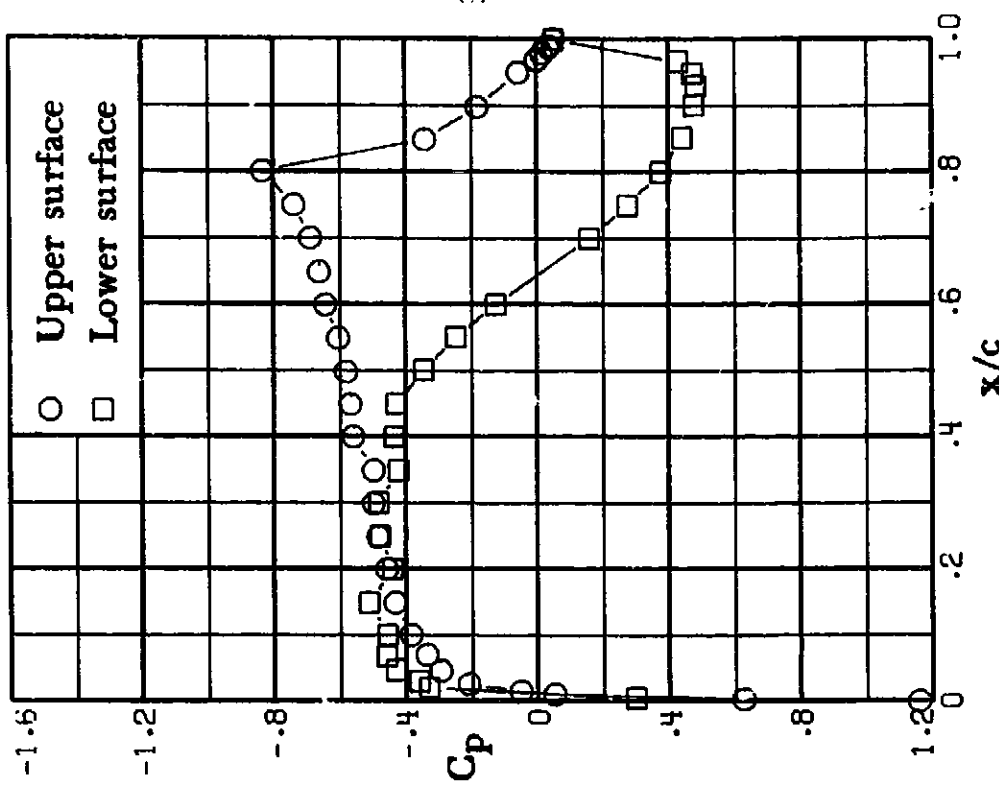


(b) $M = 0.81$; $c_n = 0.36$.

Figure 20. - Chordwise pressure distributions for 10-percent thick supercritical airfoil 33. $M = 0.81$.



(a) $M = 0.82$; $c_n = 0.17$.

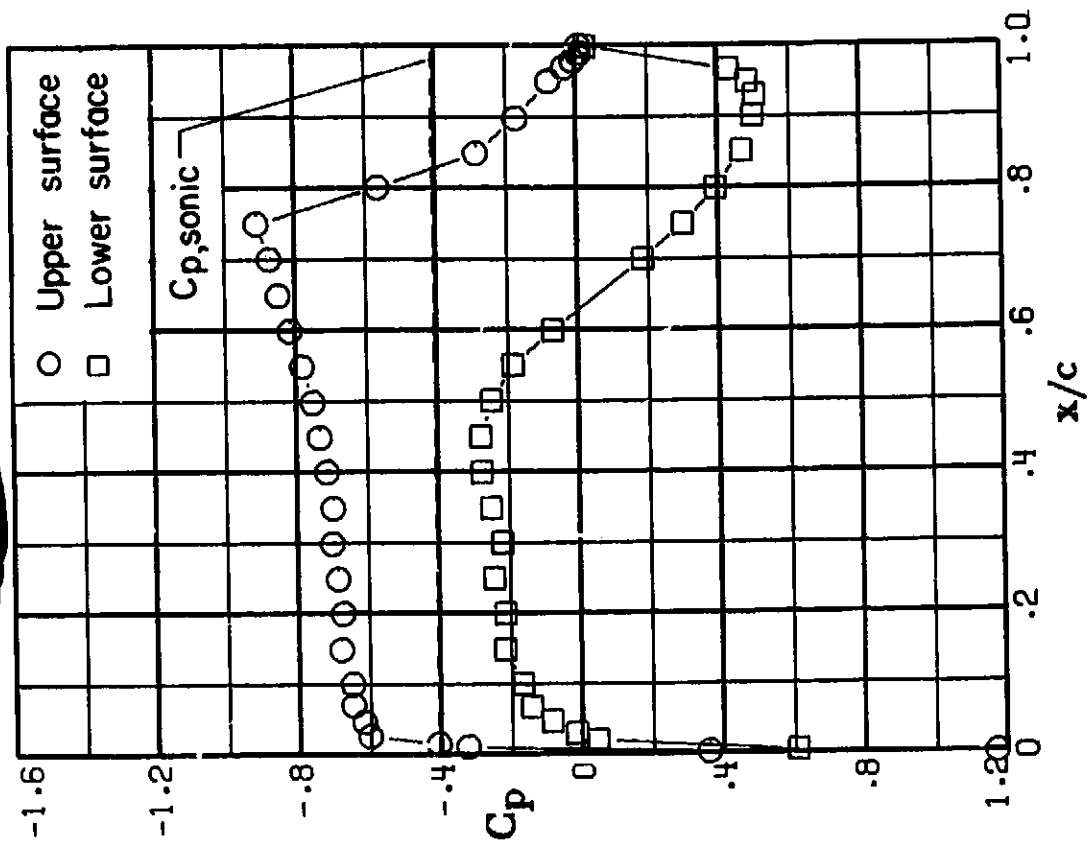


(b) $M = 0.82$; $c_n = 0.35$.

Figure 2i. - Chordwise pressure distributions for 10-percent thick supercritical airfoil 33. $M = 0.82$.

ORIGINAL FILED
 ON 11/11/54

ORIGINAL PAGE IS
OF POOR QUALITY



(e) $M = 0.81$; $c_n = 0.63$.

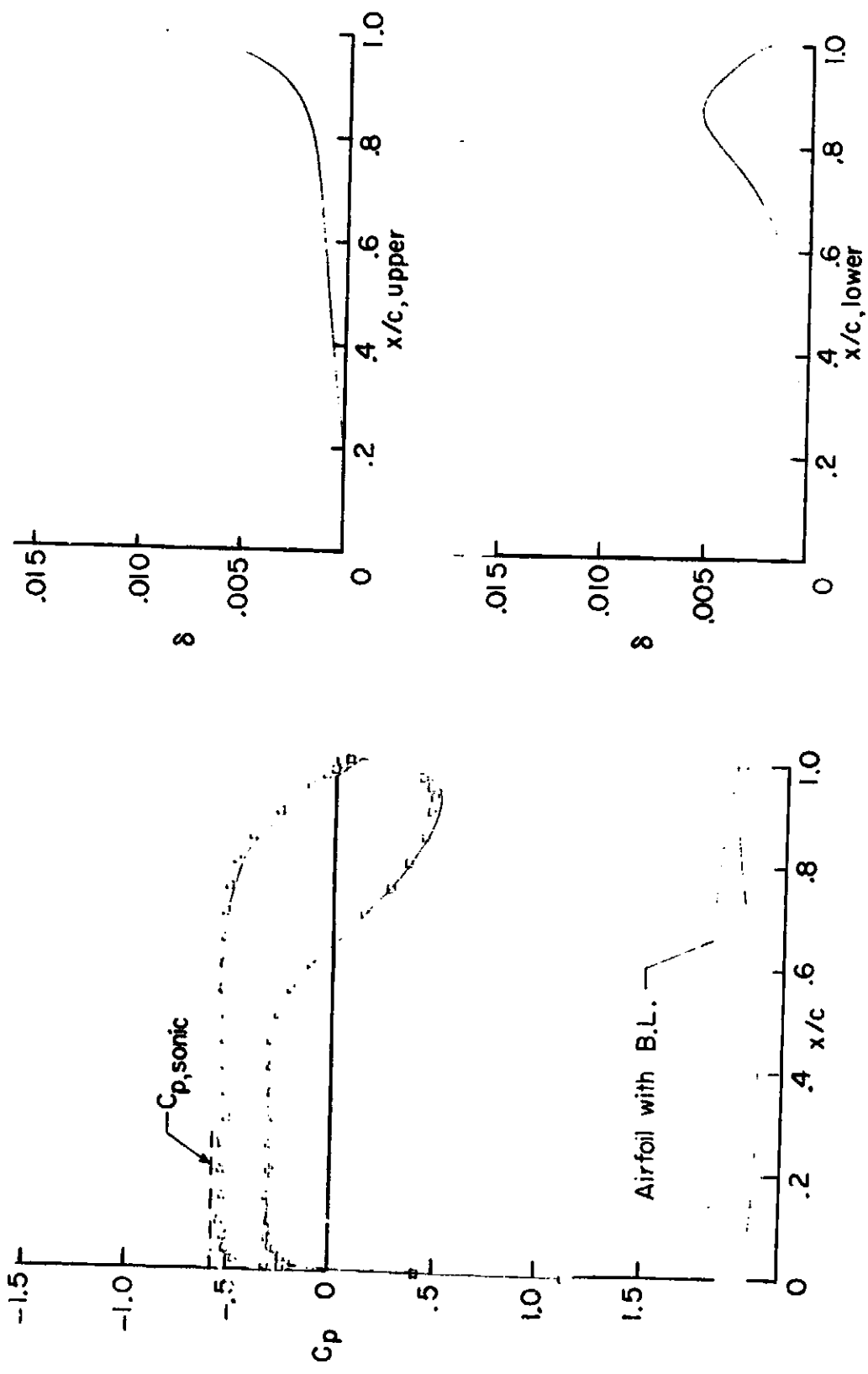
Figure 20. - Concluded.

SHEET 148

CONFIDENTIAL

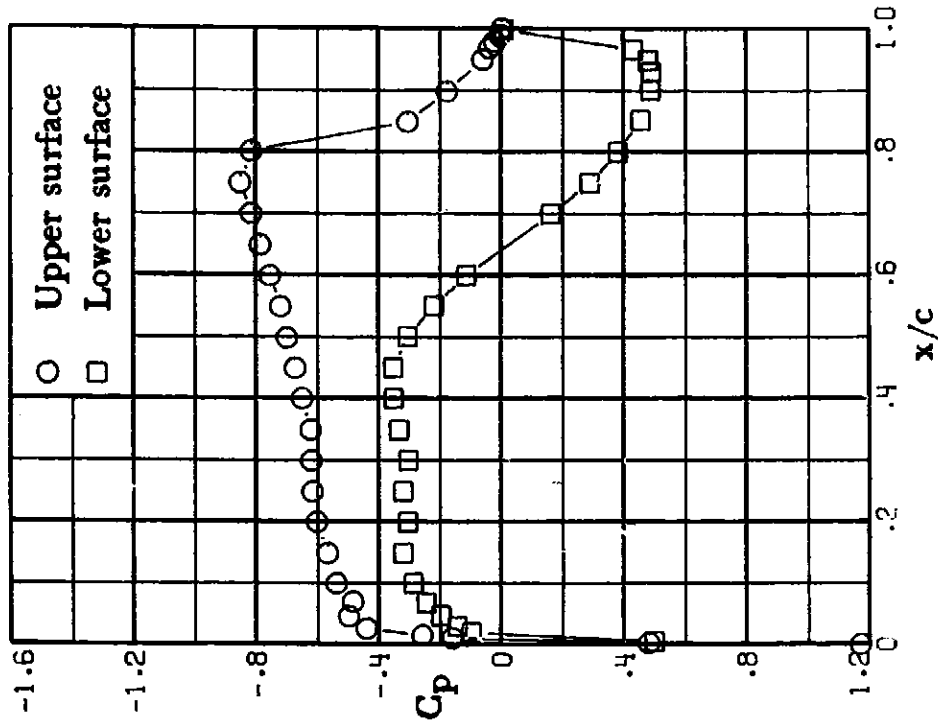
~~CONFIDENTIAL~~

— Theory M=0.758 $\alpha = -1.44^\circ$ $c_l = 0.414$ $c_d = 0.0071$
□ Experiment M=0.760 $\alpha = -1.53^\circ$ $c_l = 0.414$ $c_d = 0.0070$

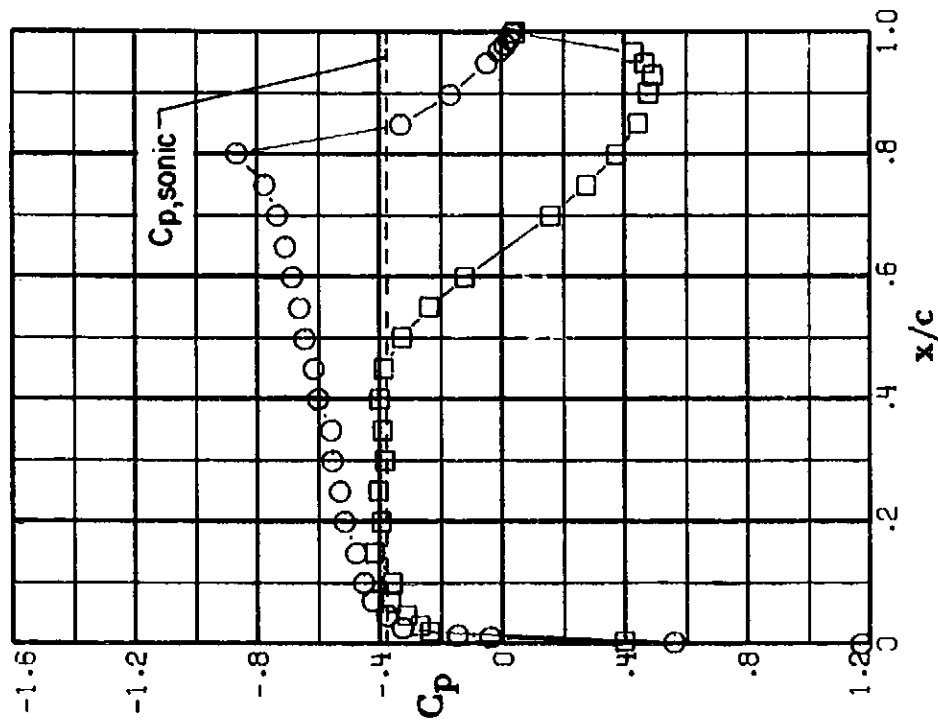


ORIGINAL PAGE IS
OF POOR QUALITY

Fig. 22. - Comparison of theoretical and experimental characteristics for the 10-percent-thick experimental supercritical airfoil 33.
 $R = 7.7 \times 10^6$.



(d) $M = 0.82$; $c_n = 0.52$.



(c) $M = 0.82$; $c_n = 0.42$.

Figure 21. - Concluded.

Theory $M=0.761$ $\alpha=-0.14^\circ$ $c_l=0.707$ $c_d=0.0076$
 Experiment $M=0.770$ $\alpha=.97^\circ$ $c_n=0.707$ $c_d=0.0077$

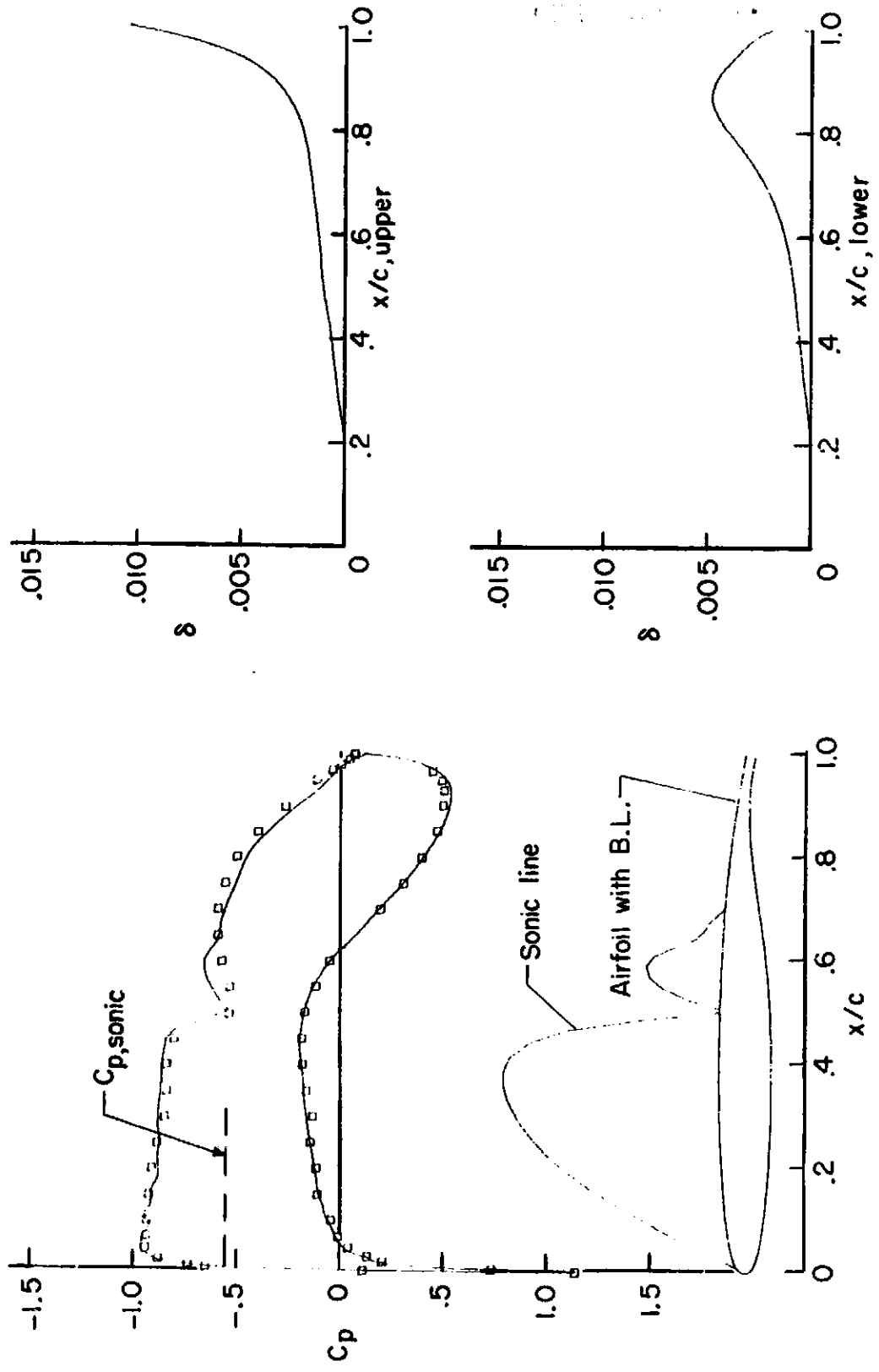
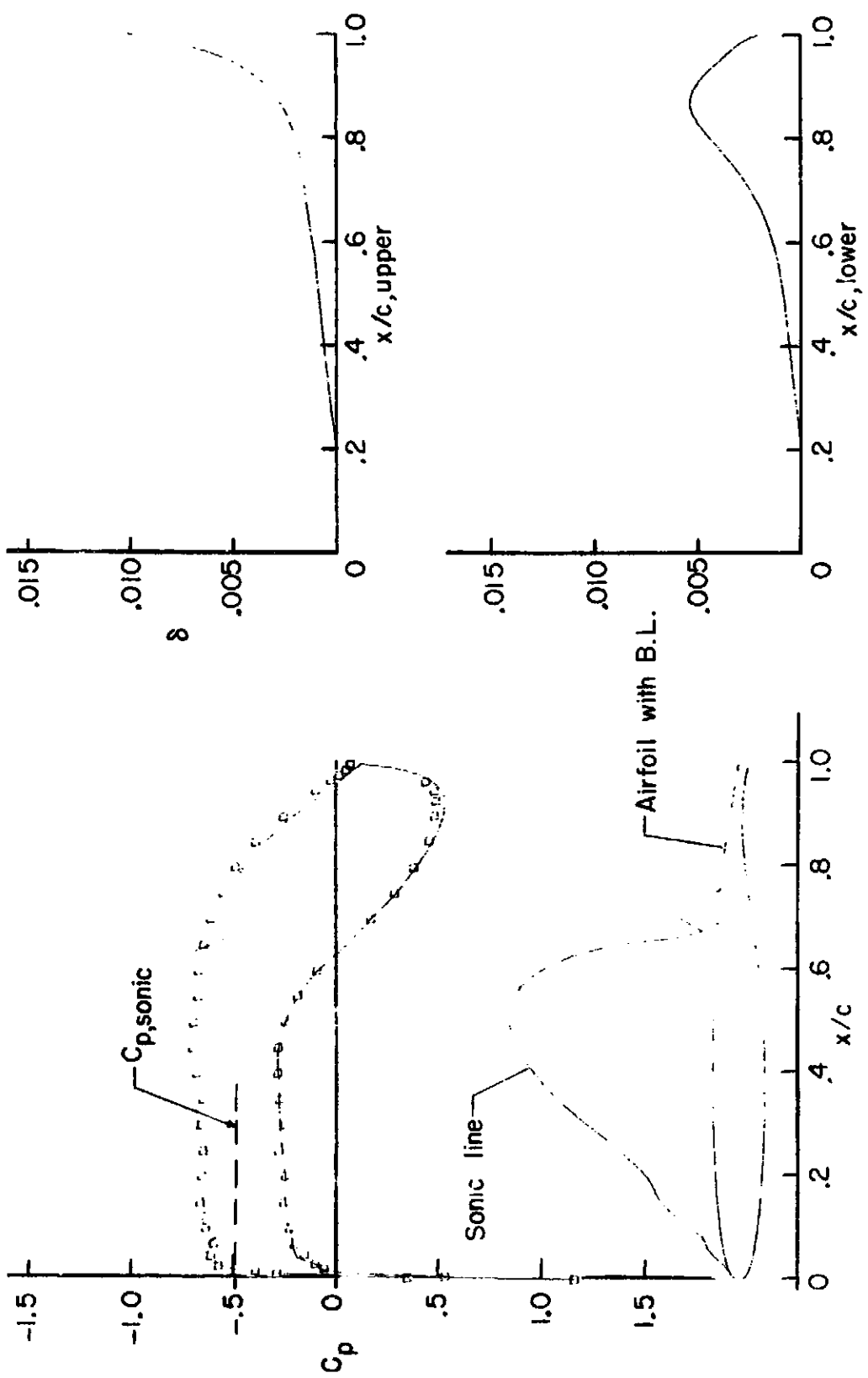


Figure 24. - Comparison of theoretical and experimental characteristics for the 10-percent-thick experimental supercritical airfoil 33.
 $R = 7.7 \times 10^6$.

— Theory $M=0.782$ $\alpha=-1.07^\circ$ $c_l=0.535$ $c_d=0.0075$
 □ Experiment $M=0.791$ $\alpha=-.03^\circ$ $c_n=0.535$ $c_d=0.0074$



ORIGINAL SOURCE
 OF INFORMATION

Figure 23.- Comparison of theoretical and experimental characteristics for the 10-percent-thick experimental supercritical airfoil 33.
 $R = 7.8 \times 10^6$.